Building A Gene Regulatory Network in Adult Mouse Skeletal Muscle Following Nerve Injury: Transcriptome Characterization and New Model for Functional *cis*-Regulatory Analysis *In Vivo*

Thesis by

Gilberto Hernandez, M.D.

In Partial Fulfillment of the Requirements

for the Degree of

Doctor of Philosophy

California Institute of Technology

Pasadena, California

2013

(Defended July 23, 2012)

To my parents, Tomasa and Gilberto Hernandez, who have provided me with the ability and motivation to always strive to live life beautifully.

Acknowledgments

I would like to thank my advisor, Barbara J. Wold, for supporting my research, despite it not being directly in accordance with the lab's focus. I have learned a great deal from our partnership. I would also like to thank, Eric H. Davidson, for literally providing me with a key to his laboratory and, by default, granting me access to the world of Gene Regulatory Networks and his team of highly talented scientists from which to learn. Special thanks to Marianne Bronner, who was my first mentor at Caltech and not only welcomed me warmly to the world of Caltech research, but provided invaluable understanding and guidance during my early graduate years in my quest to find a research focus that resonated best with my sensibilities. Naturally, I thank Professors Alexander Varshavsky and Paul Sternberg for guidance in their roles as members of my thesis committee.

I have had the privilege of learning from very talented scientists, including my first teacher of molecular biology: Leslie Dunipace; my current teacher of molecular biology: Brian Williams; my bioinformatics tutors: Christopher Hart, Henry Amrhein, Diane Trout, Anna Cecilia Therese Abelin and the rest of the Wold lab; my GRN instructors: the Davidson lab for their excellent INFOs/research/and discussions; Roger Revilla-i-Domingo, Qiang Tu, Jongmin Nam, Emmanuel Faure, Julie Hahn, Erika Vielmas, and Ping Dong all took time from their work to help me with mine. To Smadar Ben-Tabou De-Leon, Jane Rigg and Deanna Thomas for their strong and positive support throughout the years. To Miao Cui without whom I would never have arrived to any Davidson lab social event. My collaborators from the Pierce lab: Harry Choi and Colby Calvert; and from the Fraser lab: Periklis Pantazis, Thai

Truong, and Sarah Sweeney for guidance with confocal and two-photon imaging. To Igor Antoshechkin and Vijaya Kumar for assistance with RNAseq library construction and sequencing.

My *in vivo* gene transfer and skeletal muscle physiology mentors from UCLA: Julio Vergara, Marino DiFranco, and Marbella Quinonez. This project would not have been possible without the expertise provided by Professor Julio Vergara. Thanks also to Raul Serrano for his electrical engineering prowess and Phillip Tran for his technical assistance with electroporation into flexor digitorum brevis and interosseous as well as muscle fiber dissociation.

Special thanks to Libera Berghella, whose research on the *myogenin*-highly conserved element (HCE) and Msy3 protein set the stage for my dissertation work. Her patient guidance and generosity with knowledge and reporter constructs greatly assisted me throughout the development of my project. To Edoardo "Dado" Marcora for expert assistance in every possible scientific area that my project entered. To Holly Carlisle for serving as my cultural attache to the scientific community of Caltech. To Sagar Damle for his assistance in helping me overcome countless bioinformatics and experiment-related obstacles in these last few months, including defense seminar organization and for being pretty much my only source of human contact in the last 8 weeks.

I am forever grateful to Drs. Eugene Seymour, Gerald S. Levey, and Jennie B. Dorman. Dr. Seymour took the time to get to know me during a morning bike ride when I was an undergraduate at UCLA and kick started my journey towards becoming a physican-scientist through his mentorship and unconditional support. Dr. Levey took the time to get to know me during a medical student welcome BBQ and was the first person to actively stand behind my desire to explore my research interests as a member of the Caltech/UCLA Medical Scientist Training Program. Dr. Dorman has been a part of my scientific journey from even before Dr. Seymour, in the days when I studied skeletal muscle physiology by seeing how strong and fast I could make my

own muscles function. I have received nothing but support and encouragement from her through the years and her help in the construction of this written dissertation, from editing to bringing my hands to the keyboard every time I was running out of steam physically and emotionally, has been invaluable and awe inspiring.

Finally, thanks to my close family and friends (many of whom have already been mentioned above) for believing in me, appreciating my effort and for being at the finish line of this most challenging event.

Abstract

The essential functional linkages of gene regulatory networks (GRNs) consist of the interactions between *cis*-regulatory DNA sequences and *trans*-acting regulatory factors. These genomically encoded regulatory interactions govern the differential gene expression programs which direct specific biological processes during development and adulthood. Detailed analysis of GRNs during development has yielded important insights regarding the structural and functional dynamics of *cis*-regulatory modules (CRMs) and *cis*-regulatory elements (CREs). Indeed, the comprehensive GRNs that have been characterized for various developmental processes provide a model for both the methodological approach and the intellectual understanding required to explore *cis*-regulatory architecture in other biological contexts. The present study focuses on the physiological context, investigating the GRNs that govern the molecular response to nerve injury in adult mouse skeletal muscle. Until now, high-quality GRN investigations in this context have been hampered by the absence of two fundamental components: a comprehensive catalog of genes differentially expressed after nerve injury, and an effective *in vivo* gene transfer technique to functionally test putative *cis*-regulatory modules. Using RNAseq, we have compiled a comprehensive list of all differentially expressed genes at 6.0, 12.0, 24.0, and 168.0 hours following nerve injury. This data has validated previously known differentially expressed genes, as well as identified novel candidates for *cis*-regulatory analysis. The *in vivo* gene transfer technique I have adapted and advanced targets an easily accessible muscle group for minimally invasive injection and electroporation of DNA; with it, I demonstrate highly efficient, reproducible, and stable gene transfer in mouse skeletal muscle. In addition,

I have optimized the gene transfer technique not only for plasmid DNA reporter vectors, but also for BAC DNA reporter vectors, thus enabling *cis*-regulatory modules to be tested in a broad chromosomal environment. Finally, I have validated the capacity of this gene transfer method to functionally test CRMs, using a known nerve injury-associated CRM of the skeletal muscle-specific *myogenin* gene. The enhanced resolution provided by this technique allowed for qualitative and quantitative detection of increased reporter signal from a mutated version the nerve injury-associated CRM at ten days following denervation, when compared to the wild-type CRM. This result implicates a *cis*-regulatory element (CRE of 17.0 bp) within this *myogenin* CRM (1.1 kbp), as the regulatory sequence that mediates the down-regulation of *myogenin* that occurs in the weeks following denervation. This result was further supported by denervating target muscles in the hind limb of an $msy3^{-/-}$ mouse, which lacks the Msy3-binding protein of the *myogenin* CRE. In this case, the lack of the *trans*-acting repressor results in increased endogenous *myogenin* expression, which correlates with the increased reporter signal from the mutated construct of our gene transfer assay. This work lays the foundation from which a high-quality adult skeletal muscle GRN can be constructed for nerve injury and other muscle-associated disease states.

Contents

Chapter 1

Introduction

Comprehensive, validated gene regulatory network (GRN) models during early sea urchin development have provided an unprecedented perspective on how the animal body plan is encoded in the DNA [Davidson et al., 2002, Su et al., 2009, Peter and Davidson, 2009, Oliveri et al., 2008]. To date, GRNs have been implicated in controlling a wide range of biological processes, including morphogenesis, differentiation, and physiological response in various model systems [Davidson, 2006]. The essential functional linkages between *cis*-acting regulatory DNA sequences, on the one hand, and factors acting in *trans*, serve as the 'weight bearing columns' of a Gene Regulatory Network (GRN). These are the causal interactions that respond to a given regulatory state and, in turn, determine subsequent regulatory states, all of which contribute to the dynamic nature of biological responses. Functional testing of *cis*-regulatory modules (CRMs) via gene transfer of candidate *cis*-regulatory DNA sequence-driven reporter genes, reveals the general *cis*-regulatory architecture encoded in the DNA. Perturbation of validated CRMs provides further resolution of the *cis*-regulatory architecture by identifying the *cis*-regulatory elements (CREs) within each CRM. In all cases where the GRNs controlling a biological response have been well characterized, the validation of genomic network architecture and dynamics has required effective application of GRN bioscience methodologies. Central to these methodologies is the experimental validation of *cis*-acting regulatory DNA sequences via reporter gene

transfer [Revilla-i Domingo et al., 2004, Davidson et al., 2002]. To date, however, the application of GRN bioscience to adult skeletal muscle biology has been limited by existing *in vivo* gene transfer techniques, which suffer from poor or variable transfection efficiencies and often result in excessive tissue trauma. Researchers interested in adult skeletal muscle biology at the molecular-level have made many attempts at *in vivo* gene transfer into adult skeletal muscle, including both trans-epidermal and direct contact muscle-to-electrode electroporation, as well as ultrasound and viral vector infection [Taniyama et al., 2002, Mir et al., 1999, Wolff et al., 1990]. All these methods introduce confounding variables when attempted in adult skeletal muscle. In the case of electroporation, high voltage and/or the invasive survival surgery that is required to access muscle tissue result in significant trauma to target muscles and neighboring tissues [Lefesvre et al., 2002, Hartikka et al., 2001]. Viral-mediated transfection has proven effective for making transgenic mice, but its application in transient transfection experiments suffers from labor-intensive viral preparations and nonspecific infection of nontarget tissues, with resulting immune response [Lefesvre et al., 2002, Dai et al., 1995].

Consequently, the majority of the data on the *cis*-regulatory architecture of skeletal muscle centers around muscle cell differentiation, from *in vitro* experiments where gene transfer is most efficient and from *in vivo* transgenic experiments in the developing mouse embryo where reporter gene spatial and temporal expression is most easily observable [Weintraub et al., 1991b,a, Tapscott et al., 1988, Edmondson and Olson, 1989, Miner and Wold, 1990, Braun et al., 1989]. Otherwise, the majority of the regulatory network data data for adult skeletal muscle in mouse, comes from transgenic loss of function or gain of function experiments. Indeed, transgenesis has proven to be the most successful and reliable method for reporter gene transfer in adult mouse muscle. Currently, the experimental path towards functional *cis*-regulatory analysis in adult mouse skeletal muscle begins with a set of differentially expressed target genes, followed by inference of CRM function from differentiation-related *in vitro* experiments or poorly resolved *in vivo* transient transfections. Next, researchers

create a transgenic mouse to test CRM function in a physiologically relevant context. However, the cost and time required to produce a transgenic mouse is significant, especially considering that only one or two *cis*-regulatory modules can be tested at a time in this way. Thus, although genetic studies have identified many of the key regulatory and effector molecules involved in various adult skeletal muscle physiological events, how these molecules interact at the *cis* and *trans* level is still largely unknown.

My objective is to determine the genomically encoded regulatory interactions that control the physiological response capabilities of the adult skeletal muscle nerve injury-response. The first step necessary to meet this objective, is a more efficient and cost effective experimental approach to uncovering the GRNs that underlie the physiological response in adult mouse skeletal muscle. An ideal experimental pipeline would begin with a robust, stable, efficient, cost effective, short time-to-assay, and *in vivo* method for reporter gene transfer. This would allow for functional testing and reliable measurement of the reporter signals of candidate CRMs and CREs, all while in a biologically relevant context. I propose electroporation-mediated gene transfer into flexor digitorum brevis (FDB) and interosseous (IO) as an ideal *in vivo* experimental model for functional testing of candidate CRMs/CREs. In Chapter 2, I apply this experimental model to identify a functional CRE of *myogenin* that contributes to the down-regulation of *myogenin* at 10.0 days following denervation [Moresi et al., 2010]. Once a method to experimentally validate the functional CRMs and CREs which interpret the dynamic regulatory states present in skeletal muscle following nerve injury is in place, the next step is to focus on the regulatory molecules that comprise these denervation-associated regulatory states. Of particular importance are the transcription factors and signaling molecules which determine gene expression. GRN studies during embryological development in a range of model systems have provided clear evidence that transcription factors and signaling molecules are the key molecular drivers for establishing, maintaining, or transitioning between different regulatory states [Davidson, 2006]. Thus, by knowing the identity of the full

repertoire of candidate regulatory molecules, one can track their temporal and spatial expression to deduce the kinetics of their regulatory activity. In Chapter 3, I present a high-resolution transcriptome-wide RNAseq analysis for flexor digitorum brevis (FDB) and interosseous (IO) muscles at 6.0, 12.0, 24.0, and 168.0 hrs post denervation. This work moves the field forward in two important ways. First, it represents the first transcriptome-wide expression analysis for denervated FDB and IO muscles using RNAseq. Prior to this study, transcriptome-wide analysis of denervated adult mouse hind limb skeletal muscles were done using microarray assays. Tibialis anterior, extensor digitorum longus, gastrocnemius and soleus have all been assayed by microarray following sciatic nerve resection [Batt et al., 2006, Raffaello et al., 2006, Kostrominova et al., 2005, Tang et al., 2009]. RNAseq-generated data, however, has significant advantages over microarray data, including very low background, a much wider dynamic range for detecting fold changes, and higher accuracy in terms of absolute quantitation of expression across technical and biological replicates [Wang et al., 2009, Fu et al., 2009].

1.1 FDB and IO as a model system for investigation of GRNs in adult skeletal muscle

The current repertoire of skeletal muscles selected for denervation-associated studies have proven to be non ideal for gene transfer via electroporation, despite the known effectiveness of electroporation for introducting DNA or other molecules into cells [Sugar and Neumann, 1984]. A muscle group more amenable to electroporation mediated gene transfer, which also avoids the confounding trauma associated with current electroporation into adult skeletal muscle, would overcome a significant limiter to *in vivo* functional testing of candiate CRMs/CREs. Since the pioneering studies of Galvani on frog legs in the 18^{th} century, the skeletal muscles of the hind limb have served as the premier model system for research regarding nerve-muscle connec-

tivity in vertebrates (Figure 1.1A). Only as recently as the mid-20^{th} century has technology advanced enough to successfully record and characterize the excitation-contraction coupling effect first observed by Galvani in 1771 [Galvani, 1791, Sandow, 1952].

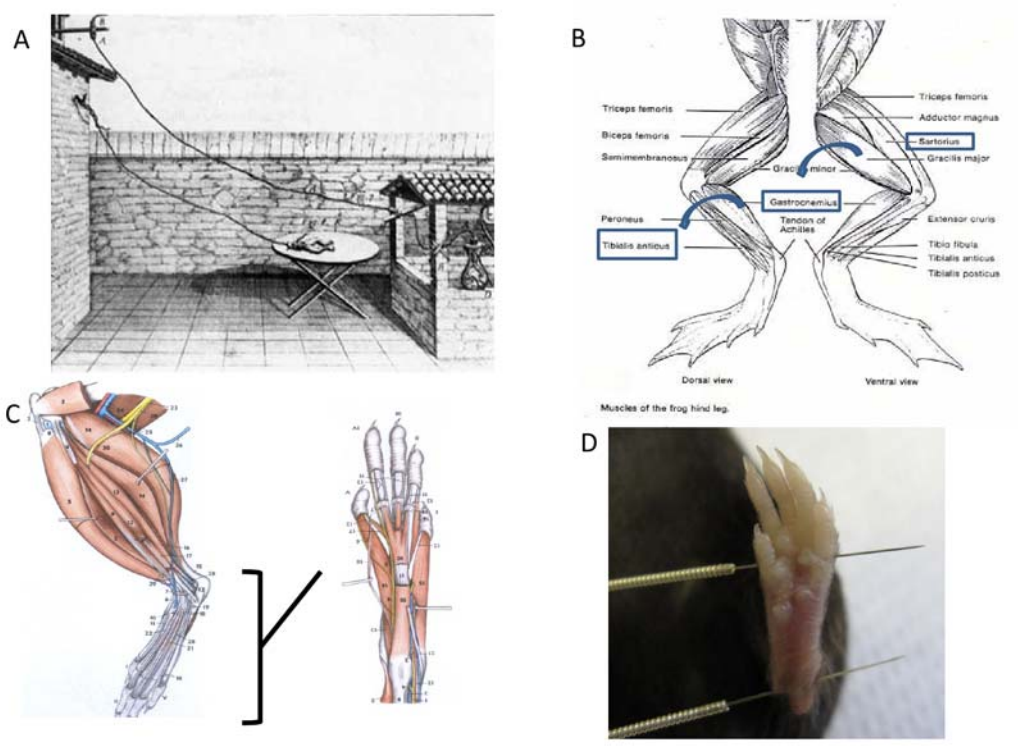

Figure 1.1: Experimental 'model muscle' groups. (A) Illustration of Galvani's experimental design for elliciting frog leg skeletal muscle contraction [Galvani, 1791]. (B) Anatomical distal trend to smaller muscles more ideal for advancing experimental technologies (sketch from Fastol.com). (C) Anatomical sketch of mouse hind limb and plantar surface views of FDB. Interosseous lies underneath the FDB and is not shown [Popesko P, Rajtova V, Horak J, Kapeller K, 1992]. (D) *in vivo* demonstration of sub-cutaneous electrode placement.

The longest muscle in the frog leg, sartorius, was the most amenable to the experimental method used in this seminal work. Since then, there has been an anatomical trend in the distal direction to the smaller skeletal muscles of the lower hind limb,

as model muscles for investigation (Figure 1.1B). Mouse gastrocnemius, plantaris, soleus, extensor digitorum longus, and tibialis anterior proved most amenable to the technological advances in experimental modalities of the second half of the 20^{th} century. However, *in vivo* electroporation into these larger muscles of the lower limb requires surgical exposure of underlying muscle and/or high voltages to penetrate the thick muscle bundles. This results in inefficient gene transfer and confounding trauma in the tissue under study.

The turn of the century marked the experimental debut of another muscle group that proved even more amenable to voltage clamp and current studies [Friedrich et al., 1999]. This group, consisting of the flexor digitorum brevis (FDB) and interosseous (IO) muscles, is located on the plantar surface of the mouse paw, and the use of FDB and IO continues the trend of employing more distal and smaller muscles (Figure 1.1C). In 2009, DiFranco et al. [2009] took advantage of the smaller size and superficial anatomical location of FDB and IO by engineering an *in vivo* electroporation method for gene transfer into this muscle group (Figure 1.1D). This highly efficient gene transfer technique has enabled them to perform protein-level analysis of key components of excitation-contraction coupling and represents a significant step towards understanding the protein-level dynamics of electrophysiological events. In the present study, we have advanced this methodology to enable transcript-level GRN experimentation, in order to test putative *cis*-regulatory modules of key genes controlling the response to nerve injury in adult skeletal muscle.

The relatively superficial location of the FDB and IO muscle groups allows for subcutaneous access to the muscle tissue, via small-diameter needles, for both introduction of DNA solution and electrode placement. Furthermore, the compartment of the plantar surface of the mouse paw can accept a volume up to 25 µL; we have confirmed that a subcutaneous injection of 10 µL of a reporter DNA solution is sufficient to fully bathe the FDB/IO muscles. Small-diameter acupuncture needles serve as electrodes, which are placed subcutaneously at the toe line and at the heel at the plantar surface of the mouse paw. Much like the gel in an electrophoresis assay, the

FDB and IO muscles lie longitudinally between the two electrodes (Figure 1.1D). Once voltage is applied, the current travels along the entire longitudinal plane of the FDB/IO muscle bundles. The result is uniform muscle coverage of both DNA solution and the applied current. We have found that the FDB and IO of one mouse paw from a 2.0 to 4.0-month-old mouse consistently yields at least 0.5 µg of total RNA, which is sufficient for both RNAseq or QRT-PCR assays.

The FDB and IO muscles are innervated exclusively by tributaries of the sciatic nerve, as are the classically studied skeletal muscles of the hind limb used for denervation experiments. Therefore, sciatic nerve resection can remain as the method of choice to induce the denervation response. In addition, FDB and IO muscles share the same fiber type composition as the classically studied muscles used for denervation studies. They are all typeIIB-fiber-type dominant or fast-twitch muscles. This is important to ensure that we can build upon prior knowledge obtained from denervation studies in the classically studied fast-twitch muscles.

1.2 Gene regulatory networks of limb skeletal muscle in the embryo and adult

Skeletal muscles of the head, body and limb have distinct embryonic and cellular origins. The trunk and limb muscles are derived from the paraxial mesoderm and the muscles of the head originate from pre-chordal and pharyngeal head mesoderm. The myogenic regulatory factors (MRFs): *myf5*, *myoD*, *myf6*, and *myogenin*, eventually direct the determination and differentiation transcriptional programs of striated skeletal muscle. However, different regulatory circuits control the deployment of the MRFs in these different anatomical regions. The next level of regulatory circuit deployment, following primary determination and differentiation of skeletal muscle (i.e. embryonic myogenesis), involves establishing the future metabolic and contractile and regenerative properties of the muscles of specific anatomical compartments (i.e. fetal

myogenesis). Finally, during post natal development the regulatory circuitry gets further refined by inputs from innervating motor neurons. In essence, the underlying core genomic regulatory apparatus for striated skeletal muscle is partially revealed as we determine the input receiving capacity of each network-associated gene as it encounters varying regulatory states throughout development and into adulthood. We will highlight some of the regulatory circuitry that governs hind limb skeletal muscle development in fast-twitch muscle (i.e. the predominant muscle type of the mouse hind limb) to provide a context from which to better frame the regulatory logic that directs the denervation response in the adult skeletal muscle. Our attention will eventually focus specifically on *myogenin* and its down-regulation after the first week of skeletal muscle denervation.

1.2.1 Regulatory circuitry during delamination and migration of progenitor cells to the limb bud

The limb musculature develops from progenitor cells that delaminate from the hypaxial region of the dermomyotome and and migrate to the limb bud. During the migration to the limb bud these progenitor cells proliferate, but do not yet differentiate. At this time they do not yet express MRFs or muscle specific proteins. The regulatory circuitry active at this point involves expression of *six1/4*, *eya1/2*, *pax3*, *c-Met*, *lbx1*, and *gab1* in the migrating progenitor cells, along with hepatocyte growth factor (HGF), secreted from neighboring tissues. Loss of function experiments confirm that Six1 and Six4 control expression of *pax3* [Grifone et al., 2005] and that Pax3 partially regulates *c-Met* [Bober et al., 1994, Goulding et al., 1994, Tajbakhsh et al., 1997, Relaix et al., 2004, 2005]. The progenitor cells are unable to undergo normal delamination or migration without Six1/4 and Pax3. Pax3 also controls expression of the homeobox-containing transcription factor ladybird,*lbx1*, and when *lbx1* is inactivated, progenitor cells cannot migrate to the limb bud [Schäfer and Braun, 1999, Gross et al., 2000, Brohmann et al., 2000]. c-Met is a tyrosine kinase receptor for

HGF and Gab1 functions in the signaling cascade downstream of c-Met and HGF When *gab1* or *hgf* is mutated, no muscles are formed in the hind limb [Sachs et al., 2000, Dietrich et al., 1999]. The regulatory circuitry at this point, from approximately embryonic day 9.0 (E9.0) to 11.0 (E11.0) in the hind limb, centers around facilitating delamination, proliferation and migration while preventing activation of the myogenic differentiation program (Figure 1.2).

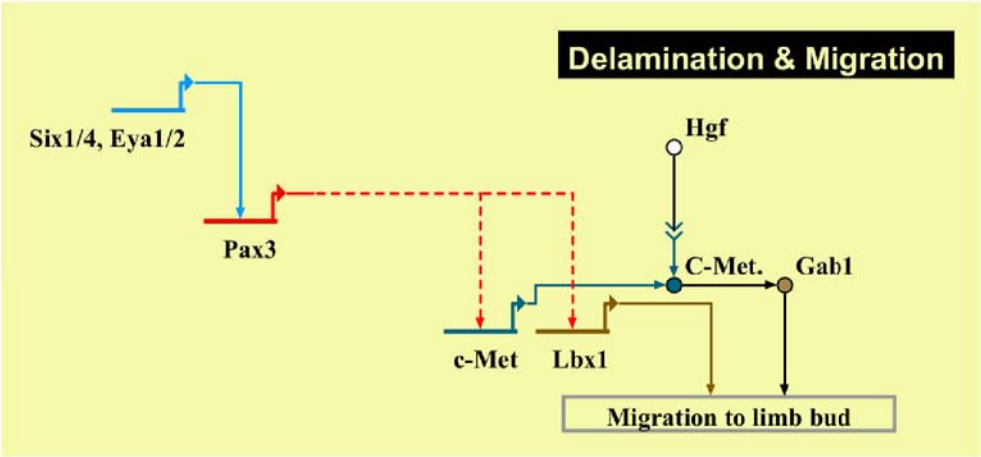

Figure 1.2: Progenitor cell regulatory subcircuit during delamination and migration to hind limb (E9.0 to E11.0). The myogenic differentiation program is not yet initiated until the progenitor cells reach the limb bud. Hgf/C-Met/Gab1 are part of a signaling mechanism that guides migration. Colored circles represent proteins of a signaling pathway and solid arrows connecting the circles represent the signaling hierarchy. Solid lines indicate a direct *cis* interaction and dotted lines indicate an indirect interaction.

1.2.2 Regulatory circuitry of hind limb muscle development in the embryo

Once progenitor cells reach the hind limb, signaling from sonic hedgehog (Shh) and bone morphogenetic protein 4 (BMP4) contribute to activation of the MRFs and the myogenic program [Krüger et al., 2001]. *six1/4*, *meox2*, *pax3*, *myf5*, *myf6*, *myoD* and *myogenin* are expressed in the progenitor cells along with regulatory co-factors (e.g. E-proteins, PBX/Meis, Eya1/2 and Mef2C) which comprise the regulatory circuitry driving primary myogenesis in the hind limb. Mutations in the homeobox gene *meox2* results in partial loss of muscle in the hind limb and down-regulation of *pax3* [Mankoo et al., 1999]. Six1/4 and Pax3 can directly activate *myf5* expression and *myf5* is the first of the MRFs to be expressed in the primary limb musculature [Giordani et al., 2007, Bajard et al., 2006]. Shortly thereafter *myoD* followed by *myogenin* and *myf6* are expressed. Six1/4 along with co-activators Eya1/2 can directly activate *myf5* once in the hind limb, whereas only Pax3 directly activated *myf5* in the dermomyotome. Mutation of *meox2* has no effect on *myoD* expression, while it does directly and indirectly affect *pax3* and *myf5* expression, respectively. In fact, myoD appears to be the primary MRF directing the myogenic program in hind limb muscle as evidenced by normal myogenesis in hind limb in *myf5*:*myf6* double mutants. In contrast, in the somites, activation of the myogenic program is delayed in *myf5*:*myf6* double mutants [Kablar et al., 1997]. Similarly, a distinct regulatory circuitry directs the temporal activation of MRFs in the trunk versus the hind limb. In the trunk, Myf6 is sufficient to direct normal myogenesis in the absence of myoD, since they are expressed at overlapping time points, whereas myogenesis is delayed in the hind limb of mutant *myoD* embryos, from E11.5 to E13.5, until *myf6* is expressed and can rescue the phenotype [Kablar et al., 1997]. Shh is thought to function in maintenance of expression of MRFs and expansion of embryonic myoblasts. Shh mutants display severe deficiencies in hind limb muscles and also result in reduced expression of *bmp4*. *in vitro* studies on explants from Shh mutant embryos showed that treatment with exogenous BMP4 increased the number of primary myotubes [Krüger et al., 2001].

These experiments suggest a regulatory hierarchy where Shh up-regulates *bmp4* and together they support the activation of the myogenic program towards the formation of primary myotubes in the hind limb. The primary muscle fibers express two contractile fiber types: fast embryonic myosin heavy chain (eMyHC) and slow MyHCβ. The regulatory circuitry at this point, from approximately E11.0 to E13.5, is centered around activation of the myogenic program and differentiation of embryonic myoblasts to primary myofibers with specific contractile properties (Figure 1.3).

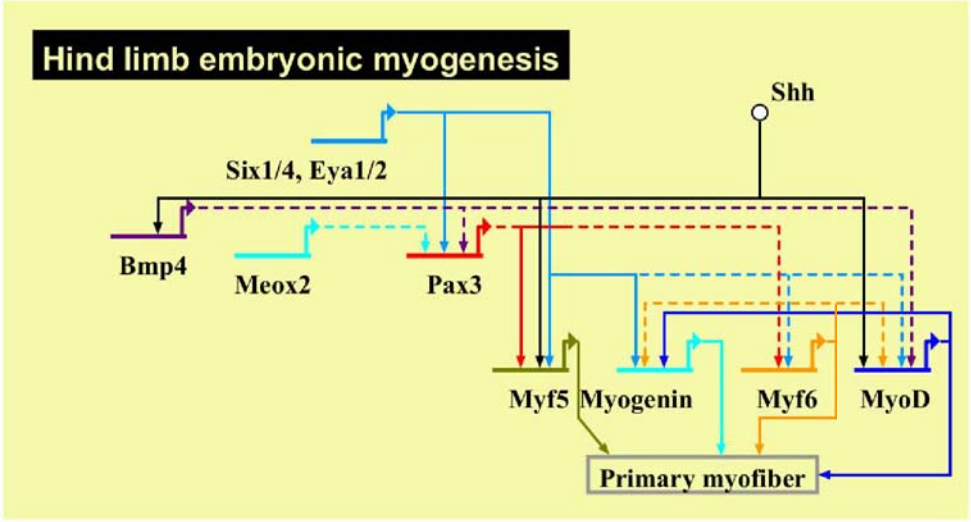

Figure 1.3: Embryonic Myogenesis. Once in the limb bud embryonic myoblasts activate the myogenic program. The white circle represents a signaling protein, Shh, acting to activate its target genes via signaling. The end result of this regulatory subcircuit is the primary myofiber. Solid lines indicate a direct *cis* interaction and dotted lines indicate an indirect interaction.

Fetal myoblasts which differentiate into secondary myotubes or myofibers during fetal development (E14.5-E17.5), follow a similar regulatory circuitry in terms of the deployment of MRFs along with their regulatory co-factors (e.g. E-proteins, PBX/Meis and Mef2C). Together the MRFs and co-factors initiate the myogenic program in fetal

myoblasts. However, *pax7*, as opposed to *pax3*, now helps to drive the differentiation regulatory program towards secondary myofiber formation [Hutcheson et al., 2009b]. *pax7* activates the myogenic program via *myoD* [Relaix et al., 2006]. *myf5* activates the myogenic program independently of *pax7*. This is in contrast to the regulatory dynamic during embryonic myogenesis, where *pax3* regulated *myf5* and *myf6*, but not *myoD* (Figure 1.3). It has been postulated that the regulatory program of fetal myoblasts is held at bay during the embryonic phase of muscle differentiation by signaling molecules, such as transforming growth factor beta (TGFβ) or β-catenin, which inhibit fetal myoblasts from differentiating, but not embryonic myoblasts during embryonic myogenesis [Cusella-De Angelis et al., 1994, Hutcheson et al., 2009a]. Secondary myofibers of the hind limb express eMyHC and perinatal MyHC. As is the case with primary myofibers, the contractile properties of the secondary myofibers at this point, as determined by the expression of different types of MyHC, occurs independently of nerve input. This suggests that the metabolic properties of the developing muscle fibers are encoded in the regulatory genome and, thus, potentially accessible to GRN analysis and discovery (Figure 1.4).

Satellite cells begin to appear midway through the fetal development phase. They take their place between the basal lamina and the developing myofibers and activate their myogenic program at this time. The regulatory circuitry of satellite cells of the hind limb is as Figure 1.4. They are *pax7* positive and activate *myoD* to initiate myogenesis. As with fetal myoblasts, TGFβ is implicated in maintaining satellite cells in the proliferative state at the start of fetal myogenesis. A possible explanation as to why they do not begin to differentiate in parallel with fetal myoblasts is that they possess a sensitivity to a different set of inhibitors of differentiation than fetal myoblasts. Platelet derived growth factor (PDGF) was found to function in this manner during muscle development in chick [Yablonka-Reuveni and Seifert, 1993]. Once differentiated, satellite cells contribute significantly to the future adult myofiber population until the late post natal period when skeletal muscle development is complete[Zhang et al., 1998]. Once in adult muscle, satellite cells are quiescent. Quiescent satellite

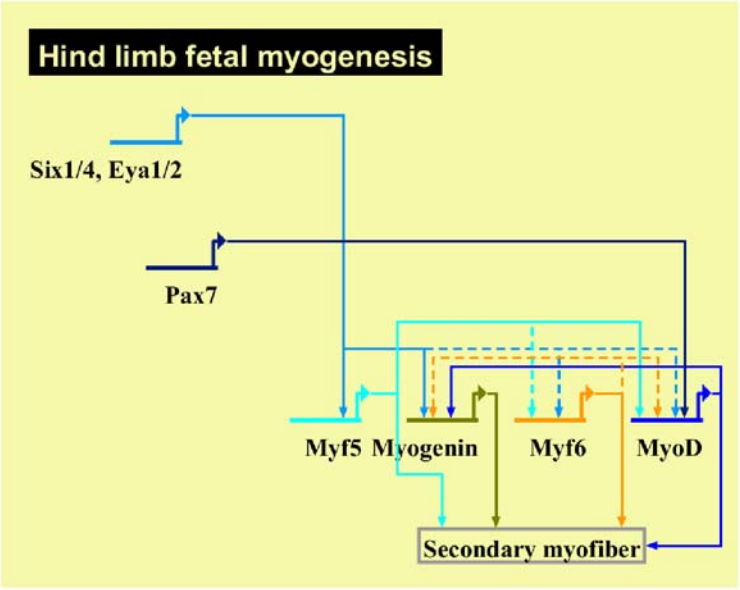

Figure 1.4: Fetal Myogenesis. Pax7 now guides the myogenic program towards secondary myofiber formation via myoD. Myf5 can also activate the myogenic program indepently of Pax7. The Six/Eya transcriptional complex directly regulates Myf5. This is also the regulatory circuitry used by satellite cells once they activate the myogenic program midway through the fetal development stage. Solid lines indicate a direct *cis* interaction and dotted lines indicate an indirect interaction.

cells remain *pax7* positive, but no longer express *myoD*. Interestingly, *pax7* loss of function studies have demonstrated that Pax7 is only required to activate the myogenic program via *myoD* up to post natal day 21.0. After day 21.0, satellite cells are still able to activate the myogenic program in the absence of *pax7* [Lepper et al., 2009]. The regulatory molecules responsible for activating the myogenic program of satellite cells after 21.0 days of post natal development have not been identified, but possible candidates include the Six family and, depending on the stimulus for regeneration of muscle, possibly direct-acting cytokines or hormones that up-regulate *myf5*, *myf6*, or *myoD*. By this time in skeletal muscle development, the regulatory circuitry has elegantly directed waves of proliferation and differentiation programs in embryonic, fetal, and satellite progenitor cells, respectively. Now that the skeletal muscle bundle is structurally and metabolically enabled, and its future regenerative capacity, via satellite cells, secured; innervation of the muscle bundle provides the major regulatory input to further advance the functional capacity of mammalian skeletal muscle.

1.2.3 Regulatory circuitry of adult hind limb muscle

Peri and post natal development is characterized by a down-regulation of the myogenic program and establishment of fiber-type specificity. The latter is driven by innervating slow and fast firing motor neurons. The MRFs, with the exception of *myoD*, are down-regulated, since further differentiation is what is called for at this stage and not further proliferation of progenitor cells. Msy3 and its co-binding factor, Pbx, along with Daschund 2 (Dach2) directly work to repress *myogenin* in innervated skeletal muscle [Berghella et al., 2008, Tang and Goldman, 2006]. *myoD* is expressed at a low level in innervated muscle, regulated in part by the Six/Eya complex [Laclef et al., 2003] (Figure 1.5). The slow and fast firing motor neurons that innervate the muscle fibers during this developmental phase, assist in stimulating the replacement of embryonic and fetal isoforms of the MyHC contractile proteins with the adult isoforms. In rodents, the major MyHC fiber-types of fast-twitch muscle are: IIA, IIX/D, and IIB

[Zhang et al., 1998, Schiaffino and Reggiani, 1994]. TypeIIA is the slowest fiber-type in fast-twitch muscle and IIB is the fastest. They are characterized by oxidative and glycolytic metabolism, respectively. Metabolic enzymes associated with glycolytic metabolism include phospho-fructo kinase (Pfk) and muscle specific enolase (Mse) (Figure 1.5). These enzymes are first expressed in secondary myofibers [Barbieri et al., 1990]. The Six/Eya transcriptional complex positively regulates the fast-type transcritional program [Grifone et al., 2004, Richard et al., 2011]. The neuronal input is conveyed to the transcriptional machinery of the muscle via calcium-dependent signaling following excitation-contraction coupling. Hdac4 is a key molecule connecting nerve activity to muscle transcription, as will be discussed in the next section [Cohen et al., 2007]. In an innervated muscle, calcium influx activates calcium-dependent kinases, which phosphorylate Hdac4 and send it out of the nucleus [McKinsey et al., 2002, Liu et al., 2005] (Figure 1.5). In addition to influencing fiber-type, innervation also maintains muscle mass and plays an important role in forming the neuromuscular junction in adult muscle. The latter we will discuss in further detail below and in Chapter 3.

1.2.4 Regulatory circuitry of denervation response in adult fast-twitch hind limb muscle

Upon denervation of fast-twitch muscles (i.e. MyHCIIB dominant) of the hind limb, calcium influx into the muscle fibers decreases and Hdac4 gets dephosphorylated and shuttled to the nucleus. Once in the nucleus, Hdac4 and its co-factor, Mef2, helps to set in motion a series of regulatory events that characterize the first 7.0 days following denervation, which I will refer to henceforth as the *early denervation* response (Figure 1.6). Hdac4/Mef2 functions to repress *pfk*, *mse*, and *myhcIIB* transcripts, which in turn represses the glycolytic and fast-twitch characteristics of the muscle bundle, respectively. This results in the muscle assuming the metabolic characteristic of the remaining fiber-types, such as MyHCIIA in Figure 1.6. This is indeed indicative of

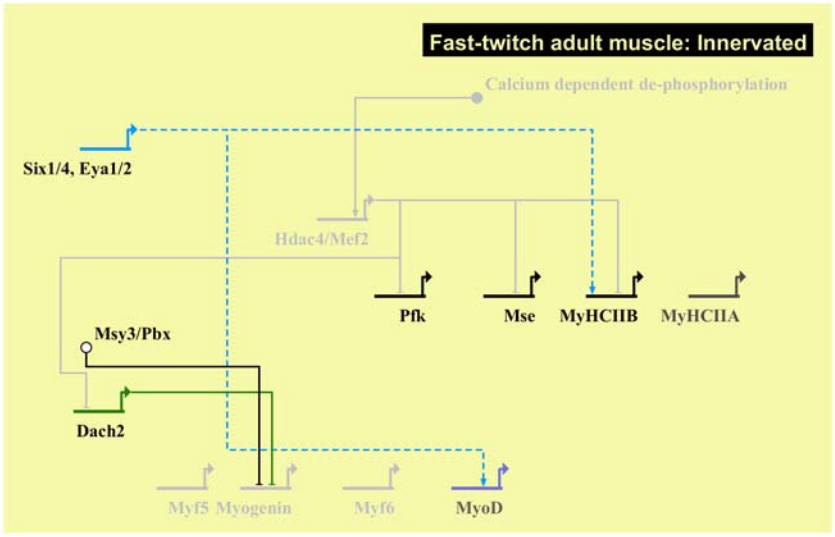

Figure 1.5: Adult fast-twitch innervated muscle is characterized by inactivity of the myogenic program and robust expression of *myhcIIB* (i.e. fast-twitch fiber-type) and *pfk* and *mse* (i.e. glycolytic enzymes). This regulatory state is influenced strongly by nerve input. All gene names in bold text represent actively expressed genes. The Six1/4,Eya1/2 transcriptional complex contributes to the robust expression level of *myhcIIB* and also to low-level *myoD* expression. Dach2 and Msy3/Pbx contribute to down-regulation of *myogenin* in innervated muscle. *myhcIIA* and *myoD* are colored in an intermediate shade to indicate low to intermediate levels of expression for these two genes in innervated muscle. The calcium influx in innervated muscle fibers maintains Hdac4 phosphorylated and in the cytoplasm (i.e. not able to regulate its denervation-associated target genes). Solid lines indicate a direct *cis* interaction and dotted lines indicate an indirect interaction. Satellite cells are quiescent during this state and only become activated following a trauma or other degenerative stimulus that requires muscle regeneration.

a fast-twitch transcriptional program driven by fast-firing motor neurons. *runx1* is activated following denervation and functions to sustain transcription of *mychIIA*, an aforementioned slow-type contractile protein; keratin-type1 cytoskeletal 18 (*krt1-18*), which links sarcomeric Z-lines with M-lines; and acetylcholine receptor subunit gamma (*chrng*), which is a subunit previously only expressed in pre-innervated late fetal and post natal muscle [Wang et al., 2005, Ursitti et al., 2004]. By acting in this manner, *runx1* functions to maintain muscle fiber structural integrity and possible re-innervation capacity in the fibers that remain. Also, as can be appreciated in Figure 1.6, by repressing *dach2*, Hdac4/Mef2 de-represses *myogenin* and indirectly activates all of the target genes of *myogenin* [Tang et al., 2009]. These target genes include *myoD*, which inturn activates itself and *myogenin* [Berkes et al., 2004]; *fbxo32* and *trim63*, which are both E3-ubiquitin ligases that are responsible for the protein degradation events that characterize neurogenic atrophy [Bodine et al., 2001, Moresi et al., 2010]; the acetylcholine subunit receptor genes alpha (*chrna*), gamma (*chrng*), and delta (*chrnd*) [Burden, 1977b]; and muscle specific kinase (*musk*). These four genes at the bottom right corner of Figure 1.6 represent components of the regulatory subcircuit of the developing neuromuscular junction, last activated during peri and post natal development [Burden, 1977b, Mazhar and Herbst, 2012].

Comparison of the different regulatory networks governing myogenesis, not only at different anatomical regions, but during the different phases of skeletal muscle development in cells of the same region, indicates an elegant regulatory design that to date is not well understood. A dedicated approach to functional testing of *cis*-acting regulatory sequences for key regulatory molecules is needed to interweave the current knowledge pertaining to the many GRNs governing skeletal muscle biology during development and during physiological response in the adult. In the present study we will introduce an stable, efficient, cost effective, short time to assay and biologically relevant gene transfer technique for functional testing of *cis*-acting regulatory sequences. We will focus on *myogenin* and its transcriptional down-regulation during the late phase of the neurogenic atrophy response.

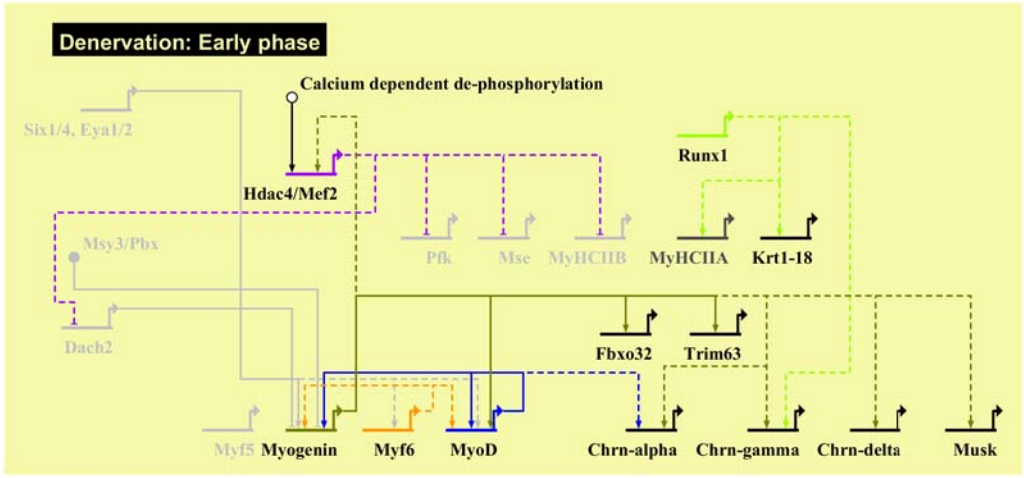

Figure 1.6: Denervation response of adult skeletal muscle out to 3.0 days after denervation (i.e. early phase). A decrease in intracellular calcium results in the dephosphorylation of Hdac4 and it gets shuttled into the nucleus to repress and activate many regulatory subcircuits including metabolic, neuromuscular junction, and neurogenic atrophy programs (see text). Solid lines indicate a direct *cis* interaction and dotted lines indicate an indirect interaction.

Chapter 2

Functional testing of the *myogenin*-highly conserved *cis*-acting element (HCE) during late phase neurogenic atrophy using a new model for functional *cis*-regulatory analysis *in vivo*

2.1 Introduction

Following denervation, fast-twitch skeletal muscles undergo a shift in their transcriptional program which results in a switch to slow-twitch dominant muscle fibers, oxidative vs. glycolytic metabolism, activation of MRFs, and neurogenic atrophy [Tang et al., 2009]. *myogenin* is a key MRF that drives the neurogenic atrophy-response in denervated muscle by directly activating *fbxo32* and *trim63*, the E3 ubiquitin ligases responsible for the protein degradation that characterizes atrophied muscle [Bodine et al., 2001, Moresi et al., 2010]. Figure 1.6 summarizes the transcritptional events of the early denervation response. However, while there is a rapid up-regulation of *myogenin* and, subsequently, of *fbxo32* and *trim63* in the first 3.0 days following denervation, the transcriptional expression of *myogenin*, *fbxo32*, and *trim63* actually

begins to decreases after peak expression at 3.0 days ([Moresi et al., 2010] and our own data). We describe the first 3.0 days after denervation as *early phase* neurogenic atrophy and the time period after 3.0 days as *late phase* neurogenic atrophy. In innervated muscle, the Msy3/Pbx complex along with Dach2 have been shown to repress *myogenin* [Berghella et al., 2008, Cohen et al., 2007] (Figure 1.5). We sought to test whether the *myogenin*-highly conserved *cis*-acting element (HCE) site was responsible for the down regulation of *myogenin* at time points greater than 7.0 days after denervation. In addition, we denervated the hind limb of $msy3^{-/-}$ and $msy3^{-/-}$ mice to confirm that Msy3 is acting in *trans* to down-regulate *myogenin* during late phase neurogenic atrophy.

We functionally test the *myogenin*-HCE utilizing a dedicated approach to uncovering the GRNs underlying the physiological response to nerve injury in adult mouse skeletal muscle. First, we overcome the confounding tissue trauma incurred by existing gene transfer techniques into adult skeletal muscle. We accomplish this by utilizing a minimally-invasive electroporation method to transfect the flexor digitorum brevis (FDB) and interosseus (IO) muscles [DiFranco et al., 2009]. FDB and IO, like most classically studied muscles of adult mouse, are fast-twitch muscle fibers. As discussed previously, their anatomical size and location make these muscles an ideal model system for both physiological and molecular level investigations. Second, we demonstrate robust and quantifiable gene transfer of both plasmid (approximately 5 kbp to 11 kbp) and BAC DNA (approximately 140 kbp to 240 kbp) reporter vectors to test candidate *cis*-regulatory DNA sequences. The ability to use BAC reporter DNA constructs for *in vivo* functional *cis*-regulatory analysis in adult skeletal muscle increases (by >100-fold) the potential for capturing *cis*-acting regulatory events. Another advantage of our skeletal muscle nerve injury model is that the time from gene transfer to muscle assay is only two weeks; an improvement in time-to-assay on the order of months, compared to transgenesis. While this study describes a means for elucidating GRNs underlying the response of skeletal muscle to nerve injury, our approach can also be applied to any adult mouse muscle disease model.

2.2 Results

2.2.1 Gene transfer of plasmid and BAC DNA towards functional testing of *cis*-regulatory modules

For plasmid DNA experiments, we utilized a previously validated functional CRM of the myogenin gene from our laboratory to drive a fluorescent reporter in FDB and IO muscles of 2.0 to 4.0-month-old C57bl/6 mice [Berghella et al., 2008]. We observed reproducible reporter gene signal across technical and biological replicates as determined by QRT-PCR; robust signal as early as 5.0 days status post gene transfer and extending out to at least 270 days; and transfection efficiency of 65 % (Figure 2.1A and 2.1B).

Co-transfection, at different ratios of DNA, of a CRM-driven reporter construct with a constitutively active promoter-driven reporter construct produced robust signals proportional to the ratio of transfected DNA (Figure 2.2).

For the BAC DNA experiments, we re-combineered reporter DNA sequences into the first exon of the myosin binding protein H (*mybph*) and *myogenin* genes [Warming et al., 2005]. BAC DNA was linearized prior to transfection into FDB and IO muscles. Strong signal was observed at 5.0 days status post transfection, compared to controls (Figure 2.3A and 2.3B). Co-transfection of BAC DNA with plasmid DNA resulted in strong signal from both constructs, yet in accordance to molar equivalent amounts of transfected DNA (Figure 2.3C and 2.3D). The capacity of our gene transfer method to co-transfect experimental and transfection control reporter plasmids and BACs in a reliable, reproducible, and efficient manner is absolutely essential for qualitative and quantitative measurements of candidate CRM or CRE activity.

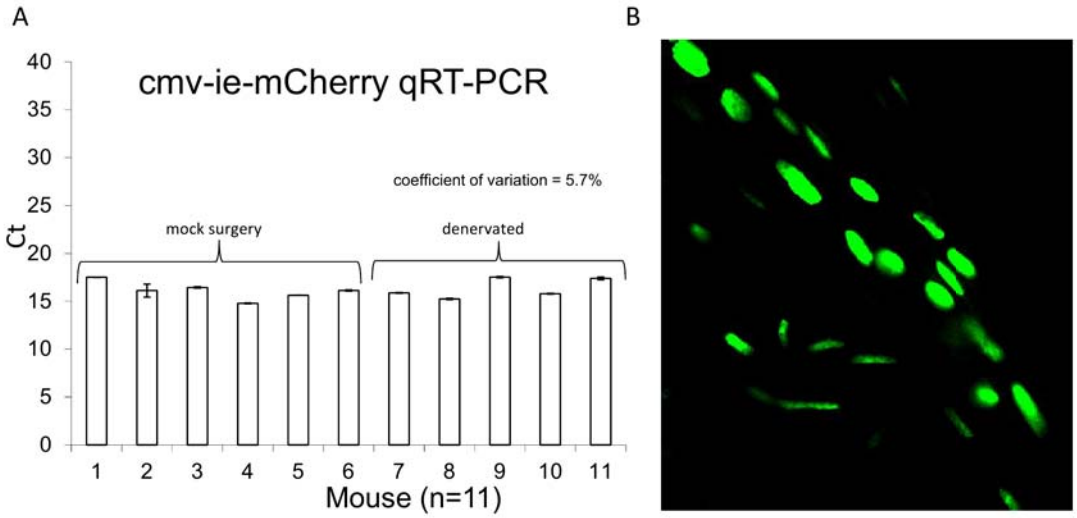

Figure 2.1: Reproducible, stable, and efficient gene transfer. (A) cmv-ie-driven mCherry reporter plasmid (15.0 µg) was transfected into FDB and IO and total RNA harvested at 14.0 days. Six mice underwent mock denervation surgery and five mice underwent sciatic nerve ressection. Ct (crossing threshold) is consistent across biological replicates. (B) Confocal image of FDB expression of functional CRM of myogenin-driven-H2B-Egfp plasmid (20.0 µg) at 22.0 days after gene transfer. Similar results have been obtained out to 270 days (data not shown). 40x oil immersion objective Confocal image. Transfection efficiency was 65 % as determined by the ratio of cmv-ie-H2B-mCherry nuclei to total number of DAPI stained nuclei (data not shown).

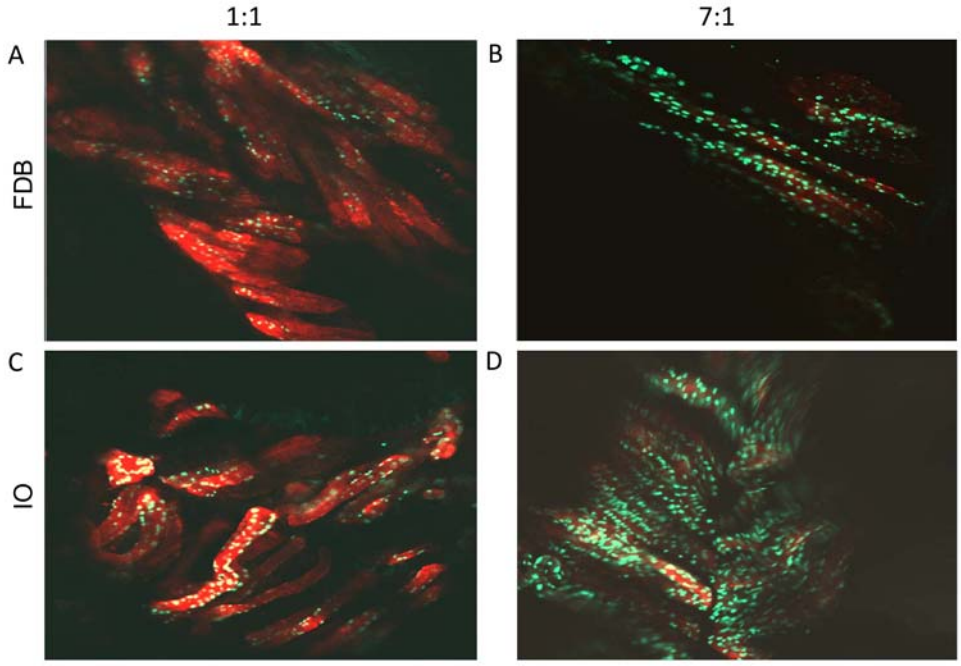

Figure 2.2: Co-transfection of plasmid DNA. FDB and IO were co-transfected with the functional CRM of myogenin-driven-H2B-Egfp plasmid and cmv-ie-membrane-mCherry. (A, C) 7.5 µg of each construct transfected. (B, D) Co-transfection with 7.5 µg of the functional CRM of myogenin-H2B-Egfp and 1.0 µg of cmv-ie-mCherry. At five days post gene transfer, signal intensity for each reporter pair is consistent with ratio amount of DNA transfected. 10x objective Confocal images.

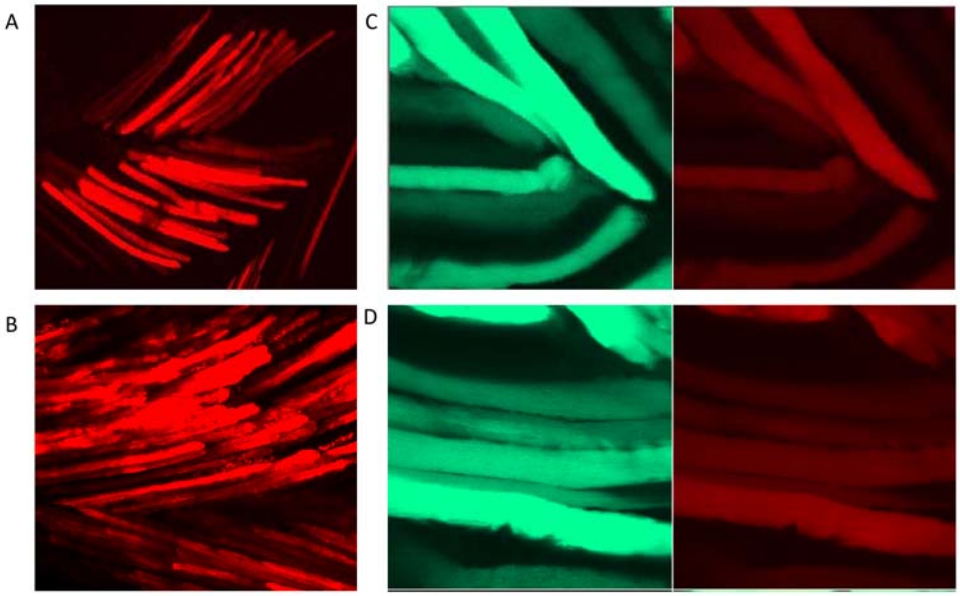

Figure 2.3: BAC gene transfer and BAC with plasmid DNA Co-transfection. (A) linearized *mybph*-mCherry reporter BAC (70.0 µg, 140 kbp). Compare to cmv-ie-driven membraneCherry reporter plasmid DNA (7.5 µg, 6.0 kbp) in (B). 10x Confocal image. (C,D) linearized *mybph*-mCherry BAC (60.0 µg), co-transfected with cmv-Egfp plasmid DNA (15.0 µg). 40x Confocal image. All images feature FDB.

2.2.2 Testing the myogenin-highly conserved *cis*-regulatory element (HCE) for regulatory activity at 10.0 days following denervation

We cloned the 1.1 kbp mutated and wild-type CRM of *myogenin* from Berghella et al. [2008] into a pCDNA (Invitrogen, Life Technologies) vector backbone containing a cytoplasmic EGFP reporter. We utilized a cmv-ie-mCherry (gift from Periklis Pantazis) plasmid as a transfection control. FDB and IO muscles (n=8.0 mice, 4.0 each per wild-type and mutant *myogenin* 1.1 kbp construct: 2.0 mice for mock surgery and 2.0 mice for denervation surgery) were co-transfected with 30.0 µg of wild-type or mutant construct and 15.0 µg of the transfection control construct. Seven days following transfection, we performed either mock surgery or denervation surgery; muscles were harvested ten days after surgical procedures (see Methods). Moresi et al. [2010] have reported that *myogenin* levels decrease by 3-fold in fast-twitch muscles beginning at 7.0 days after denervation, from their peak levels at 3.0 days. If the *myogenin*-HCE is required for the down-regulation of *myogenin*, then at 10.0days we should observe a difference between the wild-type and mutant *myogenin* reporter constructs in denervated muscles. Figure 2.4B and 2.4C-bottom panels, demonstrates this result qualitatively and 2.4D quantifies the mean reporter signal intensity as a 2.4-fold difference between the wild-type and mutant *myogenin* reporter constructs in denervated muscles.

The signal from the wild-type *myogenin* construct is similar in both mock surgery muscles (i.e. sciatic nerve intact) and denervated muscles (Figure 2.4B and 2.4D). This result is expected if the regulatory state of the fast-twitch FDB and IO muscles at 10.0days following denervation, is as demonstrated in the fast-twitch gastrocnemius and plantaris muscles of Moresi et al. [2010]. In this case, the wild-type *myogenin* construct from denervated muscle is down-regulated as is the case for endogenous *myogenin* after 7.0days. This signal level from the mutant *myogenin* construct of mock surgery muscles is similar to that from the wild type *myogenin* construct. Berghella

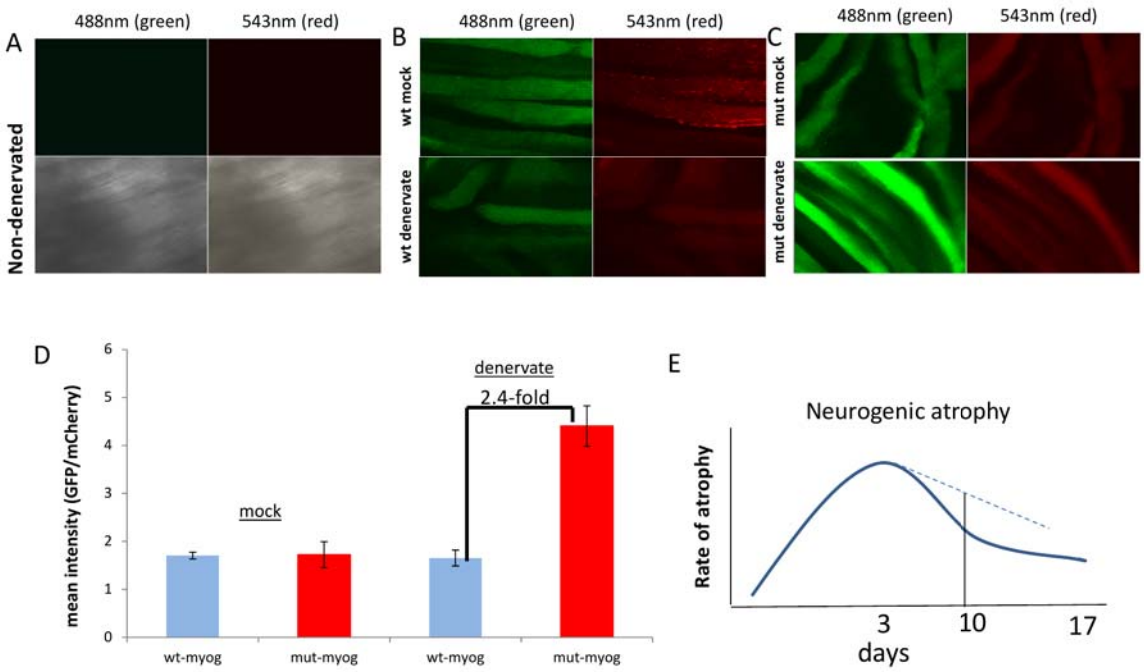

Figure 2.4: Functional testing of *myogenin*-HCE at 10.0days following denervation. (A) Contralateral non-denervated control. Non-transfected FDB from the contralateral paw, subjected to 488nm and 543nm lasers (top row: green and red channels; bottom row: phase images). (B) wild type (wt) *myogenin*-HCE-Egfp construct in mock denervated and denervated FDB. (C) mutant (mut) *myogenin*-HCE-Egfp construct in mock denervated and denervated FDB. In all conditions, 30.0 µg of wt or mut *myogenin*-HCE-Egfp reporter plasmid DNA was co-transfected with 15.0 µg of cmv-ie-mCherry reporter plasmid DNA. (D) Ratio of mean intensity signal from Egfp/mCherry reporters. A 2.4-fold up-regulation is noted with the mutant *myogenin*-HCE construct in denervated muscle compared to the wild type *myogenin*-HCE construct. (E) Schematic of neurogenic atrophy rate. Blue line represents normal rise and fall in rate of atrophy and dotted line represents effect of continued *myogenic* expression on rate of atrophy at 10.0 days. n = 2 mice per condition. 40x Confocal images of FDB muscle featured above. ImageJ software utilized to analyze reporter signal from FDB and IO. 10.0 z-stacks analyzed per animal.

et al. [2008], demonstrated an increased signal from the mutant *myogenin* construct in innervated muscle when compared to the wild type *myogenin* construct. This discrepancy can be due to the fact that their result was obtained from a transgenic mouse, with more regulatory sequence present to impart a regulatory effect. Also, their data was from a 3.0 day denervated time point, when *myogenin* expression levels are at their peak ([Moresi et al., 2010] and our own data) and thus subject to a different regulatory state than our reporter constructs. Undoubtedly, we require a finer temporal profile for endogenous *myogenin* and reporter construct data in FDB and IO to de-convolve our current results.

2.2.3 Denervation of of hind limb in the absence of Msy3 at 17.0 days after denervation

During this time, we also set out to determine if Msy3 is required, in *trans*, to down regulate *myogenin* at time points greater than 7.0 days after denervation. Specifically, neurogenic atrophy, which is mediated by *myogenin*, plateaus by 17.0 days after denervation in tibialis anterior (L. Berghella, personal communication). We denervated $msy3^{-/-}$ and $msy3^{-/-}$ mice and harvested tibialis anterior muscles at 17.0 days. We then measured the endogenous levels of *myogenin*, *myoD*, and *fbxo32* (a.k.a. atrogin-1) for each genotype (Figure 2.5).

This data confirms that Msy3 is required for the down-regulation of *myogenin* at 17.0 days following denervation. *myoD* has a candidate Msy3 site located 35 kbp upstream of its coding region and may also require Msy3 for down-regulation of its transcript at time points greater than 7.0 days after denervation [Berghella et al., 2008, Moresi et al., 2010]. The continued up-regulation of *fbxo32* is in accordance with it being a regulatory target of *myogenin* [Moresi et al., 2010]. Since *fbxo32* is a known mediator of skeletal muscle atrophy, then we would expect that we would also see a continued atrophy phenotype in the denervated muscles. Morphometric analysis on cross-sectioned muscle tissue from denervated $msy3^{-/-}$ and $msy3^{+/-}$ mice

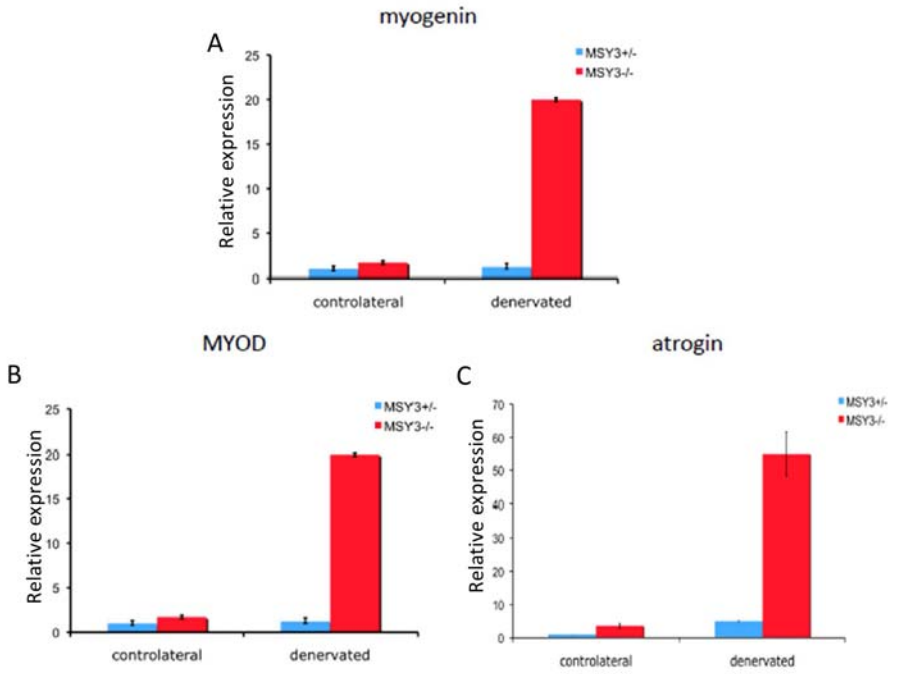

Figure 2.5: Endogenous gene expression at 17.0 days after denervation in $msy3^{-/-}$ and $msy3^{+/-}$ mice. (A) *myogenin*. (B) *myoD*. (C) *atrogin* (a.k.a. *fbxo32*). Columns represent relative expression levels normalized to *gapdh*. Contralateral non-denervated leg was used as control. In the absence of Msy3, endogenous *myogenin*, *myoD*, and *atrogin* levels remain elevated. n = 3. Data from tibialis anterior muscle.

revealed more progression of the atrophy phenotype (i.e. smaller diameter fibers) in the *msy3*$^{-/-}$ mice than in the *msy3*$^{+/-}$ mice (Figure 2.6).

These results identify the Msy3 protein as the *trans*-acting factor necessary for down-regulation of *myogenin* at 17.0 days after denervation. Our gene transfer experiment assayed at 10.0 days, provides evidence that the *myogenin*HCE site is the *cis*-acting regulatory partner for Msy3. Together they mediate the down-regulation of *myogenin* that is necessary to mediate the neurogenic skeletal muscle atrophy response. If either of the regulatory pair is absent, *myogenin* continues to be expressed and, by default, the regulatory effect on its target genes also continues resulting in a prolonged neurogenic atrophy regulatory state.

2.3 Discussion

Our ability to define the Gene Regulatory Networks (GRNs) underlying physiological events in adult skeletal muscle *in vivo* has been limited by the shortage of efficient and reliable experimental modalities in the muscles studied to date. In the case of nerve injury studies, many key differentially expressed genes have been identified and protein level interactions characterized via descriptive studies, but relatively few studies attempt to understand the *cis*-regulatory architecture encoding the expression of these denervation-associated genes [Berghella et al., 2008]. One of the most significant obstacles to understanding how GRNs govern physiological events in adult skeletal muscle has been the lack of an efficient, robust, and reproducible method for gene transfer *in vivo*. Transgenesis has proven to be the most effective method for *in vivo*validation of *cis*-regulatory sequences in mouse, but making a transgenic mouse is costly and suffers from significant time-to-discovery as well as a limited scope, since only one or two regulatory sequences can be studied at a time.

In this study, we lay the foundation for the discovery of GRNs in adult skeletal muscle following nerve injury. We propose flexor digitorum brevis (FDB) and interosseous

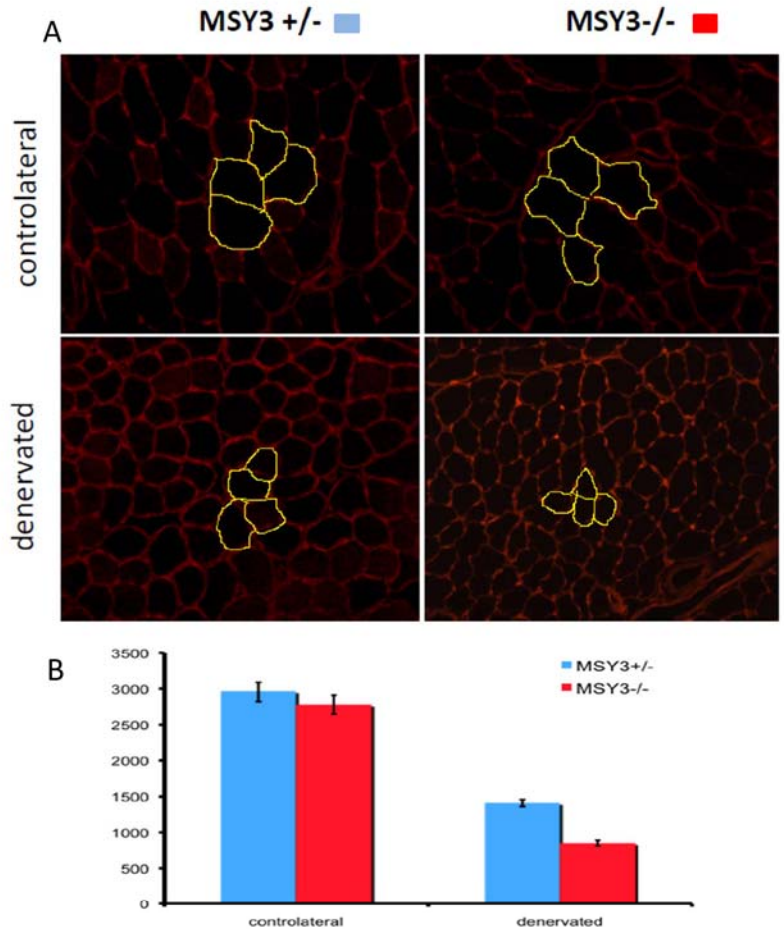

Figure 2.6: Increased neurogenic atrophy in denervated $msy3^{-/-}$ mice at 17.0 days. (A) Cross-section of contralateral non-denervated control and denervated muscle in $msy3^{-/-}$ and $msy3^{+/-}$ mice. Individual muscle fibers bordered by immuno-stain for laminin. Yellow outline of individual fibers in cross section superimposed to assist visualization. After 17.0 days of denervation, the overall diameter of each muscle fiber in denervated $msy3^{-/-}$ mice is smaller than in denervated $msy3^{+/-}$ mice 17.0 days after denervation. (B) Morphometric analysis of fibers in (A), measuring overall diameter size of each fiber for contralateral non-denervated control and denervated muscle from each mouse genotype. $msy3^{+/-}$ = blue and $msy3^{-/-}$ = red. n=2. Data from tibialis anterior muscle.

(IO) muscles as an ideal 'model system' for functional *cis*-regulatory analysis of candidate GRN target genes. The FDB/IO muscle fibers are fast-twitch, as are the classically studied muscles of the adult mouse denervation paradigm. Thus, the findings of prior studies are directly applicable and can be used to refine future *cis*-regulatory and perturbation studies in FDB and IO. Similarly, many excitability and excitation-contraction studies are now focusing on FDB and IO [Friedrich et al., 1999, DiFranco and Vergara, 2011], laying the foundation for a comprehensive knowledge-base for adult mouse fast-twitch muscle fibers in the coming years.

We adapted, extended, and further characterized the minimally-invasive, highly-efficient gene transfer method of DiFranco et al. [2009] to include functional *cis*-regulatory analysis and co-transfection of both plasmid and BAC DNA. The minimally-invasive technique avoids the confounding trauma associated with gene transfer into the larger muscles of the lower hind limb. In addition, the physical dimensions of the FDB and IO muscles and the plantar compartment of the mouse paw are ideal for complete coverage with DNA in solution and for relatively uniform passage of electrical current down the length of entire muscle bundles. Using this method, we achieve a sufficiently robust and stable transfection efficiency to enable both image-based and QRT-PCR quantification of reporter signal. We applied our method to discover a possible direct causal regulatory role for Msy3 and the HCE of *myogenin* in the context of regulating the late neurogenic atrophy response. Specifically, mutating the *myogenin*-HCE resulted in up-regulation of reporter signal compared to the wild-type HCE sequence at ten days following denervation. Increased expression of *myogenin* has been implicated in initiating the neurogenic atrophy response in skeletal muscle following denervation. However, this atrophy response begins to wane after approximately seven days. In our assay, the reporter signal driven by the mutated HCE remained strong following denervation at 10.0days. Msy3 is thought to bind the HCE site in innervated muscle [Berghella et al., 2008]. When endogenous *myogenin* expression was assayed 17.0 days following denervation in $msy3^{-/-}$ mice, transcript levels were up-regulated compared to $msy3^{+/-}$ mice, reinforcing the result of our gene

transfer assay, and providing evidence that the down-regulation of *myogenin* in the weeks following denervation is mediated by the interaction of Msy3 and the HCE site. The increased levels of endogenous *myoD* and the fact that there is an Msy3 site located 35 kbp upstream of its coding region makes *myoD* a candidate for regulation by Msy3. This *myoD* site can also be tested in our gene transfer assay.

The use of BAC DNA for transient, yet stable, gene transfer towards *in vivo* functional *cis*-regulatory analysis was not previously possible in adult mouse skeletal muscle and provides several advantages. First, BAC DNA allows testing for *cis*-regulatory activity in a more biologically relevant chromosomal environment (i.e. approximately 100-fold more intragenic DNA than with plasmid DNA). BAC versions of the *myogenin* constructs utilized in our preliminary experiments can aid in resolving our current results in this manner. Second, by utilizing BAC re-combineering techniques, functionally validated *cis* Regulatory Modules (CRMs) or *cis* Regulatory Elements (CREs) can be perturbed singly and in combination, to further resolve the underlying *cis*-regulatory architecture. The relatively short time-to-assay of this gene transfer method, in combination with the aforementioned advantages, brings functional *cis* regulatory analysis in adult skeletal muscle closer to the cutting-edge GRN bioscience modalities of the 21^{st} century. This same gene transfer technique may now be used with other modern GRN molecular tools for CRM testing, including CRM-bar coded sequence tags [Nam et al., 2010] or trans-acting molecules, such as mRNA silencing constructs. While this study describes a means for elucidating the GRNs underlying the skeletal muscle response to nerve injury, the approach can also be applied to any adult mouse muscle physiological response or disease model.

2.4 Materials and Methods

2.4.1 *Plasmid and BAC DNA constructs*

Plasmid DNA Egfp reporter constructs were made by cloning out the 1.1 kbp *myogenin* HCE sequence from the pFMYOwt*Lac*Z and pFMYOmut*Lac*Z from [Berghella et al., 2008] and inserting into pCDNA vector containing an EGFP reporter. The 1.1 kbp *myogenin* regulatory sequence had the 17.0 bp sequence of the HCE scrambled compared to wild-type. A Hpa1 restriction site was included in the scrambled sequence to allow for distinguishing from wild-type construct upon cloning verification. The cmv-ie-mCherry transfection control plasmid was generated by cloning out the membrane localization sequence from the parent pCS-cmv-ie-membrane-mCherry plasmid (a gift from Periklis Pantazis). The removal of the membrane localizing sequence to generate cmv-ie-mCherry was sequence verified by Laragen, Inc. BAC containing *myogenin* and BAC containing *mybph* were ordered from Childrens Hosptial Research Institute, Oakland, Ca. Reporter constructs for mCherry and Egfp (a gift from Julie Hahn). Re-combineering of reporters into BAC DNA was conducted as per protocol by [Warming et al., 2005]. In all cases of gene transfer into biological replicates, the experimental CRM-driven Egfp reporter was mixed with the transfection control mCherry reporter and the mixture injected into all biological replicates.

2.4.2 *Gene transfer*

The left hind limb was used for all experimental samples. A solution containing 2.0 mg/ml hyaluronidase in sterile Tyrode is prepared. Using an anesthetizing box, mouse is deeply anesthetized using 2.0 % isoflurane in oxygen with an approved gas anesthetic machine. Animal placed on a heating pad (37C) and anesthesia maintained using a rodent face mask. Anesthetic depth monitored by toe pinch reflex. Under observation with a dissection microscope, hyaluronidase injected, 10.0 µL of (2.0mg/ml), under the

footpads of left paw of the mouse using a 1.0 inch long 33.0 gauge sterile needle. Skin penetrated at a point close to the heel of the foot and needle advanced subcutaneously towards the base of the toes, care taken not to advance needle through the epidermal layer. Anesthesia discontinued and mouse placed in a recovery cage and allowed to fully recover from anesthesia. After one hour, animal anesthetized for a second time and placed on heating pad. Following the same procedure described for the hyaluronidase solution, I injected a total of 45.0 µg for co-transfection of plasmid DNA or 60.0 µg to 70.0 µg of BAC DNA. The total injection volume should be less than 25.0 µL per foot. When 25.0 µL is necessary, it is advisable to close the skin at the needle entry point with tissue glue. Once DNA was injected, anesthesia discontinued and mouse placed in a recovery cage and allowed to fully recover from anesthesia. After 10-15 min animal anesthetized for the third time and placed on heating pad. One acupuncture needle placed under the skin at heel, and a second one at the base of the toes. Electrodes are oriented parallel to each other and perpendicular to the long axis of the foot. The head of the needles (electrodes) were connected to the electrical stimulator using micro-clip connectors. Muscles electroporated by applying 20 pulses, 20 ms in duration each, at 1Hz. Depending on the spacing of the electrodes, it may be necessary to adjust the voltage amplitude of the pulses (by monitoring with an oscilloscope) to yield an electric field of 80 V/cm. No contractions in response to the stimuli should be observed if the level of anesthesia is adequate. Mouse placed in a recovery cage and allowed to fully recover from anesthesia. If the procedure went normally, the animal should regain full mobility within 10 minutes. The injections of hyaluronidase and DNA in the footpads do not have noticeable adverse effects on the animals. Once recovered from anesthesia,mice are able to ambulate normally around the cage.

2.4.3 *Sciatic nerve denervation and mock denervation surgery*

7.0 days after gene transfer, mouse is deeply anesthetized using 2.0 % isoflurane in oxygen with an approved gas anesthetic machine. The animal is placed on a heating pad (37C)) and prepared for surgery in accordance with IACUC survival surgery protocol. An 0.5cm incision is made under observation with a dissection microscope. For both mock denervated and denervated animals, blunt dissection between muscle planes is conducted until the sciatic nerve is exposed. It is important to not physically disturb the sciatic nerve in the mock denervated animals, as any traction on the nerve can injure the nerve. At this point, the skin incision in the mock surgery animals is closed with suture and glue and 0.5mg/kg buprenorphine is injected subcutaneously for pain prevention before the animal wakes from surgery. The denervated animals undergo resection of a 5.0mm section of the sciatic nerve and then the skin incision is closed with suture and glue and 0.5mg/kg buprenorphine is injected subcutaneously for pain prevention before the animal wakes from surgery. 12.0 hours after surgery the mock and denervation surgery animals are again injected subcutaneously with 0.5mg/kg buprenorphine.

2.4.4 *Total RNA isolation*

At time of muscle harvest, FDB and IO muscles are dissected and removed from animal. RNAse Zap-treated dissection instruments are used to fragment the dissected muscle and then the muscles are placed in Trizol reagent and homogenized with serial passage through 18.0, 19.0, 20.0 and 21.0 gauge needles on a 1.0ml syringe. Once tissue is homogenized in Trizol, it is placed in dry ice for 20 minutes and then placed at -80C until time for isolation of RNA. Phase separation of RNA is conducted via phenol-chloroform extraction and RNA placed in nuclease-free water, treated with TurboDNase reagent (Ambion) and quantified using Qubit fluorometer (invitrogen, Inc.). Total RNA for RNAseq quantification is and left at -80C for processing by the Millard and Muriel Jacobs Genetics and Genomics Laboratory at Caltech.

Samples for QRT-PCR are treated with TurboDNase reagent (Ambion) and cDNA synthesized using BioRad iscript synthesis kit and SYBR reagent. RFP QRT-PCR primer sequence: RFP-QF: ATGAGGCTGAAGCTGAAGGA and RFP-QR: TGGTGTAGTCCTCGTTGTGG; myogeninFOR: GGGCCCCTGGAAGAAAAG; myogenin REV: AGGAGGCGCTGTGGGAGT; MYODFOR: GCCCGCGCTCCAACTGCTCTGAT; MYODREV: CCTACGGTGGTGCGCCCTCTGC; GAPDHFOR: CGTCTTCACCACCATGGAGA; GAPDHREV: CGGCCATCACGCCACAGTTT; Atrogin F: ATGCACACTGGTGCAGAGAG; Atrogin R: TGTAAGCACACAGGCAGGTC

2.4.5 *Imaging*

Confocal imaging conducted at Caltech Biological Imaging Center(BIC). Zeiss 510 upright scope used. 488nm and 543nm lasers utilized to excite EGFP and mCherry reporters, respectively. FDB and IO muscles from the same animal are placed on a microscope slide and a 1.0micron thick glass cover slip is secured over the muscles with double sided tape. 30 % glycerol solution is used in between the microscope slide and the cover slip. Range indicator function used to avoid signal saturation for each channel and 10.0 regions imaged per muscle all at the same z-slice thickness and number of slices. Two sets of 10.0 z-stack regions were imaged at 2.55um and 4.78um slice thickness. Signal mean intensities measured using ImageJ software and autofluoresence and background correction was conducted for all z-stacks.

Chapter 3

High-resolution transcriptome in adult skeletal muscle following nerve injury

3.1 Introduction

In Chapter 2, we focused on how to functionally test the *cis*-regulatory modules (CRMs) and *cis*-regulatory elements (CREs) that interpret the dynamic regulatory states present in skeletal muscle following nerve injury. In this chapter, we focus on the regulatory molecules that comprise these denervation associated regulatory states. Of particular importance are the transcription factors and signaling molecules which determine gene expression. GRN studies during embryological development in a range of model systems have provided clear evidence that transcription factors and signaling molecules are the key molecular drivers for establishing, maintaining, or transitioning between different regulatory states [Davidson, 2006]. Thus, by knowing the identity of the full repertoire of candidate regulatory molecules, one can track their temporal and spatial expression to deduce the kinetics of their regulatory activity.

A deconvolution of the regulatory events following denervation is needed to understand the logic behind the dynamic regulatory states that, until now, have been classified as 'denervation', 'atrophy', 'degeneration' or 'regeneration' -associated responses.

In fact, these categorizations reveal a generalization that is no longer necessary once a method for functional *cis*-regulatory analysis is in place and all differentially expressed genes known. The *cis* and *trans* causal interactions can be determined experimentally and the dynamic interplay of regulatory molecules and regulatory sequences revealed.

Below, we present a high-resolution transcriptome-wide RNAseq analysis for flexor digitorum brevis (FDB) and interosseous (IO) muscles at 6.0, 12.0, 24.0, and 168.0 hours post denervation. This is the first transcriptome-wide characterization of time points less than 24.0 hours for adult skeletal muscles following sciatic nerve resection. Time points assayed to date using microarray technology have ranged from 24.0 hours to 3.0 months status post nerve resection. The time points soon after nerve resection are especially relevant for a GRN-centered study, since the initial changes to the non-denervated muscle regulatory state likely take place during this time and can aid in understanding the logic behind gene network regulatory dynamics of later time points. The added resolution provided by the RNAseq platform, along with the inclusion of earlier time points, sets the stage for the highest quality and most inclusive denervation-associated transcriptome to date. Drawing on this work, on our prior RNAseq studies studies in tibialis anterior (TA) and prior work from the field, we identify a candidate *myoD*-associated muscle system-wide transcriptional regulatory subcircuit that responds to minor muscle trauma in the innervated state; we identify *myf6* as the first denervation-associated myogenic transcription factor to be expressed as early as 6.0hours and continuing out to 168.0 hours; and we introduce *atoh8*, a bhlh transcription factor, as a candidate for mediating the redeployment, in adult skeletal muscle, of the late embryonic transcriptional subcircuit controlling the expression of acetylcholine receptor subunit genes at the developing neuromuscular junction.

3.2 Results

3.2.1 Differential expression in control vs. mock denervated muscle (at 6.0, 12.0, 24.0, and 168.0 hours), using RNAseq

To distinguish the differential gene expression resulting from our surgical procedure from that resulting from nerve injury, we first determined which genes are differentially expressed following a mock surgery that simulated every aspect of the procedure except the resection of the sciatic nerve. Briefly, the mock nerve resection surgery consisted of a 0.5cm skin incision at the level of the proximal femur, blunt dissection between fascia and individual muscle bundles, exposure of sciatic nerve without disturbing the nerve, and incision closure. It is especially important to not physically manipulate the nerve during this procedure, since any type of traction on the nerve can result in confounding nerve injury. The FDB and IO muscles of the same mouse paw were combined for each sample, total RNA isolated, and samples prepared for the RNAseq platform (see Methods). FDB and IO muscles from non-perturbed mice were used as controls. Figure 3.1 provides a summary of differential gene expression between control and mock surgery FDB and IO for all time points assayed. The systemic nature of the physiological response following the mock surgery of the hind limb is reflected in the differential gene expression that is detected in the FDB and IO muscles of the treated limb, since the FDB and IO muscles are located at the plantar surface of the mouse paw, while the incision and blunt dissection occurred at the proximal femur.

At 6.0 hours the top 100 differentially expressed up-regulated genes are predominantly ribosomal proteins and predicted genes (Appendix A:Table 1). At 12.0 hours the top 100 differentially expressed up-regulated genes still consist mainly of predicted genes, but the ribosomal protein expression is replaced by muscle-specific structural genes and some cellular proliferation genes (Appendix A: Table 2). The top 100 differentially expressed genes for 6.0, 12.0, 24.0, and 168.0 hour time points for both control vs.

mock and mock vs. denervated samples are in the subsequent Tables of Appendix A and B, respectively.

At the 24.0 hour time point, the differential expression of *myoD*, *foxo1*, *fos*, and *junB* suggest an interesting regulatory dynamic. *myoD*, and *junB* are up-regulated 3.7-fold and 2.8-fold, respectively (Figure 3.2A and 3.2C). *foxo1* and *fos* are down-regulated 2.8-fold and 4.8fold, respectively (Figure 3.2B and 3.2D). The temporal expression patterns we observe correlate well with known interactions between these factors. Fos and JunB are known to form the AP1 transcriptional complex and also to down regulate the transcriptional activity of *myoD* [Chiu et al., 1988, Sassone-Corsi et al., 1988, Li et al., 1992, Bengal et al., 1992]. Therefore, it is possible that following physical perturbation to a specific muscle bundle, as occurs in our mock surgery, albeit minimal blunt manipulation of muscle tissue, a system-wide signaling response occurs that activates a muscle damage-sensing transcriptional regulatory circuit. Our dissection for the mock surgery treated mice involves blunt dissection between muscle bundle planes to expose the sciatic nerve. This procedure occurs at the level of the proximal femur and not directly to the FDB and IO muscles located at the plantar surface of the mouse paw. The decrease in *fos* and the increase in *junB* and *myoD* mRNA levels may indicate a regulatory dynamic that shifts the regulatory state to one primed for myogenic differentiation events. Foxo1 has been shown to repress *myoD* expression *in vitro* and its concomitant down-regulation may play a role in the up-regulation of myoD *in vivo* observed at the 24.0 hour time point as well.

At 168.0 hours, the four transcription factors have all returned to their baseline levels indicating a physiological recovery from the mock surgery procedure. This conclusion is supported in the total number of differentially expressed genes between unperturbed control muscles and mock surgery muscles at 168.0 hrs. The number of up and down-regulated genes are relatively equal and the total number of differentially expressed genes drops to less than 100 (Figure 3.1).

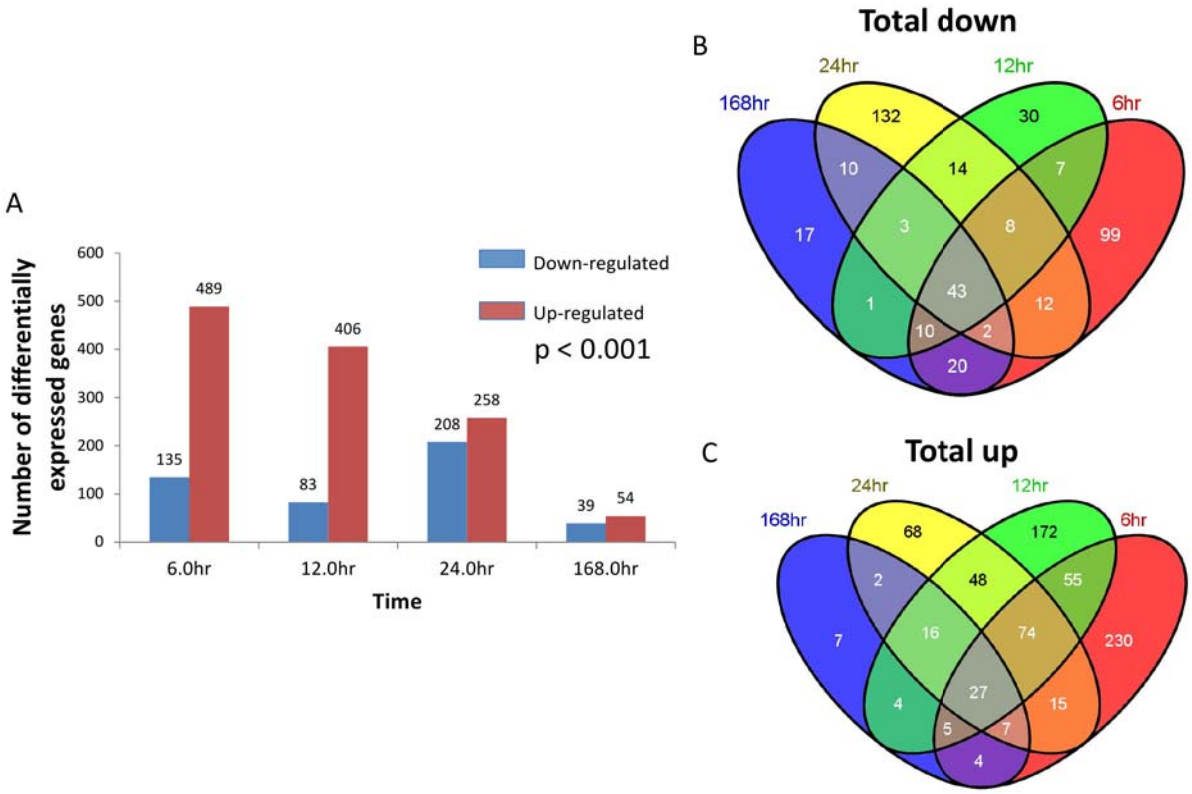

Figure 3.1: Differentially Expressed Genes In Adult FDB and IO for control vs. mock denervated. (A) Numbers on top of each column represent number of genes. By 168.0 hour time point the number of differentially expressed genes decreases, as tissues recover from mock surgery associated manipulations. p-value < 0.001 and log2 ratio value > 1. (B) Venn diagram off all down-regulated genes for each time point. (C) Venn diagram off all up-regulated genes for each time point.

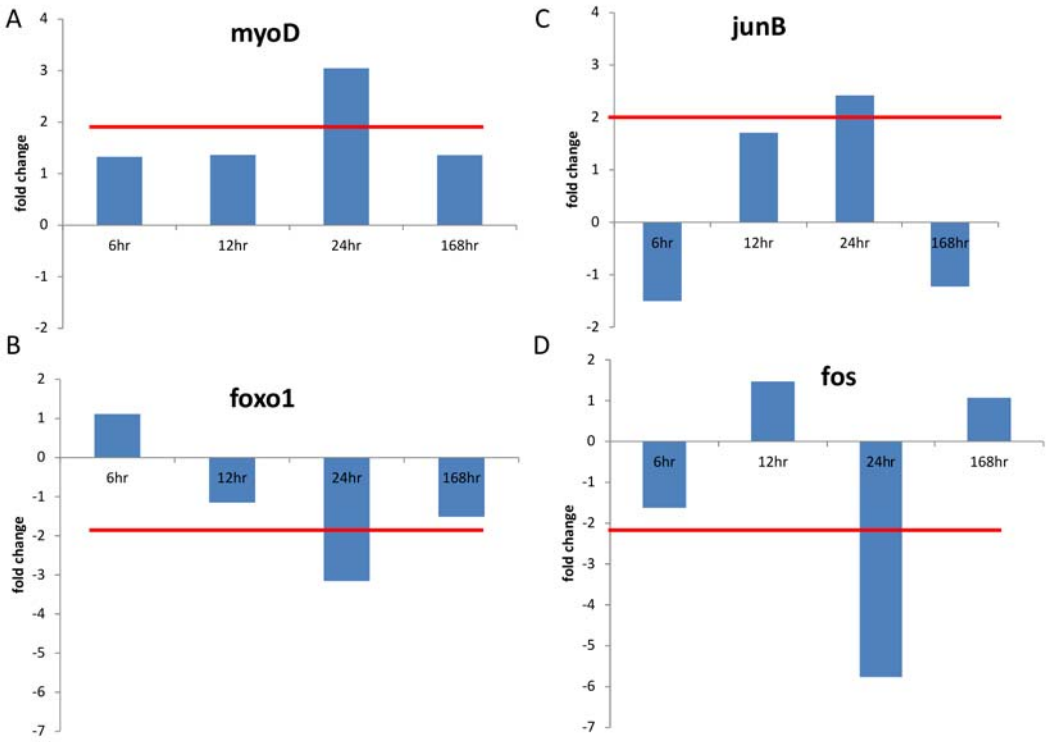

Figure 3.2: Temporal expression profile for (A) *myoD*, (B) *foxo1*, (C) *junB*, and (D) *fos* between 6.0 and 168.0 hours post mock denervation surgery. Blue columns represent fold change difference between non-manipulated control FDB and IO muscles and FDB and IO muscles from mice who underwent mock denervation surgery . Red lines demarcate the level of 2-fold change. At 24.0 hours the transcripts for known co-factors MyoD and JunB are up-regulated 3.7-fold and 2.8-fold, respectively. Also at 24.0hours, transcripts of Foxo1 and Fos, known repressors of *myoD*, are down-regulated 2.8-fold and 4.8-fold, respectively. n= 2 mice per time point.

3.2.2 Differential expression in mock denervated vs. denervated muscle (at 6.0, 12.0, 24.0, and 168.0 hours), using RNAseq

The outstanding feature of the overall differential gene expression summary for all the time points assayed is the dramatic increase in down-regulated genes at 168.0 hours in denervated muscles (Figure 3.3). When compared to Figure 3.1, this transition towards down-regulation of mRNAs at 168.0 hours suggests a key change in regulatory state that is unique to the denervation molecular response. This regulatory state change, specific to denervation, may be initiated at earlier time points or may begin sometime after 24.0 hours, or both. Further analysis of the expression data supports the idea that both are occurring. We observe striking differences in the relative expression levels of key regulatory molecules.

myf6, for example, is up-regulated by 3.7-fold at 6.0 hours status post denervation (Figure 3.4). In our analysis, *myf6* is the first of the myogenic factors to be up-regulated following nerve resection, whereas it is not differentially expressed following mock denervation. Myf6 and Myogenin play a key role in differentiated skeletal muscle and skeletal muscle maintenance [Miner and Wold, 1990, Knapp et al., 2006, Zhang et al., 1995]. They also are concomitantly expressed during embryological development of muscle [Patapoutian et al., 1993, Braun and Arnold, 1995, Bober et al., 1991, Hinterberger et al., 1991]. Thus, concomitant *myf6* and *myogenin* up-regulated expression, at 24.0 hours and out to 168.0 hours following denervation, suggests the redeployment of a muscle differentiation subcircuit reminiscent of the late myogenic program.

However, the fact that *myf6* is up-regulated as early as 6.0 hours and continues upwards out to 168.0 hours after denervation, while *myogenin* expression starts to decline after 72.0 hours following denervation, suggests that they have regulatory activities that are independent of one another (Figure 3.5). The argument for in-

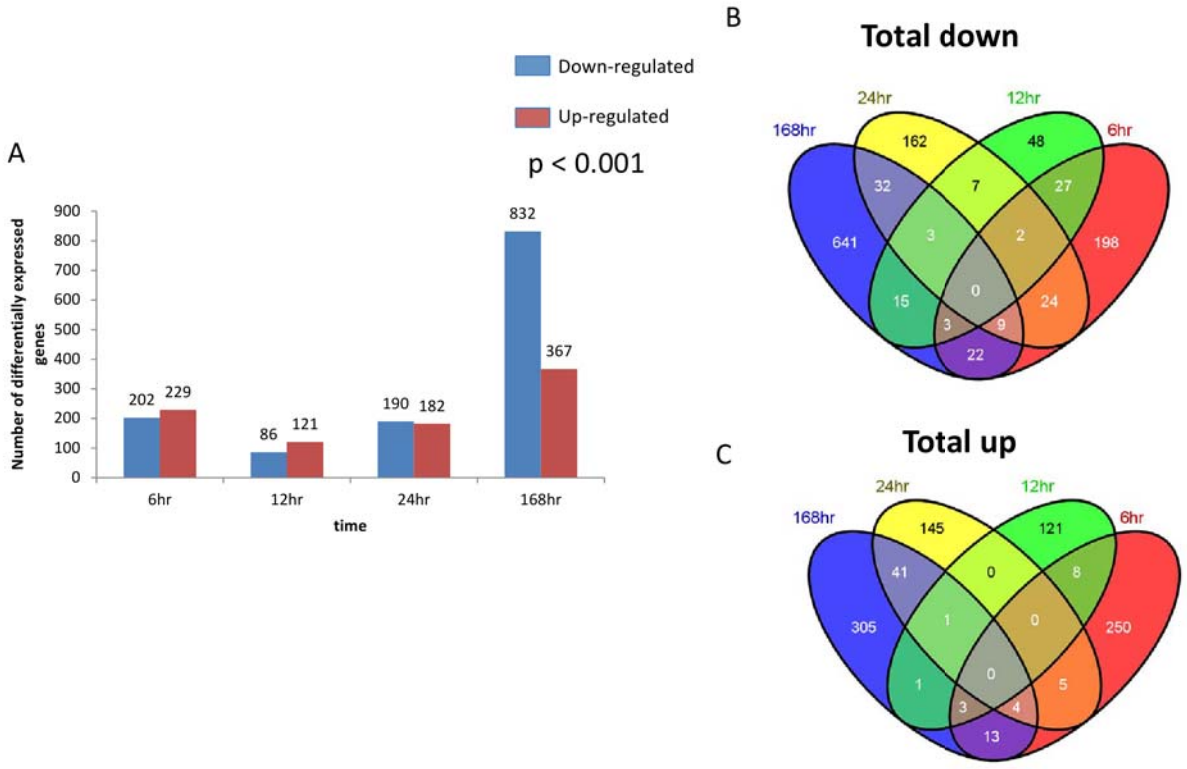

Figure 3.3: Differentially Expressed Genes In Adult FDB and IO for mock denervated vs. denervated. (A) Numbers on top of each column are number of genes. At 168.0 hours the number of down-regulated genes increases as denervation-associated regulatory state changes begin to have an effect. Compare to 168.0 hour time point of Figure 3.1 where regulatory state of FDB and IO muscles starts to return to baseline levels. p-value < 0.001 and log2 ratio value > 1. (B) Venn diagram off all down-regulated genes for each time point. (C) Venn diagram off all up-regulated genes for each time point.

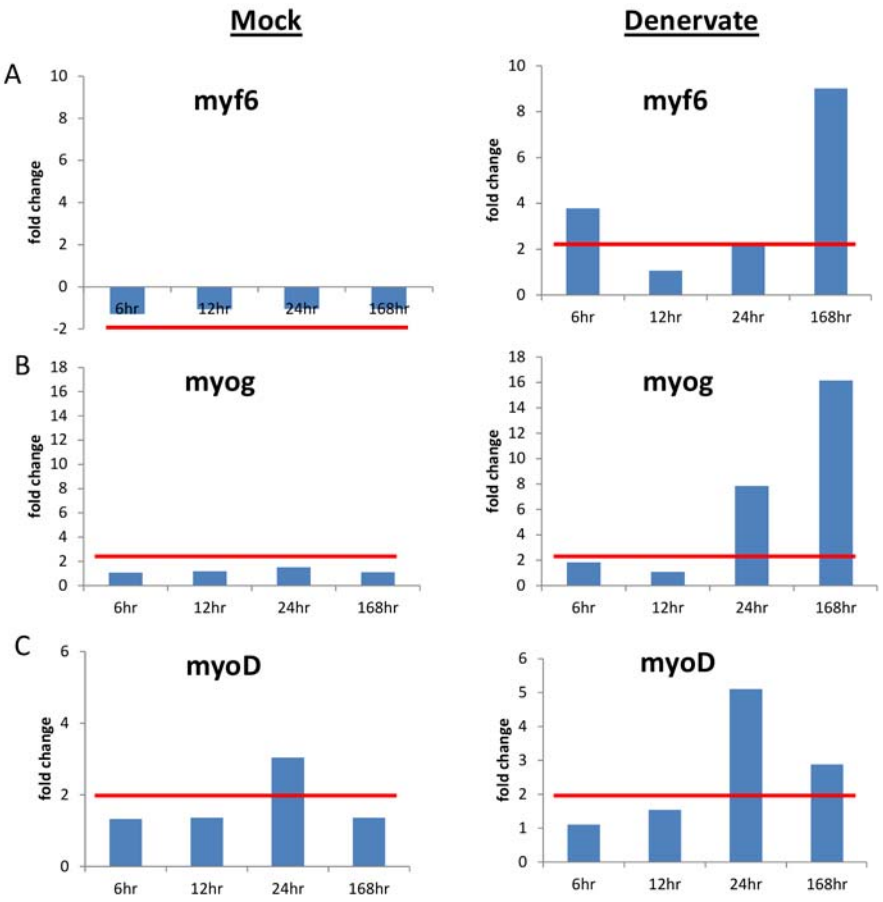

Figure 3.4: Temporal expression profile for (A) *myf6*, (B) *myog*, and (C) *myoD* between 6.0 and 168.0 hours. Blue columns in 'mock' column represent fold change difference between unmanipulated control FDB and IO muscles and FDB and IO muscles from mice who underwent mock denervation surgery. Blue columns in 'denervate' column represent fold change difference between mock denervated and denervated FDB and IO muscles. Red lines demarcate the level of 2-fold change. *myf6* is the first of the myogenic regulatory factors to be expressed as early as 6.0 hours. *myog* does not respond to mock denervation, but does become up-regulated by the 24.0 hour time point. *myoD* responds to both mock denervation and denervation by 24.0 hours and remains up-regulated at 168.0 hours relative to the earlier time points. n= 2 mice per time point.

dependent regulatory activity is supported by the fact that denervation of the hind limbs of *myf6* null mice, still results in the expected expression profile of myogenin and acetylcholine subunit genes out to 168.0 hours [Eftimie et al., 1991a, Zhang et al., 1995].

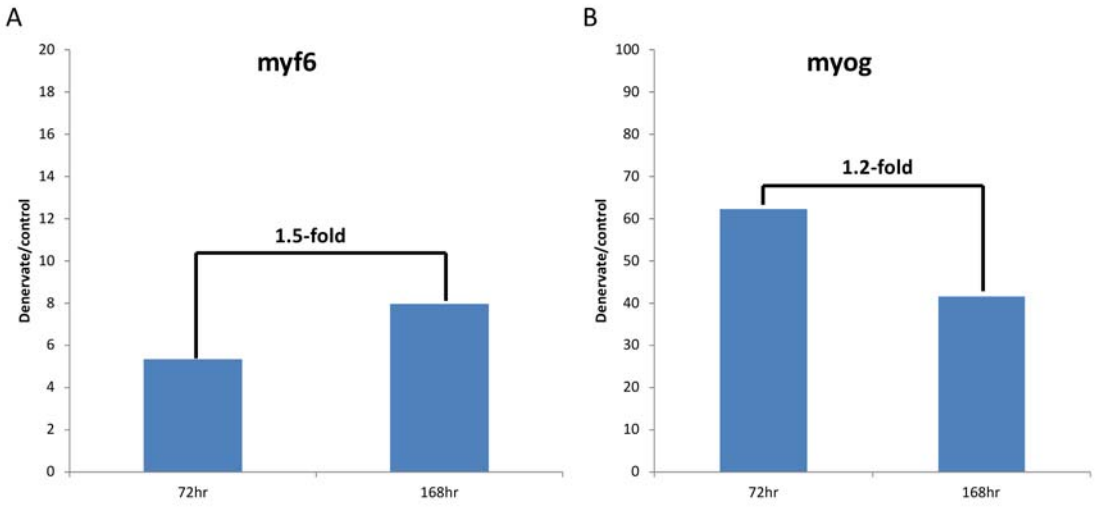

Figure 3.5: Temporal expression of (A) *myf6* and (B) *myog* from 72.0 to 168 hours. myf6 undergoes a 1.5-fold upward change from 72.0 to 168 hours, while *myog* expriences a 1.2-fold change in the downward direction. Data from RNAseq of denervated TA muscles.

There is a dramatic increase in the transcripts of the acetylcholine receptor subunits by the 168.0 hour time point following denervation. A functional acetylcholine receptor in adult skeletal muscle consists of five subunits: alpha (2), beta, delta, and epsilon. During embryonic and early post natal development, the acetylcholine receptor consists of a different subset of subunits than in the adult: alpha (2), beta, delta,

and gamma (Figure 3.6) [Burden, 1977a, Merlie, 1984, Kues et al., 1995, Duclert et al., 1996]. Furthermore, at this early stage of neuromuscular junction development, all myonuclei share the same transcriptional program [Buonanno and Merlie, 1986, Baldwin et al., 1988]. However, once the maturing skeletal muscle receives input from the nerve, the transcriptional program that activates the acetylcholine receptor subunit genes becomes restricted to the nuclei that are localized near the innervating nerve, which are called junctional or subsynaptic nuclei [Anderson and Cohen, 1977, Burden, 1977b, Merlie and Sanes, Sanes et al., 1991, Simon et al., 1992, Piette et al., 1993, Gilmour et al., 1995]. Following denervation, however, there is a recapitulation of the transcriptional program of late embryonic and early post natal development [Merlie et al., 1984, Goldman et al., 1988]. This up-regulation of *chrng*, *chrnd*, and *chrna1* is unique to the transcriptional response following denervation and is not seen in the muscles from our mock surgery mice. Myogenic factors have been implicated in the regulation of the acetylcholine subunits following denervation [Eftimie et al., 1991b, Prody and Merlie, 1991, Duclert et al., 1991, Gilmour et al., 1991, Dutton et al., 1993, Merlie et al., 1994]. We have identified a novel candidate for acetylcholine subunit transcriptional regulation, *atoh8* (a.k.a. *math6*) (Figure 3.7). Atoh8 is basic loop helix transcription factor of the atonal family of proteins. At 24.0 hours, it is up-regulated by 5.6-fold. The temporal expression profile depicted in Figure 3.7 place it at the right time point, kinetically, to be a potential up-stream regulator of *chrng*, *chrnd*, and *chrna1*. Although Atoh8 has not previously been assigned a function in mammalian adult skeletal muscle, it has recently been found to have a role in differentiated muscle fibers during somite morphogensis in zebrafish [Yao et al., 2010]. Atoh1, an atonal family member, has been been shown to regulate *chrna1* and be necessary for the induction of *chrng* in hair cells of the inner ear in mouse [Scheffer et al., 2007] . The regulatory control of *chrna1* is mediated in *cis* via two E-box sites located upstream of the *chrna1* coding sequence [Piette et al., 1990]. *chrng* and *chrnd* also have conserved E-box sites proximal to the start of translation [Simon and Burden, 1993]. In the case of *chrng* and *chrnd*, they are located adjacent to each other on the chromosome, separated by only 5.7 kbp. This close proximity

allows them to be captured in one BAC. Recombineering a reporter for each gene within the same BAC and testing the candidate regulatory sequences in combination *in vivo* using our gene tranfer system, would allow for an unprecedented insight into the *cis* -regulatory architecture controlling these genes following denervation.

3.3 Discussion

The advent of high-throughput and high-resolution transcriptome characterization has greatly expanded our view of the output of the regulatory genome. This is especially important for capturing subtle changes in RNA levels across multiple time points in a reproducible manner with relatively low variability. We have taken advantage of this technology to explore the early time points (i.e. 6.0 and 12.0 hours) following denervation of skeletal muscle, as well as the time points more commonly studied (i.e. 24.0 and 168 hours). As mentioned previously, high-quality transcriptional data of the early time points following a major physiological event, like denervation, are very important for a GRN-dedicated study. This is even more important for GRN directed studies focused on characterizing a physiological event in adult, where there are multiple gene batteries in motion and protein-level regulatory interactions concomitantly occurring. Focusing on transcription factors and signaling molecules, the first responders to the commands of the regulatory genome, aids in keeping a foot hold on the scaffolding of the underlying physiological GRNs. In addition, in the case of skeletal muscle denervation biology, there is already a large body of work that has identified many of the major regulatory events for the time points most studied. What remains is to consolidate and explain this information by linking every molecular event to the *cis* and *trans* interactions that set them in motion. We took this combined approach of utilizing high-quality and high-resolution expression data, prior work in the field, and focusing on transcription factors and signaling molecules to: identify a candidate *myoD*-associated muscle system-wide transcriptional regulatory subcircuit that responds to minor muscle trauma in the innervated state; identify *myf6* as the

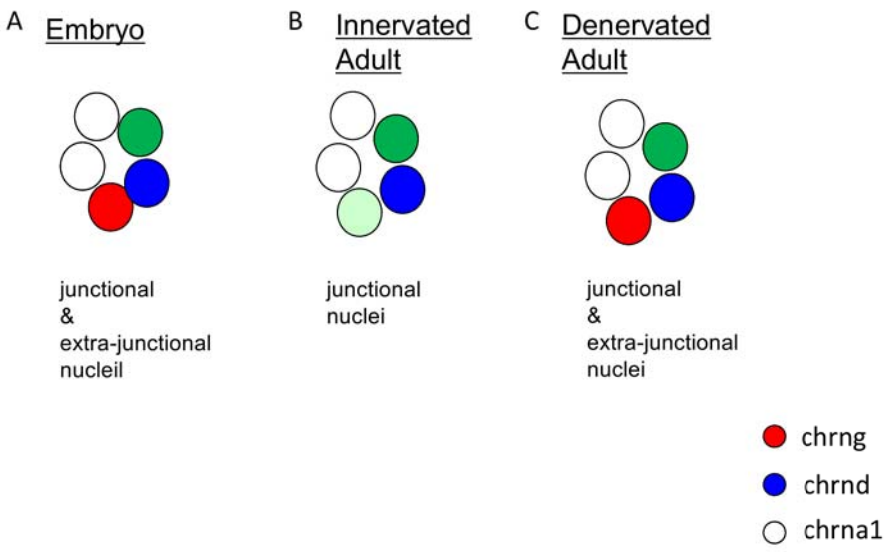

Figure 3.6: Acetylcholine receptor subunit composition of skeletal muscle during: late embryological development (A), in innervated adult muscle (B), and in adult muscle after denervation (C). The black outlined circles represent the proteins of the five subunits that comprise the acetylcholine receptor (top view). Color code to identify relevant protein subunits at bottom right corner of figure. Junctional nuclei = nuclei that are located at the neuromuscular junction; extra-junctional nuclei = all other nuclei not at the neuromuscular junction. During late embryological development and again after denervation, the composition of the acetylcholine receptor is the same. Compare (A) to (C). The spatial expression of *chrng*, *chrnd*, and *chrna1* is localized at both junctional and extra-junctional nuclei during development and after denervation.

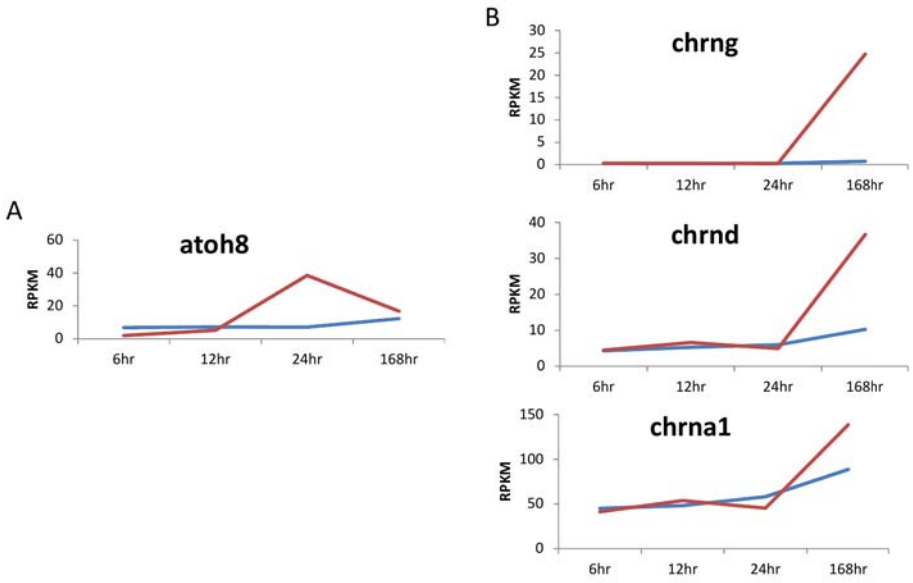

Figure 3.7: Temporal expression profile for *atoh8*, *chrng*, *chrnd*, and *chrna1*. Blue line is mRNA level for mock denervated FDB and IO muscles. Red line is mRNA levels for denervated FDB and IO muscles. *atoh8* levels are elevated at 24.0 hours (A), followed by mRNA levels rising for acetylcholine receptor subunits *chrng*, *chrnd*, and *chrna1* by 168.0 hours (B). The temporal expression pattern suggests *atoh8* as an initiator of the acetylcholine subunit transcriptional changes following denervation.

first denervation-associated myogenic transcription factor to be expressed as early as 6.0 hours and continuing out to 168.0 hours; introduce *atoh8*, a bhlh transcription factor, as a candidate for mediating the redeployment, in adult skeletal muscle, of the late embryonic transcriptional subcircuit controlling the expression of acetylcholine receptor subunit genes at the developing neuromuscular junction. In Chapter 2 we introduced a dedicated method for gene transfer to experimentally validate the candidate CRMs or CREs, in both plasmid and BAC DNA formats, responsible for the differential expression of key regulatory molecules. FDB and IO muscles are an excellent model to study fast-twitch muscle groups and while we are currently focused on the GRNs underlying the denervation response, the GRNs underlying any mouse skeletal muscle disease model that affects fast-twitch muscle groups, can be studied using our gene transfer system on FDB and IO muscles.

3.4 Materials and Methods

3.4.1 *RNAseq*

Sciatic nerve denervation and mock denervation surgeries were conducted as per Chapter 2 methods. The control samples were from unperturbed left TA, FDB, IO muscles. Total RNA was isolated from left TA, FDB and IO muscles of 2.0 to 4.0-month-old C57Bl/6 female mice. Two sets of FDB and IO muscles per time point: 6.0, 12.0, 24.0, and 168 hour. One TA muscle for 6.0 and 168.0 hour time points. Two TA muscles for 72.0 hour time point. At time of muscle harvest, TA, FDB and IO muscles are dissected and removed from animal. RNAse Zap-treated dissection instruments are used to fragment the dissected muscle and then the muscles are placed in Trizol reagent and homogenized with serial passage through 18.0, 19.0, 20.0 and 21.0 gauge needles on a 1.0ml syringe. Once tissue is homogenized in Trizol, it is placed in dry ice for 20 minutes and then placed at -80C until time for isolation of RNA. Phase separation of RNA is conducted via phenol-chloroform extraction and

RNA placed in nuclease-free water, treated with TurboDNase reagent (Ambion) and quantified using Qubit fluorometer (invitrogen, Inc.). Total RNA for RNAseq quantification is and left at -80C for library construction by the Millard and Muriel Jacobs Genetics and Genomics Laboratory at Caltech.

An Illumina Genome Analyzer IIx sequencer at the Millard and Muriel Jacobs Genetics and Genomics Laboratory was used for multi-plex HiSeq (100bp, single end reads) sequencing. RNAseq analysis was conducted using an analysis pipeline consisting of published and customized software by Edoardo Marcora, Ph.D.: Bowtie v0.12.7 [v0.12.7], TopHat 1.3.3 [v1.2.0], Cufflinks v1.3.0 [v0.9.3], Htseq v0.5.3p3 [v0.4.7], DESeq v.1.6.1 [v1.4.0], mm9 UCSC.

Chapter 4

Conclusion

The regulatory genome has been well characterized in the context of developmental biology. The most comprehensive example and characterization of regulatory genome dynamics has been conducted in the sea urchin embryo [Davidson et al., 2002]. However, the tipping point from mere postulation to the highly detailed network model that exists today for the first 30.0 hrs of endomesoderm development in sea urchin, occurred when the causal mechanisms of body plan evolution became experimentally accessible [Britten and Davidson, 1971]. The work presented in this study introduces a methodology which makes GRN discovery and validation in adult skeletal muscle following denervation experimentally accessible. We propose flexor digitorum brevis and interosseous muscles as a model muscle group to study the regulatory genome governing fast-twitch muscle fibers. Using this methodology, we provide evidence to explain the causal mechanism that down-regulates *myogenin*, a key denervation-associated transcription factor, at 10.0 and 17.0 days after denervation. Finally, we utilize high-throughput and high-resolution transcriptome sequencing, at early (i.e. 6.0 and 12.0 hours) and later (i.e. 24.0 to 168.0 hours) time points, to generate a comprehensive catalog of differentially expressed genes to aid in identifying candidates to test using our GRN-dedicated experimental model system.

It is clear from the distinct regulatory circuitry governing myogenesis at various anatomical regions throughout development and in response to varying stimuli in

adult, that there is much to be discovered regarding how modular components of GRNs are activated and integrated with other subcircuits over time. Gain and loss of function studies have identified and outlined many regulatory relationships, but what is lacking is the exact mechanism in *cis* and *trans* that explains each interaction. Our experimental model lays the foundation for systematic functional testing of *cis*-acting regulatory regions of genes that have been previously identified to be major contributors to many skeletal muscle transcriptional programs. The efficiency of the gene transfer into FDB and IO also is promising for the implementation of multi-plex cis-functional testing (i.e. functional testing of many candidate CRMs at once in the same transefction), which would solve the problem of throughput when testing only one or two CRMs at a time[Nam et al., 2010]. The efficient gene transfer also bodes well for the reliable introduction of RNA interference molecules to perturb regulatory interactions in *trans*. Utilization of nuclear-targeted reporter genes will be very helpful in providing spatial and temporal regulatory information to further resolve the unique transcriptional programs of junctional and non-junctional nuclei. As demonstrated in Chapter 3, high-throughput sequencing technology provides excellent resolution of all differentially expressed genes. Taken together, all the pieces to building a gene regulatory network in adult mouse skeletal muscle following nerve injury are now in place. While this study describes a means for elucidating the GRNs underlying the skeletal muscle response to nerve injury, the approach can also be applied to any adult mouse muscle physiological response or disease model. In time, we can begin to integrate, organize, and understand skeletal muscle disease-associated gene regulatory networks. The ultimate objective will be to learn how to modulate these transcriptional networks to preserve non-pathological phenotypes.

Bibliography

M J Anderson and M W Cohen. Nerve-induced and spontaneous redistribution of acetylcholine receptors on cultured muscle cells. *The Journal of physiology*, 268(3):757–73, July 1977. ISSN 0022-3751. URL http://www.ncbi.nlm.nih.gov/pubmed/69707http://www.pubmedcentral.nih.gov/articlerender.fcgi?artid=1283687&tool=pmcentrez&rendertype=abstract.

Lola Bajard, Frédéric Relaix, Mounia Lagha, Didier Rocancourt, Philippe Daubas, and Margaret E Buckingham. A novel genetic hierarchy functions during hypaxial myogenesis: Pax3 directly activates Myf5 in muscle progenitor cells in the limb. *Genes & development*, 20(17):2450–64, September 2006. ISSN 0890-9369. doi: 10.1101/gad.382806. URL http://www.pubmedcentral.nih.gov/articlerender.fcgi?artid=1560418&tool=pmcentrez&rendertype=abstract.

T J Baldwin, C M Yoshihara, K Blackmer, C R Kintner, and S J Burden. Regulation of acetylcholine receptor transcript expression during development in Xenopus laevis. *The Journal of cell biology*, 106(2):469–78, February 1988. ISSN 0021-9525. URL http://www.ncbi.nlm.nih.gov/pubmed/3339098http://www.pubmedcentral.nih.gov/articlerender.fcgi?artid=2114983&tool=pmcentrez&rendertype=abstract.

G Barbieri, L De Angelis, S Feo, G Cossu, and A Giallongo. Differential expression of muscle-specific enolase in embryonic and fetal myogenic cells during mouse development. *Differentiation; research in biological diversity*, 45(3):179–84, December 1990. ISSN 0301-4681. URL http://www.ncbi.nlm.nih.gov/pubmed/2090519.

Jane Batt, James Bain, Jason Goncalves, Bernadeta Michalski, Pamela Plant, Margaret Fahnestock, and Jim Woodgett. Differential gene expression profiling of short and long term denervated muscle. *FASEB journal : official publication of the Federation of American Societies for Experimental Biology*, 20 (1):115–7, January 2006. ISSN 1530-6860. doi: 10.1096/fj.04-3640fje. URL http://www.ncbi.nlm.nih.gov/pubmed/16291642.

E Bengal, L Ransone, R Scharfmann, V J Dwarki, S J Tapscott, H Weintraub, and I M Verma. Functional antagonism between c-Jun and MyoD proteins: a direct physical association. *Cell*, 68(3):507–19, February 1992. ISSN 0092-8674. URL http://www.ncbi.nlm.nih.gov/pubmed/1310896.

Libera Berghella, Luciana De Angelis, Tristan De Buysscher, Ali Mortazavi, Stefano Biressi, Sonia V Forcales, Dario Sirabella, Giulio Cossu, and Barbara J Wold. A highly conserved molecular switch binds MSY-3 to regulate myogenin repression in postnatal muscle. *Genes & development*, 22(15):2125–38, August 2008. ISSN 0890-9369. doi: 10.1101/gad.468508. URL http://www.pubmedcentral.nih.gov/articlerender.fcgi?artid=2492748&tool=pmcentrez&rendertype=abstract.

Charlotte A Berkes, Donald A Bergstrom, Bennett H Penn, Karen J Seaver, Paul S Knoepfler, and Stephen J Tapscott. Pbx marks genes for activation by MyoD indicating a role for a homeodomain protein in establishing myogenic potential. *Molecular cell*, 14(4):465–77, May 2004. ISSN 1097-2765. URL http://www.ncbi.nlm.nih.gov/pubmed/15149596.

E Bober, G E Lyons, T Braun, G Cossu, M Buckingham, and H H Arnold. The muscle regulatory gene, Myf-6, has a biphasic pattern of expression during early mouse development. *The Journal of cell biology*, 113(6):1255–65, June 1991. ISSN 0021-9525. URL http://www.pubmedcentral.nih.gov/articlerender.fcgi?artid=2289041&tool=pmcentrez&rendertype=abstract.

E Bober, T Franz, H H Arnold, P Gruss, and P Tremblay. Pax-3 is required for the

development of limb muscles: a possible role for the migration of dermomyotomal muscle progenitor cells. *Development (Cambridge, England)*, 120(3):603–12, March 1994. ISSN 0950-1991. URL http://www.ncbi.nlm.nih.gov/pubmed/8162858.

S C Bodine, E Latres, S Baumhueter, V K Lai, L Nunez, B A Clarke, W T Poueymirou, F J Panaro, E Na, K Dharmarajan, Z Q Pan, D M Valenzuela, T M DeChiara, T N Stitt, G D Yancopoulos, and D J Glass. Identification of ubiquitin ligases required for skeletal muscle atrophy. *Science (New York, N.Y.)*, 294(5547): 1704–8, November 2001. ISSN 0036-8075. doi: 10.1126/science.1065874. URL http://www.ncbi.nlm.nih.gov/pubmed/11679633.

T Braun and H H Arnold. Inactivation of Myf-6 and Myf-5 genes in mice leads to alterations in skeletal muscle development. *The EMBO journal*, 14(6):1176–86, March 1995. ISSN 0261-4189. URL http://www.pubmedcentral.nih.gov/articlerender.fcgi?artid=398195&tool=pmcentrez&rendertype=abstract.

T Braun, G Buschhausen-Denker, E Bober, E Tannich, and H H Arnold. A novel human muscle factor related to but distinct from MyoD1 induces myogenic conversion in 10T1/2 fibroblasts. *The EMBO journal*, 8(3):701–9, March 1989. ISSN 0261-4189. URL http://www.pubmedcentral.nih.gov/articlerender.fcgi?artid=400865&tool=pmcentrez&rendertype=abstract.

R J Britten and E H Davidson. Repetitive and non-repetitive DNA sequences and a speculation on the origins of evolutionary novelty. *The Quarterly review of biology*, 46(2):111–38, June 1971. ISSN 0033-5770. URL http://www.ncbi.nlm.nih.gov/pubmed/5160087.

H Brohmann, K Jagla, and C Birchmeier. The role of Lbx1 in migration of muscle precursor cells. *Development (Cambridge, England)*, 127(2):437–45, January 2000. ISSN 0950-1991. URL http://www.ncbi.nlm.nih.gov/pubmed/10603359.

A Buonanno and J P Merlie. Transcriptional regulation of nicotinic acetylcholine receptor genes during muscle development. *The Journal of biological chemistry*,

261(25):11452–5, September 1986. ISSN 0021-9258. URL http://www.ncbi.nlm.nih.gov/pubmed/3745150.

S Burden. Development of the neuromuscular junction in the chick embryo: the number, distribution, and stability of acetylcholine receptors. *Developmental biology*, 57 (2):317–29, June 1977a. ISSN 0012-1606. URL http://www.ncbi.nlm.nih.gov/pubmed/873051.

S Burden. Acetylcholine receptors at the neuromuscular junction: developmental change in receptor turnover. *Developmental biology*, 61(1):79–85, November 1977b. ISSN 0012-1606. URL http://www.ncbi.nlm.nih.gov/pubmed/924025.

R Chiu, W J Boyle, J Meek, T Smeal, T Hunter, and M Karin. The c-Fos protein interacts with c-Jun/AP-1 to stimulate transcription of AP-1 responsive genes. *Cell*, 54(4):541–52, August 1988. ISSN 0092-8674. URL http://www.ncbi.nlm.nih.gov/pubmed/3135940.

Todd J Cohen, David S Waddell, Tomasa Barrientos, Zhonghua Lu, Guoping Feng, Gregory A Cox, Sue C Bodine, and Tso-Pang Yao. The histone deacetylase HDAC4 connects neural activity to muscle transcriptional reprogramming. *The Journal of biological chemistry*, 282(46):33752–9, November 2007. ISSN 0021-9258. doi: 10.1074/jbc.M706268200. URL http://www.ncbi.nlm.nih.gov/pubmed/17873280.

M G Cusella-De Angelis, S Molinari, A Le Donne, M Coletta, E Vivarelli, M Bouche, M Molinaro, S Ferrari, and G Cossu. Differential response of embryonic and fetal myoblasts to TGF beta: a possible regulatory mechanism of skeletal muscle histogenesis. *Development (Cambridge, England)*, 120(4):925–33, April 1994. ISSN 0950-1991. URL http://www.ncbi.nlm.nih.gov/pubmed/7600968.

Y Dai, E M Schwarz, D Gu, W W Zhang, N Sarvetnick, and I M Verma. Cellular and humoral immune responses to adenoviral vectors containing factor IX gene: tolerization of factor IX and vector antigens allows for long-term expression. *Proceedings*

of the National Academy of Sciences of the United States of America, 92(5):1401–5, February 1995. ISSN 0027-8424. URL http://www.pubmedcentral.nih.gov/articlerender.fcgi?artid=42527&tool=pmcentrez&rendertype=abstract.

E H Davidson. *The Regulatory Genome: Gene Regulatory Networks in Development and Evolution*. academic press/Elsevier, San Diego, 2006. ISBN 978-0-12-088563-3.

Eric H Davidson, Jonathan P Rast, Paola Oliveri, Andrew Ransick, Cristina Calestani, Chiou-Hwa Yuh, Takuya Minokawa, Gabriele Amore, Veronica Hinman, César Arenas-Mena, Ochan Otim, C Titus Brown, Carolina B Livi, Pei Yun Lee, Roger Revilla, Maria J Schilstra, Peter J C Clarke, Alistair G Rust, Zhengjun Pan, Maria I Arnone, Lee Rowen, R Andrew Cameron, David R McClay, Leroy Hood, and Hamid Bolouri. A provisional regulatory gene network for specification of endomesoderm in the sea urchin embryo. *Developmental biology*, 246 (1):162–90, June 2002. ISSN 0012-1606. doi: 10.1006/dbio.2002.0635. URL http://www.ncbi.nlm.nih.gov/pubmed/12027441.

S Dietrich, F Abou-Rebyeh, H Brohmann, F Bladt, E Sonnenberg-Riethmacher, T Yamaai, A Lumsden, B Brand-Saberi, and C Birchmeier. The role of SF/HGF and c-Met in the development of skeletal muscle. *Development (Cambridge, England)*, 126(8):1621–9, April 1999. ISSN 0950-1991. URL http://www.ncbi.nlm.nih.gov/pubmed/10079225.

Marino DiFranco and Julio L Vergara. The Na conductance in the sarcolemma and the transverse tubular system membranes of mammalian skeletal muscle fibers. *The Journal of general physiology*, 138(4):393–419, October 2011. ISSN 1540-7748. doi: 10.1085/jgp.201110682. URL http://www.pubmedcentral.nih.gov/articlerender.fcgi?artid=3182446&tool=pmcentrez&rendertype=abstract.

Marino DiFranco, Marbella Quinonez, Joana Capote, and Julio Vergara. DNA transfection of mammalian skeletal muscles using in vivo electroporation. *Journal of visualized experiments : JoVE*, (32), January 2009. ISSN 1940-087X. doi:

10.3791/1520. URL http://www.ncbi.nlm.nih.gov/pubmed/19841615http://www.pubmedcentral.nih.gov/articlerender.fcgi?artid=2793085&tool=pmcentrez&rendertype=abstract.

A Duclert, J Piette, and J P Changeux. Influence of innervation of myogenic factors and acetylcholine receptor alpha-subunit mRNAs. *Neuroreport*, 2(1):25–8, January 1991. ISSN 0959-4965. URL http://www.ncbi.nlm.nih.gov/pubmed/1768845.

A Duclert, N Savatier, L Schaeffer, and J P Changeux. Identification of an element crucial for the sub-synaptic expression of the acetylcholine receptor epsilon-subunit gene. *The Journal of biological chemistry*, 271(29):17433–8, July 1996. ISSN 0021-9258. URL http://www.ncbi.nlm.nih.gov/pubmed/8663316.

E K Dutton, A M Simon, and S J Burden. Electrical activity-dependent regulation of the acetylcholine receptor delta-subunit gene, MyoD, and myogenin in primary myotubes. *Proceedings of the National Academy of Sciences of the United States of America*, 90(5):2040–4, March 1993. ISSN 0027-8424. URL http://www.pubmedcentral.nih.gov/articlerender.fcgi?artid=46016&tool=pmcentrez&rendertype=abstract.

D G Edmondson and E N Olson. A gene with homology to the myc similarity region of MyoD1 is expressed during myogenesis and is sufficient to activate the muscle differentiation program. *Genes & development*, 3(5):628–40, May 1989. ISSN 0890-9369. URL http://www.ncbi.nlm.nih.gov/pubmed/2473006.

R Eftimie, H R Brenner, and A Buonanno. Myogenin and MyoD join a family of skeletal muscle genes regulated by electrical activity. *Proc Natl Acad Sci U S A*, 88(4):1349–1353, 1991a. URL http://www.ncbi.nlm.nih.gov/pubmed/1705035.

R Eftimie, H R Brenner, and A Buonanno. Myogenin and MyoD join a family of skeletal muscle genes regulated by electrical activity. *Proceedings of the National Academy of Sciences of the United States of America*, 88(4):1349–53,

February 1991b. ISSN 0027-8424. URL http://www.pubmedcentral.nih.gov/articlerender.fcgi?artid=51015&tool=pmcentrez&rendertype=abstract.

O Friedrich, T Ehmer, and R H Fink. Calcium currents during contraction and shortening in enzymatically isolated murine skeletal muscle fibres. *The Journal of physiology*, 517 (Pt 3:757–70, June 1999. ISSN 0022-3751. URL http://www.pubmedcentral.nih.gov/articlerender.fcgi?artid=2269387&tool=pmcentrez&rendertype=abstract.

Xing Fu, Ning Fu, Song Guo, Zheng Yan, Ying Xu, Hao Hu, Corinna Menzel, Wei Chen, Yixue Li, Rong Zeng, and Philipp Khaitovich. Estimating accuracy of RNA-Seq and microarrays with proteomics. *BMC genomics*, 10:161, January 2009. ISSN 1471-2164. doi: 10.1186/1471-2164-10-161. URL http://www.pubmedcentral.nih.gov/articlerender.fcgi?artid=2676304&tool=pmcentrez&rendertype=abstract.

Luigi Galvani. De viribus electricitatis in motu musculari commentarius, 1791.

B P Gilmour, G R Fanger, C Newton, S M Evans, and P D Gardner. Multiple binding sites for myogenic regulatory factors are required for expression of the acetylcholine receptor gamma-subunit gene. *The Journal of biological chemistry*, 266(30):19871–4, October 1991. ISSN 0021-9258. URL http://www.ncbi.nlm.nih.gov/pubmed/1657903.

B P Gilmour, D Goldman, K G Chahine, and P D Gardner. Electrical activity suppresses nicotinic acetylcholine receptor gamma subunit promoter activity. *Developmental biology*, 168(2):416–28, April 1995. ISSN 0012-1606. doi: 10.1006/dbio.1995.1091. URL http://www.ncbi.nlm.nih.gov/pubmed/7729578.

Julien Giordani, Lola Bajard, Josiane Demignon, Philippe Daubas, Margaret Buckingham, and Pascal Maire. Six proteins regulate the activation of Myf5 expression in embryonic mouse limbs. *Proceedings of the National Academy of Sciences of the United States of America*, 104(27):11310–5, July 2007. ISSN 0027-

8424. doi: 10.1073/pnas.0611299104. URL http://www.pubmedcentral.nih.gov/articlerender.fcgi?artid=2040895&tool=pmcentrez&rendertype=abstract.

D Goldman, H R Brenner, and S Heinemann. Acetylcholine receptor alpha-, beta-, gamma-, and delta-subunit mRNA levels are regulated by muscle activity. *Neuron*, 1(4):329–33, June 1988. ISSN 0896-6273. URL http://www.ncbi.nlm.nih.gov/pubmed/3272739.

M Goulding, A Lumsden, and A J Paquette. Regulation of Pax-3 expression in the dermomyotome and its role in muscle development. *Development (Cambridge, England)*, 120(4):957–71, April 1994. ISSN 0950-1991. URL http://www.ncbi.nlm.nih.gov/pubmed/7600971.

Raphaelle Grifone, Christine Laclef, François Spitz, Soledad Lopez, Josiane Demignon, Jacques-Emmanuel Guidotti, Kiyoshi Kawakami, Pin-Xian Xu, Robert Kelly, Basil J Petrof, Dominique Daegelen, Jean-Paul Concordet, and Pascal Maire. Six1 and Eya1 expression can reprogram adult muscle from the slow-twitch phenotype into the fast-twitch phenotype. *Molecular and cellular biology*, 24(14):6253–67, July 2004. ISSN 0270-7306. doi: 10.1128/MCB.24.14.6253-6267.2004. URL http://www.pubmedcentral.nih.gov/articlerender.fcgi?artid=434262&tool=pmcentrez&rendertype=abstract.

Raphaelle Grifone, Josiane Demignon, Christophe Houbron, Evelyne Souil, Claire Niro, Mary J Seller, Ghislaine Hamard, and Pascal Maire. Six1 and Six4 homeoproteins are required for Pax3 and Mrf expression during myogenesis in the mouse embryo. *Development (Cambridge, England)*, 132(9):2235–49, May 2005. ISSN 0950-1991. doi: 10.1242/dev.01773. URL http://www.ncbi.nlm.nih.gov/pubmed/15788460.

M K Gross, L Moran-Rivard, T Velasquez, M N Nakatsu, K Jagla, and M Goulding. Lbx1 is required for muscle precursor migration along a lateral pathway into the limb. *Development (Cambridge, England)*, 127(2):413–24, January 2000. ISSN

0950-1991. URL http://www.ncbi.nlm.nih.gov/pubmed/10603357.

J Hartikka, L Sukhu, C Buchner, D Hazard, V Bozoukova, M Margalith, W K Nishioka, C J Wheeler, M Manthorp, and M Sawdey. Electroporation-facilitated delivery of plasmid DNA in skeletal muscle: plasmid dependence of muscle damage and effect of poloxamer 188. *Molecular therapy : the journal of the American Society of Gene Therapy*, 4(5):407–15, November 2001. ISSN 1525-0016. doi: 10.1006/mthe.2001.0483. URL http://www.ncbi.nlm.nih.gov/pubmed/11708877.

T J Hinterberger, D A Sassoon, S J Rhodes, and S F Konieczny. Expression of the muscle regulatory factor MRF4 during somite and skeletal myofiber development. *Developmental biology*, 147(1):144–56, September 1991. ISSN 0012-1606. URL http://www.ncbi.nlm.nih.gov/pubmed/1715299.

David A Hutcheson, Jia Zhao, Allyson Merrell, Malay Haldar, and Gabrielle Kardon. Embryonic and fetal limb myogenic cells are derived from developmentally distinct progenitors and have different requirements for beta-catenin. *Genes & development*, 23(8):997–1013, April 2009a. ISSN 1549-5477. doi: 10.1101/gad.1769009. URL http://www.pubmedcentral.nih.gov/articlerender.fcgi?artid=2675868&tool=pmcentrez&rendertype=abstract.

David A Hutcheson, Jia Zhao, Allyson Merrell, Malay Haldar, and Gabrielle Kardon. Embryonic and fetal limb myogenic cells are derived from developmentally distinct progenitors and have different requirements for beta-catenin. *Genes & development*, 23(8):997–1013, April 2009b. ISSN 1549-5477. doi: 10.1101/gad.1769009. URL http://www.pubmedcentral.nih.gov/articlerender.fcgi?artid=2675868&tool=pmcentrez&rendertype=abstract.

B Kablar, K Krastel, C Ying, A Asakura, S J Tapscott, and M A Rudnicki. MyoD and Myf-5 differentially regulate the development of limb versus trunk skeletal muscle. *Development (Cambridge, England)*, 124(23):4729–38, December 1997. ISSN 0950-1991. URL http://www.ncbi.nlm.nih.gov/pubmed/9428409.

Jennifer R Knapp, Judith K Davie, Anita Myer, Eric Meadows, Eric N Olson, and William H Klein. Loss of myogenin in postnatal life leads to normal skeletal muscle but reduced body size. *Development (Cambridge, England)*, 133(4): 601–10, February 2006. ISSN 0950-1991. doi: 10.1242/dev.02249. URL `http://www.ncbi.nlm.nih.gov/pubmed/16407395`.

Tatiana Y Kostrominova, Douglas E Dow, Robert G Dennis, Richard A Miller, and John A Faulkner. Comparison of gene expression of 2-mo denervated, 2-mo stimulated-denervated, and control rat skeletal muscles. *Physiological genomics*, 22 (2):227–43, July 2005. ISSN 1531-2267. doi: 10.1152/physiolgenomics.00210.2004. URL `http://www.ncbi.nlm.nih.gov/pubmed/15840640`.

M Krüger, D Mennerich, S Fees, R Schäfer, S Mundlos, and T Braun. Sonic hedgehog is a survival factor for hypaxial muscles during mouse development. *Development (Cambridge, England)*, 128(5):743–52, March 2001. ISSN 0950-1991. URL `http://www.ncbi.nlm.nih.gov/pubmed/11171399`.

W A Kues, B Sakmann, and V Witzemann. Differential expression patterns of five acetylcholine receptor subunit genes in rat muscle during development. *The European journal of neuroscience*, 7(6):1376–85, June 1995. ISSN 0953-816X. URL `http://www.ncbi.nlm.nih.gov/pubmed/7582112`.

Christine Laclef, Ghislaine Hamard, Josiane Demignon, Evelyne Souil, Christophe Houbron, and Pascal Maire. Altered myogenesis in Six1-deficient mice. *Development (Cambridge, England)*, 130(10):2239–52, May 2003. ISSN 0950-1991. URL `http://www.ncbi.nlm.nih.gov/pubmed/12668636`.

Pierre Lefesvre, Joline Attema, and Dirk van Bekkum. A comparison of efficacy and toxicity between electroporation and adenoviral gene transfer. *BMC molecular biology*, 3:12, August 2002. ISSN 1471-2199. URL `http://www.pubmedcentral.nih.gov/articlerender.fcgi?artid=122059&tool=pmcentrez&rendertype=abstract`.

Christoph Lepper, Simon J Conway, and Chen-Ming Fan. Adult satellite cells and embryonic muscle progenitors have distinct genetic requirements. *Nature*, 460(7255):627–31, July 2009. ISSN 1476-4687. doi: 10.1038/nature08209. URL http://www.pubmedcentral.nih.gov/articlerender.fcgi?artid=2767162&tool=pmcentrez&rendertype=abstract.

L Li, J C Chambard, M Karin, and E N Olson. Fos and Jun repress transcriptional activation by myogenin and MyoD: the amino terminus of Jun can mediate repression. *Genes Dev*, 6(4):676–689, 1992. URL http://www.ncbi.nlm.nih.gov/pubmed/1313772.

Yewei Liu, William R Randall, and Martin F Schneider. Activity-dependent and -independent nuclear fluxes of HDAC4 mediated by different kinases in adult skeletal muscle. *The Journal of cell biology*, 168(6):887–97, March 2005. ISSN 0021-9525. doi: 10.1083/jcb.200408128. URL http://www.pubmedcentral.nih.gov/articlerender.fcgi?artid=2171787&tool=pmcentrez&rendertype=abstract.

B S Mankoo, N S Collins, P Ashby, E Grigorieva, L H Pevny, A Candia, C V Wright, P W Rigby, and V Pachnis. Mox2 is a component of the genetic hierarchy controlling limb muscle development. *Nature*, 400(6739):69–73, July 1999. ISSN 0028-0836. doi: 10.1038/21892. URL http://www.ncbi.nlm.nih.gov/pubmed/10403250.

Sania Mazhar and Ruth Herbst. The formation of complex acetylcholine receptor clusters requires MuSK kinase activity and structural information from the MuSK extracellular domain. *Molecular and cellular neurosciences*, 49(4):475–86, April 2012. ISSN 1095-9327. doi: 10.1016/j.mcn.2011.12.007. URL http://www.pubmedcentral.nih.gov/articlerender.fcgi?artid=3359500&tool=pmcentrez&rendertype=abstract.

Timothy A McKinsey, Chun Li Zhang, and Eric N Olson. Signaling chromatin to make muscle. *Current opinion in cell biology*, 14(6):763–72, December 2002. ISSN 0955-0674. URL http://www.ncbi.nlm.nih.gov/pubmed/12473352.

J P Merlie. Biogenesis of the acetylcholine receptor, a multisubunit integral membrane protein. *Cell*, 36(3):573–5, March 1984. ISSN 0092-8674. URL http://www.ncbi.nlm.nih.gov/pubmed/6697388.

J P Merlie and J R Sanes. Concentration of acetylcholine receptor mRNA in synaptic regions of adult muscle fibres. *Nature*, 317(6032):66–8. ISSN 0028-0836. URL http://www.ncbi.nlm.nih.gov/pubmed/3839905.

J P Merlie, K E Isenberg, S D Russell, and J R Sanes. Denervation supersensitivity in skeletal muscle: analysis with a cloned cDNA probe. *The Journal of cell biology*, 99(1 Pt 1):332–5, July 1984. ISSN 0021-9525. URL http://www.pubmedcentral.nih.gov/articlerender.fcgi?artid=2275635&tool=pmcentrez&rendertype=abstract.

J P Merlie, J Mudd, T C Cheng, and E N Olson. Myogenin and acetylcholine receptor alpha gene promoters mediate transcriptional regulation in response to motor innervation. *The Journal of biological chemistry*, 269(4):2461–7, January 1994. ISSN 0021-9258. URL http://www.ncbi.nlm.nih.gov/pubmed/8300573.

J H Miner and B Wold. Herculin, a fourth member of the MyoD family of myogenic regulatory genes. *Proceedings of the National Academy of Sciences of the United States of America*, 87(3):1089–93, February 1990. ISSN 0027-8424. URL http://www.pubmedcentral.nih.gov/articlerender.fcgi?artid=53416&tool=pmcentrez&rendertype=abstract.

L M Mir, M F Bureau, J Gehl, R Rangara, D Rouy, J M Caillaud, P Delaere, D Branellec, B Schwartz, and D Scherman. High-efficiency gene transfer into skeletal muscle mediated by electric pulses. *Proceedings of the National Academy of Sciences of the United States of America*, 96(8):4262–7, April 1999. ISSN 0027-8424. URL http://www.pubmedcentral.nih.gov/articlerender.fcgi?artid=16320&tool=pmcentrez&rendertype=abstract.

Viviana Moresi, Andrew H Williams, Eric Meadows, Jesse M Flynn, Matthew J

Potthoff, John McAnally, John M Shelton, Johannes Backs, William H Klein, James A Richardson, Rhonda Bassel-Duby, and Eric N Olson. Myogenin and class II HDACs control neurogenic muscle atrophy by inducing E3 ubiquitin ligases. *Cell*, 143(1):35–45, October 2010. ISSN 1097-4172. doi: 10.1016/j.cell.2010.09.004. URL http://www.pubmedcentral.nih.gov/articlerender.fcgi?artid=2982779&tool=pmcentrez&rendertype=abstract.

Jongmin Nam, Ping Dong, Ryan Tarpine, Sorin Istrail, and Eric H Davidson. Functional cis-regulatory genomics for systems biology. *Proceedings of the National Academy of Sciences of the United States of America*, 107(8):3930–5, February 2010. ISSN 1091-6490. doi: 10.1073/pnas.1000147107. URL http://www.pubmedcentral.nih.gov/articlerender.fcgi?artid=2840491&tool=pmcentrez&rendertype=abstract.

Paola Oliveri, Qiang Tu, and Eric H Davidson. Global regulatory logic for specification of an embryonic cell lineage. *Proceedings of the National Academy of Sciences of the United States of America*, 105(16):5955–62, April 2008. ISSN 1091-6490. doi: 10.1073/pnas.0711220105. URL http://www.pubmedcentral.nih.gov/articlerender.fcgi?artid=2329687&tool=pmcentrez&rendertype=abstract.

A Patapoutian, J H Miner, G E Lyons, and B Wold. Isolated sequences from the linked Myf-5 and MRF4 genes drive distinct patterns of muscle-specific expression in transgenic mice. *Development (Cambridge, England)*, 118(1):61–9, May 1993. ISSN 0950-1991. URL http://www.ncbi.nlm.nih.gov/pubmed/8375340.

Isabelle S Peter and Eric H Davidson. Genomic control of patterning. *The International journal of developmental biology*, 53(5-6):707–16, January 2009. ISSN 1696-3547. doi: 10.1387/ijdb.072495ip. URL http://www.ncbi.nlm.nih.gov/pubmed/19378258.

J Piette, J L Bessereau, M Huchet, and J P Changeux. Two adjacent MyoD1-binding sites regulate expression of the acetylcholine receptor alpha-subunit gene.

Nature, 345(6273):353–5, May 1990. ISSN 0028-0836. doi: 10.1038/345353a0. URL http://www.ncbi.nlm.nih.gov/pubmed/2342565.

J Piette, M Huchet, D Houzelstein, and J P Changeux. Compartmentalized expression of the alpha- and gamma-subunits of the acetylcholine receptor in recently fused myofibers. *Developmental biology*, 157(1):205–13, May 1993. ISSN 0012-1606. doi: 10.1006/dbio.1993.1124. URL http://www.ncbi.nlm.nih.gov/pubmed/8482411.

Popesko P, Rajtova V, Horak J, Kapeller K. *A Color Atlas of Anatomy of Small Laboratory Animals: Mouse, the Rat, the Hamster v.2.* Mosby, 1992. ISBN 9780723418238.

C A Prody and J P Merlie. A developmental and tissue-specific enhancer in the mouse skeletal muscle acetylcholine receptor alpha-subunit gene regulated by myogenic factors. *The Journal of biological chemistry*, 266(33):22588–96, November 1991. ISSN 0021-9258. URL http://www.ncbi.nlm.nih.gov/pubmed/1658001.

Anna Raffaello, Paolo Laveder, Chiara Romualdi, Camilla Bean, Luana Toniolo, Elena Germinario, Aram Megighian, Daniela Danieli-Betto, Carlo Reggiani, and Gerolamo Lanfranchi. Denervation in murine fast-twitch muscle: short-term physiological changes and temporal expression profiling. *Physiological genomics*, 25(1): 60–74, March 2006. ISSN 1531-2267. doi: 10.1152/physiolgenomics.00051.2005. URL http://www.ncbi.nlm.nih.gov/pubmed/16380408.

Frédéric Relaix, Didier Rocancourt, Ahmed Mansouri, and Margaret Buckingham. Divergent functions of murine Pax3 and Pax7 in limb muscle development. *Genes & development*, 18(9):1088–105, May 2004. ISSN 0890-9369. doi: 10.1101/gad.301004. URL http://www.pubmedcentral.nih.gov/articlerender.fcgi?artid=406297&tool=pmcentrez&rendertype=abstract.

Frédéric Relaix, Didier Rocancourt, Ahmed Mansouri, and Margaret Buckingham. A Pax3/Pax7-dependent population of skeletal muscle progenitor cells. *Nature*,

435(7044):948–53, June 2005. ISSN 1476-4687. doi: 10.1038/nature03594. URL http://www.ncbi.nlm.nih.gov/pubmed/15843801.

Frédéric Relaix, Didier Montarras, Stéphane Zaffran, Barbara Gayraud-Morel, Didier Rocancourt, Shahragim Tajbakhsh, Ahmed Mansouri, Ana Cumano, and Margaret Buckingham. Pax3 and Pax7 have distinct and overlapping functions in adult muscle progenitor cells. *The Journal of cell biology*, 172(1):91–102, January 2006. ISSN 0021-9525. doi: 10.1083/jcb.200508044. URL http://www.pubmedcentral.nih.gov/articlerender.fcgi?artid=2063537&tool=pmcentrez&rendertype=abstract.

Roger Revilla-i Domingo, Takuya Minokawa, and Eric H Davidson. R11: a cis-regulatory node of the sea urchin embryo gene network that controls early expression of SpDelta in micromeres. *Developmental biology*, 274(2):438–51, October 2004. ISSN 0012-1606. doi: 10.1016/j.ydbio.2004.07.008. URL http://www.ncbi.nlm.nih.gov/pubmed/15385170.

Anne-Françoise Richard, Josiane Demignon, Iori Sakakibara, Julien Pujol, Maryline Favier, Laure Strochlic, Fabien Le Grand, Nicolas Sgarioto, Anthony Guernec, Alain Schmitt, Nicolas Cagnard, Ruijin Huang, Claire Legay, Isabelle Guillet-Deniau, and Pascal Maire. Genesis of muscle fiber-type diversity during mouse embryogenesis relies on Six1 and Six4 gene expression. *Developmental biology*, 359 (2):303–20, November 2011. ISSN 1095-564X. doi: 10.1016/j.ydbio.2011.08.010. URL http://www.ncbi.nlm.nih.gov/pubmed/21884692.

M Sachs, H Brohmann, D Zechner, T Müller, J Hülsken, I Walther, U Schaeper, C Birchmeier, and W Birchmeier. Essential role of Gab1 for signaling by the c-Met receptor in vivo. *The Journal of cell biology*, 150(6):1375–84, September 2000. ISSN 0021-9525. URL http://www.pubmedcentral.nih.gov/articlerender.fcgi?artid=2150711&tool=pmcentrez&rendertype=abstract.

A Sandow. Excitation-contraction coupling in muscular response. *The Yale*

journal of biology and medicine, 25(3):176–201, December 1952. ISSN 0044-0086. URL http://www.pubmedcentral.nih.gov/articlerender.fcgi?artid=2599245&tool=pmcentrez&rendertype=abstract.

J R Sanes, Y R Johnson, P T Kotzbauer, J Mudd, T Hanley, J C Martinou, and J P Merlie. Selective expression of an acetylcholine receptor-lacZ transgene in synaptic nuclei of adult muscle fibers. *Development (Cambridge, England)*, 113(4):1181–91, December 1991. ISSN 0950-1991. URL http://www.ncbi.nlm.nih.gov/pubmed/1811935.

P Sassone-Corsi, L J Ransone, W W Lamph, and I M Verma. Direct interaction between fos and jun nuclear oncoproteins: role of the 'leucine zipper' domain. *Nature*, 336(6200):692–5, December 1988. ISSN 0028-0836. doi: 10.1038/336692a0. URL http://www.ncbi.nlm.nih.gov/pubmed/3143919.

K Schäfer and T Braun. Early specification of limb muscle precursor cells by the homeobox gene Lbx1h. *Nature genetics*, 23(2):213–6, October 1999. ISSN 1061-4036. doi: 10.1038/13843. URL http://www.ncbi.nlm.nih.gov/pubmed/10508520.

Deborah Scheffer, Cyrille Sage, Paola V Plazas, Mingqian Huang, Carolina Wedemeyer, Duan-Sun Zhang, Zheng-Yi Chen, A Belen Elgoyhen, David P Corey, and Veronique Pingault. The $\alpha 1$ subunit of nicotinic acetylcholine receptors in the inner ear: transcriptional regulation by ATOH1 and co-expression with the γ subunit in hair cells. *Journal of neurochemistry*, 103(6):2651–64, December 2007. ISSN 1471-4159. doi: 10.1111/j.1471-4159.2007.04980.x. URL http://www.ncbi.nlm.nih.gov/pubmed/17961150.

S Schiaffino and C Reggiani. Myosin isoforms in mammalian skeletal muscle. *Journal of applied physiology (Bethesda, Md. : 1985)*, 77(2):493–501, August 1994. ISSN 8750-7587. URL http://www.ncbi.nlm.nih.gov/pubmed/8002492.

A M Simon and S J Burden. An E box mediates activation and repression of the acetylcholine receptor delta-subunit gene during myogenesis.

Molecular and cellular biology, 13(9):5133–40, September 1993. ISSN 0270-7306. URL http://www.pubmedcentral.nih.gov/articlerender.fcgi?artid=360201&tool=pmcentrez&rendertype=abstract.

A M Simon, P Hoppe, and S J Burden. Spatial restriction of AChR gene expression to subsynaptic nuclei. *Development (Cambridge, England)*, 114(3):545–53, March 1992. ISSN 0950-1991. URL http://www.ncbi.nlm.nih.gov/pubmed/1618127.

Yi-Hsien Su, Enhu Li, Gary K Geiss, William J R Longabaugh, Alexander Krämer, and Eric H Davidson. A perturbation model of the gene regulatory network for oral and aboral ectoderm specification in the sea urchin embryo. *Developmental biology*, 329(2):410–21, May 2009. ISSN 1095-564X. doi: 10.1016/j.ydbio.2009.02.029. URL http://www.pubmedcentral.nih.gov/articlerender.fcgi?artid=2677136&tool=pmcentrez&rendertype=abstract.

I P Sugar and E Neumann. Stochastic model for electric field-induced membrane pores. Electroporation. *Biophysical chemistry*, 19(3):211–25, May 1984. ISSN 0301-4622. URL http://www.ncbi.nlm.nih.gov/pubmed/6722274.

S Tajbakhsh, D Rocancourt, G Cossu, and M Buckingham. Redefining the genetic hierarchies controlling skeletal myogenesis: Pax-3 and Myf-5 act upstream of MyoD. *Cell*, 89(1):127–38, April 1997. ISSN 0092-8674. URL http://www.ncbi.nlm.nih.gov/pubmed/9094721.

Huibin Tang and Daniel Goldman. Activity-dependent gene regulation in skeletal muscle is mediated by a histone deacetylase (HDAC)-Dach2-myogenin signal transduction cascade. *Proceedings of the National Academy of Sciences of the United States of America*, 103(45):16977–82, November 2006. ISSN 0027-8424. doi: 10.1073/pnas.0601565103. URL http://www.pubmedcentral.nih.gov/articlerender.fcgi?artid=1636564&tool=pmcentrez&rendertype=abstract.

Huibin Tang, Peter Macpherson, Michael Marvin, Eric Meadows, William H Klein, Xiang-Jiao Yang, and Daniel Goldman. A histone deacetylase 4/myogenin posi-

tive feedback loop coordinates denervation-dependent gene induction and suppression. *Molecular biology of the cell*, 20(4):1120–31, February 2009. ISSN 1939-4586. doi: 10.1091/mbc.E08-07-0759. URL http://www.pubmedcentral.nih.gov/articlerender.fcgi?artid=2642751&tool=pmcentrez&rendertype=abstract.

Y Taniyama, K Tachibana, K Hiraoka, M Aoki, S Yamamoto, K Matsumoto, T Nakamura, T Ogihara, Y Kaneda, and R Morishita. Development of safe and efficient novel nonviral gene transfer using ultrasound: enhancement of transfection efficiency of naked plasmid DNA in skeletal muscle. *Gene therapy*, 9 (6):372–80, March 2002. ISSN 0969-7128. doi: 10.1038/sj.gt.3301678. URL http://www.ncbi.nlm.nih.gov/pubmed/11960313.

S J Tapscott, R L Davis, M J Thayer, P F Cheng, H Weintraub, and A B Lassar. MyoD1: a nuclear phosphoprotein requiring a Myc homology region to convert fibroblasts to myoblasts. *Science (New York, N.Y.)*, 242(4877):405–11, October 1988. ISSN 0036-8075. URL http://www.ncbi.nlm.nih.gov/pubmed/3175662.

Jeanine A Ursitti, Pervis C Lee, Wendy G Resneck, Minda M McNally, Amber L Bowman, Andrea O'Neill, Michele R Stone, and Robert J Bloch. Cloning and characterization of cytokeratins 8 and 19 in adult rat striated muscle. Interaction with the dystrophin glycoprotein complex. *The Journal of biological chemistry*, 279 (40):41830–8, October 2004. ISSN 0021-9258. doi: 10.1074/jbc.M400128200. URL http://www.ncbi.nlm.nih.gov/pubmed/15247274.

Xiaoxia Wang, Chris Blagden, Jihua Fan, Scott J Nowak, Ichiro Taniuchi, Dan R Littman, and Steven J Burden. Runx1 prevents wasting, myofibrillar disorganization, and autophagy of skeletal muscle. *Genes & development*, 19(14):1715–22, July 2005. ISSN 0890-9369. doi: 10.1101/gad.1318305. URL http://www.pubmedcentral.nih.gov/articlerender.fcgi?artid=1176009&tool=pmcentrez&rendertype=abstract.

Zhong Wang, Mark Gerstein, and Michael Snyder. RNA-Seq: a revolutionary tool

for transcriptomics. *Nature reviews. Genetics*, 10(1):57–63, January 2009. ISSN 1471-0064. doi: 10.1038/nrg2484. URL http://www.pubmedcentral.nih.gov/articlerender.fcgi?artid=2949280&tool=pmcentrez&rendertype=abstract.

Sø ren Warming, Nina Costantino, Donald L Court, Nancy a Jenkins, and Neal G Copeland. Simple and highly efficient BAC recombineering using galK selection. *Nucleic acids research*, 33(4):e36, January 2005. ISSN 1362-4962. doi: 10.1093/nar/gni035. URL http://www.pubmedcentral.nih.gov/articlerender.fcgi?artid=549575&tool=pmcentrez&rendertype=abstract.

H Weintraub, R Davis, S Tapscott, M Thayer, M Krause, R Benezra, T K Blackwell, D Turner, R Rupp, and S Hollenberg. The myoD gene family: nodal point during specification of the muscle cell lineage. *Science (New York, N.Y.)*, 251(4995):761–6, February 1991a. ISSN 0036-8075. URL http://www.ncbi.nlm.nih.gov/pubmed/1846704.

H Weintraub, V J Dwarki, I Verma, R Davis, S Hollenberg, L Snider, A Lassar, and S J Tapscott. Muscle-specific transcriptional activation by MyoD. *Genes & development*, 5(8):1377–86, August 1991b. ISSN 0890-9369. URL http://www.ncbi.nlm.nih.gov/pubmed/1651276.

J A Wolff, R W Malone, P Williams, W Chong, G Acsadi, A Jani, and P L Felgner. Direct gene transfer into mouse muscle in vivo. *Science (New York, N.Y.)*, 247 (4949 Pt 1):1465–8, March 1990. ISSN 0036-8075. URL http://www.ncbi.nlm.nih.gov/pubmed/1690918.

Z Yablonka-Reuveni and R A Seifert. Proliferation of chicken myoblasts is regulated by specific isoforms of platelet-derived growth factor: evidence for differences between myoblasts from mid and late stages of embryogenesis. *Developmental biology*, 156(2):307–18, April 1993. ISSN 0012-1606. doi: 10.1006/dbio.1993.1079. URL http://www.ncbi.nlm.nih.gov/pubmed/8462733.

Jihua Yao, Jingyao Zhou, Qiaoling Liu, Daru Lu, Lu Wang, Xiaojing Qiao,

and William Jia. Atoh8, a bHLH transcription factor, is required for the development of retina and skeletal muscle in zebrafish. *PloS one*, 5 (6):e10945, January 2010. ISSN 1932-6203. doi: 10.1371/journal.pone.0010945. URL http://www.pubmedcentral.nih.gov/articlerender.fcgi?artid=2880597&tool=pmcentrez&rendertype=abstract.

M Zhang, K Koishi, and I S McLennan. Skeletal muscle fibre types: detection methods and embryonic determinants. *Histology and histopathology*, 13(1):201–7, January 1998. ISSN 0213-3911. URL http://www.ncbi.nlm.nih.gov/pubmed/9476649.

W Zhang, R R Behringer, and E N Olson. Inactivation of the myogenic bHLH gene MRF4 results in up-regulation of myogenin and rib anomalies. *Genes & development*, 9(11):1388–99, June 1995. ISSN 0890-9369. URL http://www.ncbi.nlm.nih.gov/pubmed/7797078.

Appendices

Appendix A

Control vs. mock denervated muscle: top 100 differentially expressed genes

Table A.1: 6.0hr up-regulated genes sorted by fold change. rpkm1 = mock; rpkm2 = control. log 2(fold change) = control/mock. rpkm = reads per kilobase per million base pairs.

gene symbol	**log2(fold change)**	**rpkm1**	**rpkm2**	**ENSEMBL ID**
Rpl23a	−3.22	241.1	95.6	ENSMUSG00000058546
Rpl31	−2.62	38.6	17.8	ENSMUSG00000073702
Rpl32-ps	−2.33	32.3	13.5	ENSMUSG00000068969
Gm11826	−2.27	104.5	27.8	ENSMUSG00000083328
Rpl17	−2.15	41	21.5	ENSMUSG00000062328
Gm5526	−2.06	118	80.7	ENSMUSG00000084817
Gm16276	−2	69.8	15.8	ENSMUSG00000084755
Atp5k	−1.97	227.6	50.1	ENSMUSG00000050856
Gm13365	−1.95	8.5	4.7	ENSMUSG00000082632
Rpl35a	−1.84	192.4	56.8	ENSMUSG00000060636
Gm11918	−1.72	142.6	41.4	ENSMUSG00000080911
Gm15776	−1.68	159.6	63.7	ENSMUSG00000082241

Table A.1: 6.0hr up-regulated genes sorted by fold change. rpkm1 = mock; rpkm2 = control. log 2(fold change) = control/mock. rpkm = reads per kilobase per million base pairs.

gene symbol	**log2(fold change)**	**rpkm1**	**rpkm2**	**ENSEMBL ID**
Myh4	−1.67	340.6	129.1	ENSMUSG00000057003
Gm14303	−1.64	1,078.70	326.1	ENSMUSG00000081344
Gm14539	−1.63	1,118.80	354.9	ENSMUSG00000084830
Uqcr11	−1.6	586.5	185.2	ENSMUSG00000020163
Myl6	−1.58	70.3	35.2	ENSMUSG00000090841
C920021L13Rik	−1.53	13.8	3.5	ENSMUSG00000080727
Gm9846	−1.46	897.3	773.4	ENSMUSG00000050621
Rps21	−1.45	682.8	277.3	ENSMUSG00000039001
G0s2	−1.45	19.7	6.9	ENSMUSG00000009633
Gapdh	−1.42	183.1	112.2	ENSMUSG00000057666
Gm5560	−1.38	32.6	15.3	ENSMUSG00000067161
Gm14450	−1.36	878.8	343	ENSMUSG00000081661
Gm12338	−1.36	3,251.80	1,679.70	ENSMUSG00000081485
Rpl18a	−1.34	159.6	62.2	ENSMUSG00000045128
Gm12389	−1.3	326.9	125.9	ENSMUSG00000081352
Usmg5	−1.3	65.2	25.2	ENSMUSG00000071528
Hist1h4i	−1.27	18.5	9.1	ENSMUSG00000060639
Gm6265	−1.25	2,000.10	911.9	ENSMUSG00000066491
Arntl	−1.25	6.6	2.8	ENSMUSG00000055116
Gm16379	−1.21	40	18.7	ENSMUSG00000059658
Gm9763	−1.19	136.1	59	ENSMUSG00000037438
Gm16124	−1.18	23.8	10.4	ENSMUSG00000086914
Gm6181	−1.16	152.2	72.7	ENSMUSG00000074092
Oaz1	−1.14	434.5	273.3	ENSMUSG00000035242
Gm4604	−1.13	340.9	271	ENSMUSG00000091845

Table A.1: 6.0hr up-regulated genes sorted by fold change. rpkm1 = mock; rpkm2 = control. log 2(fold change) = control/mock. rpkm = reads per kilobase per million base pairs.

gene symbol	**log2(fold change)**	**rpkm1**	**rpkm2**	**ENSEMBL ID**
Gm6415	−1.12	276.7	120.2	ENSMUSG00000083820
2900053A13Rik	−1.12	17.5	8.1	ENSMUSG00000087687
Gm7536	−1.11	626.3	466.7	ENSMUSG00000057036
Gm5829	−1.1	30.8	15.3	ENSMUSG00000067744
Gm9493	−1.1	309.2	184.9	ENSMUSG00000044424
Ndufs5	−1.08	204.9	103.1	ENSMUSG00000028648
Ldha-ps2	−1.06	133.5	109.4	ENSMUSG00000083836
Rpsa-ps4	−1.06	33.4	16.1	ENSMUSG00000081076
Tnfrsf12a	−1.06	48.4	21	ENSMUSG00000023905
Apoo	−1.05	32.1	18.7	ENSMUSG00000079508
Snrpd2	−1.05	89.3	46.5	ENSMUSG00000040824
Msrb2	−1.04	10.9	5.5	ENSMUSG00000023094
Gm10039	−1.02	1,063.20	569.9	ENSMUSG00000091478
Psenen	−1.02	37.7	22.4	ENSMUSG00000036835
Rpl30	−1.02	250.5	105.6	ENSMUSG00000058600
Ift27	−1.01	20.3	10.1	ENSMUSG00000016637
Gm14706	−1.01	155.2	77.4	ENSMUSG00000083482
Cox7b	−0.99	1,682.20	974.7	ENSMUSG00000031231
Gm8017	−0.98	349.9	234.9	ENSMUSG00000063427
A330094K24Rik	−0.98	16.9	8.4	ENSMUSG00000090400
Gm11808	−0.96	757.4	411.4	ENSMUSG00000068240
Gm6293	−0.95	137.5	71.1	ENSMUSG00000051133
Gm11221	−0.92	46.3	25.4	ENSMUSG00000082998
Tnmd	−0.91	26	13.4	ENSMUSG00000031250
Hist1h4h	−0.91	113.8	58.4	ENSMUSG00000060981

Table A.1: 6.0hr up-regulated genes sorted by fold change. rpkm1 = mock; rpkm2 = control. log 2(fold change) = control/mock. rpkm = reads per kilobase per million base pairs.

gene symbol	**log2(fold change)**	**rpkm1**	**rpkm2**	**ENSEMBL ID**
2810001G20Rik	−0.9	12.9	7.1	ENSMUSG00000087497
B330016D10Rik	−0.9	9.6	4.9	ENSMUSG00000048406
Mgst3	−0.89	267	143.3	ENSMUSG00000026688
Gm15430	−0.89	1,469.40	906.4	ENSMUSG00000036305
Gm3724	−0.88	156.7	86.7	ENSMUSG00000061468
Gm8659	−0.87	310	189.4	ENSMUSG00000082076
Rplp2	−0.87	66.3	36.9	ENSMUSG00000025508
S100a1	−0.86	340.5	177.7	ENSMUSG00000044080
Riiad1	−0.86	40.2	22	ENSMUSG00000028139
Romo1	−0.86	221.6	138.7	ENSMUSG00000067847
Gm10196	−0.86	228.9	115.4	ENSMUSG00000067058
2310075C17Rik	−0.86	90.2	50	ENSMUSG00000089718
Gm14088	−0.86	509.9	271.5	ENSMUSG00000081413
Lsmd1	−0.85	59.8	36.3	ENSMUSG00000059278
Ost4	−0.85	72.2	43	ENSMUSG00000038803
Tmem150c	−0.85	6.5	2.7	ENSMUSG00000050640
Map1lc3a	−0.85	418.3	229.8	ENSMUSG00000027602
Myl1	−0.84	8,190.60	4,609.10	ENSMUSG00000061816
Rps25-ps1	−0.84	414.4	210.9	ENSMUSG00000067344
Klf10	−0.84	6.2	3.5	ENSMUSG00000037465
Atp5o	−0.84	404.3	231.4	ENSMUSG00000022956
Gm15920	−0.84	623.5	346.4	ENSMUSG00000080893
Rpl22l1	−0.83	49.2	31.3	ENSMUSG00000039221
Nedd8	−0.83	186.6	105.4	ENSMUSG00000010376
Klk1b26	−0.83	49.8	29.1	ENSMUSG00000053719

Table A.1: 6.0hr up-regulated genes sorted by fold change. rpkm1 = mock; rpkm2 = control. log 2(fold change) = control/mock. rpkm = reads per kilobase per million base pairs.

gene symbol	**log2(fold change)**	**rpkm1**	**rpkm2**	**ENSEMBL ID**
Bloc1s1	−0.83	123.9	76.6	ENSMUSG00000090247
Rpl36-ps2	−0.83	194.1	89.6	ENSMUSG00000024205
Gm8430	−0.82	471.4	308.8	ENSMUSG00000055093
Pebp1	−0.82	181	99.6	ENSMUSG00000032959
Nudt8	−0.82	29	15.9	ENSMUSG00000024869
Scg3	−0.82	6.9	3.9	ENSMUSG00000032181
Gm16418	−0.82	423.1	230.1	ENSMUSG00000084093
Gm12693	−0.82	146.4	88.4	ENSMUSG00000083179
Ddt	−0.81	69	42.7	ENSMUSG00000001666
Glb1l2	−0.81	5.2	3	ENSMUSG00000036395
Gm4799	−0.81	29.8	15.8	ENSMUSG00000071151
Chchd1	−0.8	240.7	129.4	ENSMUSG00000063787
Sepx1	−0.8	230.3	128	ENSMUSG00000075705

Table A.2: 12.0hr up-regulated genes sorted by fold change. rpkm1 = mock; rpkm2 = control. log 2(fold change) = control/mock. rpkm = reads per kilobase per million base pairs.

gene symbol	**log2(fold change)**	**rpkm1**	**rpkm2**	**ENSEMBL ID**
Gm10020	−4.4	118.6	63.2	ENSMUSG00000057262
Gm6635	−4.1	5.7	0.22	ENSMUSG00000058607
Gm15148	−4.1	21	0.9	ENSMUSG00000082423
S100g	−3.6	11.3	0.55	ENSMUSG00000040808
Gm5786	−3.2	91	69.8	ENSMUSG00000066487
Gm11918	−2.8	261.3	43.01	ENSMUSG00000080911
Gm9846	−2.8	1,492.60	800.97	ENSMUSG00000050621
Gm14303	−2.7	2,057.50	338.26	ENSMUSG00000081344
Gm6644	−2.6	128.6	80.41	ENSMUSG00000073674
G0s2	−2.6	55.3	7.17	ENSMUSG00000009633
Gm12191	−2.6	370.4	321.52	ENSMUSG00000083061
Ankrd2	−2.5	437.6	74.59	ENSMUSG00000025172
Gm4604	−2.5	478.7	281.09	ENSMUSG00000091845
Tnfrsf12a	−2.5	131	21.79	ENSMUSG00000023905
Gm13253	−2.4	124.8	113.07	ENSMUSG00000083757
Gm14337	−2.3	1,627.70	324.58	ENSMUSG00000081700
Atp5k	−2.2	256.5	51.93	ENSMUSG00000050856
Gm9844	−2.1	28.3	5.51	ENSMUSG00000050347
Mybph	−2.1	229.6	50.87	ENSMUSG00000042451
Gm14539	−2.1	1,585.50	367.28	ENSMUSG00000084830
Gm13433	−2	57.4	16.13	ENSMUSG00000083043
Spinkl	−2	7.7	1.61	ENSMUSG00000053729
Gm12497	−2	185	43.93	ENSMUSG00000049231
Inmt	−2	65.3	17.14	ENSMUSG00000003477

Table A.2: 12.0hr up-regulated genes sorted by fold change. rpkm1 = mock; rpkm2 = control. log 2(fold change) = control/mock. rpkm = reads per kilobase per million base pairs.

gene symbol	**log2(fold change)**	**rpkm1**	**rpkm2**	**ENSEMBL ID**
Gm15501	−2	260.2	148.78	ENSMUSG00000087412
Rplp2	−1.9	135.7	38.25	ENSMUSG00000025508
Gm11826	−1.9	109.5	28.77	ENSMUSG00000083328
Gm15459	−1.8	350.2	260.19	ENSMUSG00000083840
Rpl31	−1.8	37	18.52	ENSMUSG00000073702
Gm5526	−1.8	122.2	83.76	ENSMUSG00000084817
Gm12599	−1.8	11.6	7.1	ENSMUSG00000081325
Gm14567	−1.8	387.8	102.22	ENSMUSG00000080896
Gm10036	−1.8	194.5	123.73	ENSMUSG00000058064
Gm6293	−1.8	211.8	73.88	ENSMUSG00000051133
Rpl35a	−1.8	206.3	58.93	ENSMUSG00000060636
Myl6	−1.8	77.1	36.49	ENSMUSG00000090841
Gm15776	−1.7	166	66.07	ENSMUSG00000082241
Ankrd1	−1.7	34.4	10.57	ENSMUSG00000024803
Scara5	−1.6	18.3	6.3	ENSMUSG00000022032
Klf10	−1.6	11.1	3.67	ENSMUSG00000037465
Gm6181	−1.6	196.5	75.47	ENSMUSG00000074092
Gsta3	−1.6	14.7	4.66	ENSMUSG00000025934
Gm7536	−1.6	756.8	482.94	ENSMUSG00000057036
Gck	−1.6	6.4	1.71	ENSMUSG00000041798
Rpl30	−1.6	354.8	109.67	ENSMUSG00000058600
Gm11222	−1.5	14.1	5.88	ENSMUSG00000085627
Nov	−1.5	55.5	19.56	ENSMUSG00000037362
Cxcl14	−1.5	68.2	24.27	ENSMUSG00000021508
Oaz1	−1.5	508.9	283.62	ENSMUSG00000035242

Table A.2: 12.0hr up-regulated genes sorted by fold change. rpkm1 = mock; rpkm2 = control. log 2(fold change) = control/mock. rpkm = reads per kilobase per million base pairs.

gene symbol	**log2(fold change)**	**rpkm1**	**rpkm2**	**ENSEMBL ID**
Twist1	−1.5	6.8	2.18	ENSMUSG00000035799
Gm9493	−1.5	333.3	191.81	ENSMUSG00000044424
Rps21	−1.5	826.1	287.84	ENSMUSG00000039001
Myoc	−1.5	264	90.26	ENSMUSG00000026697
Lmcd1	−1.5	639.9	210.9	ENSMUSG00000057604
Gm16276	−1.5	50.8	16.38	ENSMUSG00000084755
Gm15430	−1.4	2,435.50	939.34	ENSMUSG00000036305
Gm16418	−1.4	595	238.59	ENSMUSG00000084093
Igfbp6	−1.4	196.4	67.75	ENSMUSG00000023046
Snrpd2	−1.4	104.1	48.22	ENSMUSG00000040824
Gdf10	−1.4	12.7	5.19	ENSMUSG00000021943
Rpl23a	−1.4	206.1	99.11	ENSMUSG00000058546
Pcolce2	−1.3	35.2	11.27	ENSMUSG00000015354
Galntl2	−1.3	18.4	8.38	ENSMUSG00000021903
Cmklr1	−1.3	7.6	2.22	ENSMUSG00000042190
Pim1	−1.3	13.9	5.2	ENSMUSG00000024014
2900053A13Rik	−1.3	19.2	8.36	ENSMUSG00000087687
Gapdh	−1.3	204.2	116.18	ENSMUSG00000057666
Ndufs5	−1.3	233.2	106.94	ENSMUSG00000028648
Csrp3	−1.3	4,632.30	1,673.00	ENSMUSG00000030470
Serpina3n	−1.3	10.3	4.23	ENSMUSG00000021091
Gm16379	−1.3	44.8	19.38	ENSMUSG00000059658
Ms4a4d	−1.3	6.4	2.68	ENSMUSG00000024678
Dpep1	−1.3	12.3	5.07	ENSMUSG00000019278
4921517L17Rik	−1.3	6.2	2.81	ENSMUSG00000038085

Table A.2: 12.0hr up-regulated genes sorted by fold change. rpkm1 = mock; rpkm2 = control. log 2(fold change) = control/mock. rpkm = reads per kilobase per million base pairs.

gene symbol	**log2(fold change)**	**rpkm1**	**rpkm2**	**ENSEMBL ID**
Angptl7	−1.3	173.3	76.27	ENSMUSG00000028989
Wisp2	−1.3	15.1	5.34	ENSMUSG00000027656
Atp5l	−1.3	343.8	144.25	ENSMUSG00000038717
Sfrp4	−1.3	14.6	5.27	ENSMUSG00000021319
Gm8017	−1.3	420	244.03	ENSMUSG00000063427
Gm10705	−1.3	98.4	53.19	ENSMUSG00000074506
Rps17	−1.3	729.2	349.99	ENSMUSG00000061787
Zfp503	−1.2	20.8	8.1	ENSMUSG00000039081
Hist1h4h	−1.2	150.2	60.55	ENSMUSG00000060981
Timm23	−1.2	167.4	79.14	ENSMUSG00000013701
Usmg5	−1.2	74.8	26.07	ENSMUSG00000071528
Slc43a3	−1.2	16.8	8.79	ENSMUSG00000027074
Rps2	−1.2	544.4	257.36	ENSMUSG00000044533
2310030G06Rik	−1.2	14.3	6.3	ENSMUSG00000032062
Gm5406	−1.2	34.8	17.94	ENSMUSG00000080715
Pi16	−1.2	62.3	27.57	ENSMUSG00000024011
Gpx3	−1.2	253.4	107.41	ENSMUSG00000018339
Gm6415	−1.2	304.2	124.7	ENSMUSG00000083820
Gm6969	−1.2	142	68.87	ENSMUSG00000066553
Gm14450	−1.2	872	356.29	ENSMUSG00000081661
Gm5560	−1.1	31.3	15.86	ENSMUSG00000067161
Ier2	−1.1	10.3	4.63	ENSMUSG00000053560
Bloc1s1	−1.1	161.2	79.56	ENSMUSG00000090247
Fbln1	−1.1	16.5	7.89	ENSMUSG00000006369
Gm10196	−1.1	325.2	119.9	ENSMUSG00000067058

Table A.2: 12.0hr up-regulated genes sorted by fold change. rpkm1 = mock; rpkm2 = control. log 2(fold change) = control/mock. rpkm = reads per kilobase per million base pairs.

gene symbol	**log2(fold change)**	**rpkm1**	**rpkm2**	**ENSEMBL ID**
Serpinf1	−1.1	253.2	111.34	ENSMUSG00000000753

Table A.3: 6.0hr genes sorted by p-value. rpkm1 = mock; rpkm2 = control. log 2(fold change) = control/mock. rpkm = reads per kilobase per million base pairs. $p < 0.001$.

gene symbol	**log2(fold change)**	**rpkm1**	**rpkm2**	**ENSEMBL ID**
Krt2	11.16	$0.00E+00$	30.3	ENSMUSG00000064201
Lor	9.41	$2.80E-02$	26.4	ENSMUSG00000043165
Krt1	9.45	$0.00E+00$	20.8	ENSMUSG00000046834
Krt10	3.95	$2.50E+00$	40.9	ENSMUSG00000019761
Myh4	-1.67	$3.40E+02$	129.1	ENSMUSG00000057003
Rpl23a	-3.22	$2.40E+02$	95.6	ENSMUSG00000058546
Krt14	8.11	$0.00E+00$	13.4	ENSMUSG00000045545
Krt5	7.82	$0.00E+00$	8.5	ENSMUSG00000061527
Flg	7.64	$0.00E+00$	11.9	ENSMUSG00000091340
Perp	3.04	$1.20E+00$	10.5	ENSMUSG00000019851
Rpl35a	-1.84	$1.90E+02$	56.8	ENSMUSG00000060636
Krt17	6.99	$0.00E+00$	6.3	ENSMUSG00000035557
mt-Co2	3.88	$0.00E+00$	29,055.90	ENSMUSG00000064354
Dmkn	4.43	$1.00E+00$	10.8	ENSMUSG00000060962
Gm11826	-2.27	$1.00E+02$	27.8	ENSMUSG00000083328
Lce1a1	6.74	$0.00E+00$	15.8	ENSMUSG00000057609
Myl1	-0.84	$8.20E+03$	4,609.10	ENSMUSG00000061816
Cox7b	-0.99	$1.70E+03$	974.7	ENSMUSG00000031231
Mylpf	-0.79	$4.10E+04$	19,680.30	ENSMUSG00000030672
Zfp36	1.34	$8.10E+00$	21.3	ENSMUSG00000044786
Atp5o	-0.84	$4.00E+02$	231.4	ENSMUSG00000022956
Gm15920	-0.84	$6.20E+02$	346.4	ENSMUSG00000080893
Ly6d	5.91	$6.20E-02$	14.1	ENSMUSG00000034634
Gm6415	-1.12	$2.80E+02$	120.2	ENSMUSG00000083820

Table A.3: 6.0hr genes sorted by p-value. rpkm1 = mock; rpkm2 = control. log 2(fold change) = control/mock. rpkm = reads per kilobase per million base pairs. $p < 0.001$.

gene symbol	**log2(fold change)**	**rpkm1**	**rpkm2**	**ENSEMBL ID**
Uqcr10	-0.79	$1.20E+03$	692.5	ENSMUSG00000059534
Sbsn	1.93	$2.30E+00$	8.5	ENSMUSG00000046056
mt-Nd3	2.85	$1.80E+04$	16,499.40	ENSMUSG00000064360
Rpl31	-2.62	$3.90E+01$	17.8	ENSMUSG00000073702
Lce1d	6.09	$0.00E+00$	10.7	ENSMUSG00000078658
Ndufv2	-0.74	$6.50E+02$	370	ENSMUSG00000024099
Gm5526	-2.06	$1.20E+02$	80.7	ENSMUSG00000084817
Lce1a2	6.04	$0.00E+00$	10.8	ENSMUSG00000068890
Atp5j2	-0.8	$5.90E+02$	282.2	ENSMUSG00000038690
Slc7a2	1.12	$6.40E+00$	13.5	ENSMUSG00000031596
Retnla	2.77	$2.10E+01$	152.3	ENSMUSG00000061100
Rps25-ps1	-0.84	$4.10E+02$	210.9	ENSMUSG00000067344
Nedd8	-0.83	$1.90E+02$	105.4	ENSMUSG00000010376
Gbp10	1.11	$9.30E+00$	19.2	ENSMUSG00000054588
S100a1	-0.86	$3.40E+02$	177.7	ENSMUSG00000044080
Sepx1	-0.8	$2.30E+02$	128	ENSMUSG00000075705
Nfkbia	0.96	$2.00E+01$	39.9	ENSMUSG00000021025
Rpl30	-1.02	$2.50E+02$	105.6	ENSMUSG00000058600
Ndufb6	-0.73	$3.60E+02$	216.6	ENSMUSG00000071014
Fam25c	4.32	$4.30E-01$	9.5	ENSMUSG00000043681
Adrb2	0.97	$1.30E+01$	25.8	ENSMUSG00000045730
Lce1m	5.81	$0.00E+00$	6.9	ENSMUSG00000027912
Gm16276	-2	$7.00E+01$	15.8	ENSMUSG00000084755
Gm11478	-0.67	$6.80E+02$	429	ENSMUSG00000083992
Lce1g	5.77	$0.00E+00$	6.1	ENSMUSG00000027919

Table A.3: 6.0hr genes sorted by p-value. rpkm1 = mock; rpkm2 = control. log 2(fold change) = control/mock. rpkm = reads per kilobase per million base pairs. $p < 0.001$.

gene symbol	**log2(fold change)**	**rpkm1**	**rpkm2**	**ENSEMBL ID**
Cox7a2	-0.68	$4.50E+02$	280.7	ENSMUSG00000032330
Tnni2	-0.62	$1.70E+04$	10,506.80	ENSMUSG00000031097
Gm9763	-1.19	$1.40E+02$	59	ENSMUSG00000037438
Lce1c	5.74	$0.00E+00$	9.7	ENSMUSG00000042092
Ddr2	0.89	$3.60E+00$	7.2	ENSMUSG00000026674
Uqcrq	-0.74	$1.50E+03$	818.4	ENSMUSG00000044894
Gm15430	-0.89	$1.50E+03$	906.4	ENSMUSG00000036305
Gm8017	-0.98	$3.50E+02$	234.9	ENSMUSG00000063427
Cox6c	-0.66	$8.40E+02$	518.3	ENSMUSG00000014313
Lce1f	5.67	$0.00E+00$	9	ENSMUSG00000042124
Ndufc2	-0.69	$4.10E+02$	252.5	ENSMUSG00000030647
Arntl	-1.25	$6.60E+00$	2.8	ENSMUSG00000055116
Mb	-0.59	$1.70E+04$	11,492.40	ENSMUSG00000018893
Gm7536	-1.11	$6.30E+02$	466.7	ENSMUSG00000057036
Ndufa6	-0.72	$6.90E+02$	397.6	ENSMUSG00000022450
Gm94	5.62	$0.00E+00$	5.9	ENSMUSG00000071858
Rpl4	-0.61	$5.70E+02$	377.8	ENSMUSG00000032399
Rps3	-0.66	$5.80E+02$	355.3	ENSMUSG00000030744
Cst3	-0.6	$2.30E+03$	1,456.50	ENSMUSG00000027447
Cox6b1	-0.71	$1.20E+03$	714.2	ENSMUSG00000036751
Csrp3	-0.59	$2.40E+03$	1,612.50	ENSMUSG00000030470
Romo1	-0.86	$2.20E+02$	138.7	ENSMUSG00000067847
Usmg5	-1.3	$6.50E+01$	25.2	ENSMUSG00000071528
Ndufa11	-0.68	$5.90E+01$	37.9	ENSMUSG00000002379
Map1lc3a	-0.85	$4.20E+02$	229.8	ENSMUSG00000027602

Table A.3: 6.0hr genes sorted by p-value. rpkm1 = mock; rpkm2 = control. log 2(fold change) = control/mock. rpkm = reads per kilobase per million base pairs. $p < 0.001$.

gene symbol	**log2(fold change)**	**rpkm1**	**rpkm2**	**ENSEMBL ID**
Timm8b	−0.76	$3.20E+02$	188.1	ENSMUSG00000039016
Sdhb	−0.63	$3.50E+02$	209.9	ENSMUSG00000009863
Idh3b	−0.61	$3.70E+02$	247.6	ENSMUSG00000027406
Lce1b	5.55	$0.00E+00$	8.3	ENSMUSG00000027923
Chchd1	−0.8	$2.40E+02$	129.4	ENSMUSG00000063787
Ndufa4	−0.59	$1.90E+03$	1,290.10	ENSMUSG00000029632
Itgb1bp2	−0.65	$1.50E+02$	99	ENSMUSG00000031312
Brp44	−0.61	$3.70E+02$	253.5	ENSMUSG00000026568
Gm14088	−0.86	$5.10E+02$	271.5	ENSMUSG00000081413
Tigd4	0.79	$1.60E+01$	29.5	ENSMUSG00000047819
Aldoa	−0.56	$8.60E+03$	5,914.00	ENSMUSG00000030695
Psma7	−0.67	$3.40E+02$	187.4	ENSMUSG00000027566
Atp5k	−1.97	$2.30E+02$	50.1	ENSMUSG00000050856
Gm11918	−1.72	$1.40E+02$	41.4	ENSMUSG00000080911
Gm12693	−0.82	$1.50E+02$	88.4	ENSMUSG00000083179
Gm6181	−1.16	$1.50E+02$	72.7	ENSMUSG00000074092
Rpl18a	−1.34	$1.60E+02$	62.2	ENSMUSG00000045128
Myoz1	−0.57	$1.60E+03$	1,071.60	ENSMUSG00000068697
Snrpd2	−1.05	$8.90E+01$	46.5	ENSMUSG00000040824
Mrps18c	−0.78	$2.00E+02$	124.6	ENSMUSG00000016833
Tpt1-ps3	−0.56	$4.50E+03$	2,917.40	ENSMUSG00000084319
Cox4i1	−0.57	$1.40E+03$	938	ENSMUSG00000031818
Gm9493	−1.1	$3.10E+02$	184.9	ENSMUSG00000044424
Gm5560	−1.38	$3.30E+01$	15.3	ENSMUSG00000067161
Ndufa10	−0.61	$1.30E+02$	90.1	ENSMUSG00000026260

Table A.3: 6.0hr genes sorted by p-value. rpkm1 = mock; rpkm2 = control. log 2(fold change) = control/mock. rpkm = reads per kilobase per million base pairs. $p < 0.001$.

gene symbol	**log2(fold change)**	**rpkm1**	**rpkm2**	**ENSEMBL ID**
Ndufv3	-0.65	$4.70E+02$	282.6	ENSMUSG00000024038

Table A.4: 12.0hr genes sorted by p-value. rpkm1 = mock; rpkm2 = control. log 2(fold change) = control/mock. rpkm = reads per kilobase per million base pairs. $p < 0.001$.

gene symbol	**log2(fold change)**	**rpkm1**	**rpkm2**	**ENSEMBL ID**
Krt2	10.96	$0.00E+00$	31.6	ENSMUSG00000064201
Mybph	-2.09	$2.30E+02$	50.9	ENSMUSG00000042451
Lor	8.6	$3.90E-02$	27.4	ENSMUSG00000043165
Lmcd1	-1.49	$6.40E+02$	210.9	ENSMUSG00000057604
Gm4604	-2.46	$4.80E+02$	281.1	ENSMUSG00000091845
Csrp3	-1.31	$4.60E+03$	1,673.00	ENSMUSG00000030470
Gm11918	-2.83	$2.60E+02$	43	ENSMUSG00000080911
Calm4	5.51	$5.50E-01$	25.3	ENSMUSG00000033765
G0s2	-2.57	$5.50E+01$	7.2	ENSMUSG00000009633
Krt10	3.58	$3.20E+00$	42.5	ENSMUSG00000019761
Ankrd2	-2.51	$4.40E+02$	74.6	ENSMUSG00000025172
Rpl30	-1.56	$3.50E+02$	109.7	ENSMUSG00000058600
Rplp2	-1.94	$1.40E+02$	38.2	ENSMUSG00000025508
Gm15430	-1.43	$2.40E+03$	939.3	ENSMUSG00000036305
Krt14	7.91	$0.00E+00$	13.9	ENSMUSG00000045545
Rpl35a	-1.77	$2.10E+02$	58.9	ENSMUSG00000060636
Scara5	-1.63	$1.80E+01$	6.3	ENSMUSG00000022032
Gsn	-1.08	$1.60E+03$	743.5	ENSMUSG00000026879
Krt5	7.62	$0.00E+00$	8.8	ENSMUSG00000061527
Rps2	-1.19	$5.40E+02$	257.4	ENSMUSG00000044533
Dcn	-1.05	$9.80E+02$	479.4	ENSMUSG00000019929
Rps17	-1.25	$7.30E+02$	350	ENSMUSG00000061787
Dmkn	4.12	$1.80E+00$	11.2	ENSMUSG00000060962
Tnfrsf12a	-2.46	$1.30E+02$	21.8	ENSMUSG00000023905

Table A.4: 12.0hr genes sorted by p-value. rpkm1 = mock; rpkm2 = control. log 2(fold change) = control/mock. rpkm = reads per kilobase per million base pairs. $p < 0.001$.

gene symbol	**log2(fold change)**	**rpkm1**	**rpkm2**	**ENSEMBL ID**
Flg	7.44	$0.00E+00$	12.3	ENSMUSG00000091340
Gm8017	−1.26	$4.20E+02$	244	ENSMUSG00000063427
Inmt	−1.99	$6.50E+01$	17.1	ENSMUSG00000003477
Rpl13a	−1.01	$1.80E+03$	845	ENSMUSG00000074129
Arrdc3	1.26	$2.90E+01$	79.6	ENSMUSG00000074794
Mgp	−1.02	$6.80E+02$	314.7	ENSMUSG00000030218
Gm6181	−1.61	$2.00E+02$	75.5	ENSMUSG00000074092
Gm9493	−1.5	$3.30E+02$	191.8	ENSMUSG00000044424
Zfp503	−1.25	$2.10E+01$	8.1	ENSMUSG00000039081
Gadd45g	1.68	$3.20E+01$	107	ENSMUSG00000021453
Snrpd2	−1.38	$1.00E+02$	48.2	ENSMUSG00000040824
Fbln2	−1.09	$5.10E+01$	23.6	ENSMUSG00000064080
Cd63-ps	−1.02	$2.90E+02$	150.6	ENSMUSG00000085939
Rnase4	−1.01	$1.20E+02$	59.4	ENSMUSG00000021876
Gm11826	−1.92	$1.10E+02$	28.8	ENSMUSG00000083328
Gm6415	−1.16	$3.00E+02$	124.7	ENSMUSG00000083820
Gm16418	−1.39	$5.90E+02$	238.6	ENSMUSG00000084093
Gpx3	−1.16	$2.50E+02$	107.4	ENSMUSG00000018339
Pcolce2	−1.35	$3.50E+01$	11.3	ENSMUSG00000015354
Sparc	−0.86	$3.10E+02$	176.9	ENSMUSG00000018593
Mmp2	−0.98	$5.60E+01$	29.1	ENSMUSG00000031740
Hspb7	−0.82	$7.40E+02$	402.6	ENSMUSG00000006221
Gm15501	−1.96	$2.60E+02$	148.8	ENSMUSG00000087412
Krt17	6.8	$0.00E+00$	6.6	ENSMUSG00000035557
Serping1	−0.93	$1.50E+02$	80.7	ENSMUSG00000023224

Table A.4: 12.0hr genes sorted by p-value. rpkm1 = mock; rpkm2 = control. log 2(fold change) = control/mock. rpkm = reads per kilobase per million base pairs. $p < 0.001$.

gene symbol	**log2(fold change)**	**rpkm1**	**rpkm2**	**ENSEMBL ID**
Ndufb11	-0.88	$4.90E+02$	255.7	ENSMUSG00000031059
Mylpf	-0.8	$3.80E+04$	20,390.20	ENSMUSG00000030672
Ecm1	-1.02	$8.70E+01$	46.6	ENSMUSG00000028108
Rplp2-ps1	-0.93	$1.50E+03$	705.3	ENSMUSG00000091018
Rplp1	-0.81	$2.10E+03$	1,118.00	ENSMUSG00000007892
Atp5k	-2.22	$2.60E+02$	51.9	ENSMUSG00000050856
Ltbp4	-0.98	$8.20E+01$	45.6	ENSMUSG00000040488
Myoc	-1.49	$2.60E+02$	90.3	ENSMUSG00000026697
Gm10196	-1.13	$3.30E+02$	119.9	ENSMUSG00000067058
Gm15459	-1.84	$3.50E+02$	260.2	ENSMUSG00000083840
Gm7536	-1.58	$7.60E+02$	482.9	ENSMUSG00000057036
Ubl5	-0.98	$4.40E+02$	197.8	ENSMUSG00000084786
Cygb	-1.06	$3.80E+01$	17.8	ENSMUSG00000020810
Rps3	-0.79	$7.20E+02$	368.8	ENSMUSG00000030744
Rpl38-ps2	-1.07	$1.20E+03$	577.7	ENSMUSG00000080921
Lox	-0.96	$2.90E+01$	15.1	ENSMUSG00000024529
Lce1a1	6.54	$0.00E+00$	16.4	ENSMUSG00000057609
Gdf10	-1.38	$1.30E+01$	5.2	ENSMUSG00000021943
Id3	-1	$1.10E+02$	47.1	ENSMUSG00000007872
Igfbp6	-1.39	$2.00E+02$	67.7	ENSMUSG00000023046
Klf10	-1.62	$1.10E+01$	3.7	ENSMUSG00000037465
Ank1	-0.84	$5.30E+02$	351.1	ENSMUSG00000031543
Bloc1s1	-1.14	$1.60E+02$	79.6	ENSMUSG00000090247
Gm15920	-0.87	$6.40E+02$	359.5	ENSMUSG00000080893
Gm14539	-2.07	$1.60E+03$	367.3	ENSMUSG00000084830

Table A.4: 12.0hr genes sorted by p-value. rpkm1 = mock; rpkm2 = control. log 2(fold change) = control/mock. rpkm = reads per kilobase per million base pairs. $p < 0.001$.

gene symbol	**log2(fold change)**	**rpkm1**	**rpkm2**	**ENSEMBL ID**
2310050C09Rik	6.48	$0.00E+00$	7.5	ENSMUSG00000090314
Bgn	-0.83	$1.10E+02$	58.3	ENSMUSG00000031375
Perp	2.79	$1.40E+00$	10.9	ENSMUSG00000019851
Plekho1	-0.91	$1.10E+02$	60.7	ENSMUSG00000015745
Rps15-ps2	-0.88	$1.20E+03$	588.4	ENSMUSG00000071419
Atp5e	-0.8	$3.00E+03$	1,527.10	ENSMUSG00000016252
Galntl2	-1.34	$1.80E+01$	8.4	ENSMUSG00000021903
Rpl22-ps1	-0.98	$2.60E+02$	125.1	ENSMUSG00000080877
Cox8b	-0.76	$2.30E+03$	1,314.90	ENSMUSG00000025488
Col1a2	-0.76	$8.60E+01$	46.7	ENSMUSG00000029661
Cox6b1	-0.75	$1.30E+03$	741.4	ENSMUSG00000036751
Pcolce	-0.88	$1.00E+02$	50.9	ENSMUSG00000029718
Timm23	-1.22	$1.70E+02$	79.1	ENSMUSG00000013701
Tpt1	-0.76	$1.50E+03$	938.2	ENSMUSG00000060126
Cox7b	-0.77	$1.60E+03$	1,013.50	ENSMUSG00000031231
Zfp52	-0.94	$2.20E+01$	11.4	ENSMUSG00000051341
Nov	-1.55	$5.50E+01$	19.6	ENSMUSG00000037362
Ndufb3	-0.8	$2.90E+02$	176.1	ENSMUSG00000026032
Gm5526	-1.82	$1.20E+02$	83.8	ENSMUSG00000084817
Sepx1	-0.81	$2.30E+02$	132.9	ENSMUSG00000075705
Dpt	-0.79	$1.20E+02$	65.6	ENSMUSG00000026574
Slc43a3	-1.22	$1.70E+01$	8.8	ENSMUSG00000027074
2900010M23Rik	-0.8	$3.50E+02$	200.1	ENSMUSG00000024208
Uqcrq	-0.7	$1.40E+03$	849.3	ENSMUSG00000044894
Ppp1r15a	-0.94	$3.80E+01$	17.4	ENSMUSG00000040435

Table A.4: 12.0hr genes sorted by p-value. rpkm1 = mock; rpkm2 = control. log 2(fold change) = control/mock. rpkm = reads per kilobase per million base pairs. $p < 0.001$.

gene symbol	**log2(fold change)**	**rpkm1**	**rpkm2**	**ENSEMBL ID**
Myl6	-1.75	$7.70E+01$	36.5	ENSMUSG00000090841

Table A.5: 24.0hr genes sorted by p-value. rpkm1 = mock; rpkm2 = control. log 2(fold change) = control/mock. rpkm = reads per kilobase per million base pairs. $p < 0.001$.

gene symbol	**log2(fold change)**	**rpkm1**	**rpkm2**	**ENSEMBL ID**
Krt2	10.52	$3.70E-02$	32.95	ENSMUSG00000064201
Krt1	8.81	$3.60E-02$	22.52	ENSMUSG00000046834
Calm4	6.4	$3.40E-01$	26.38	ENSMUSG00000033765
Ddit4	3.47	$1.10E+01$	109.64	ENSMUSG00000020108
Gm11826	-2.5	$2.10E+02$	29.87	ENSMUSG00000083328
Ppp1r3c	1.96	$3.90E+01$	112.47	ENSMUSG00000067279
Krt5	7.18	$5.00E-02$	9.25	ENSMUSG00000061527
Klf10	-2.36	$3.00E+01$	3.81	ENSMUSG00000037465
Dmkn	3.91	$2.30E+00$	11.64	ENSMUSG00000060962
Flg	7.51	$0.00E+00$	12.77	ENSMUSG00000091340
Myod1	-1.61	$4.10E+01$	11.16	ENSMUSG00000009471
Inmt	-2.01	$7.50E+01$	17.8	ENSMUSG00000003477
Rpl35a	-1.6	$2.30E+02$	61.24	ENSMUSG00000060636
Krt14	5.47	$1.60E-01$	14.44	ENSMUSG00000045545
Gsn	-0.97	$1.60E+03$	772.34	ENSMUSG00000026879
Rpl30	-1.28	$4.60E+02$	113.97	ENSMUSG00000058600
Rplp2-ps1	-1.08	$2.00E+03$	733.1	ENSMUSG00000091018
Clec2d	-1.14	$1.70E+02$	61.34	ENSMUSG00000030157
Itgb1bp3	-1.87	$2.40E+01$	4.55	ENSMUSG00000004939
Dll1	-1.88	$1.70E+01$	3.25	ENSMUSG00000014773
Tfrc	1.04	$1.10E+02$	162.33	ENSMUSG00000022797
Atp5e	-0.9	$3.80E+03$	$1,586.25$	ENSMUSG00000016252
G0s2	-1.86	$2.90E+01$	7.45	ENSMUSG00000009633
Asprv1	4.59	$2.90E-01$	6.35	ENSMUSG00000033508

Table A.5: 24.0hr genes sorted by p-value. rpkm1 = mock; rpkm2 = control. log 2(fold change) = control/mock. rpkm = reads per kilobase per million base pairs. $p < 0.001$.

gene symbol	**log2(fold change)**	**rpkm1**	**rpkm2**	**ENSEMBL ID**
Ggta1	1.36	$1.70E+01$	37.83	ENSMUSG00000035778
Htra3	-1.13	$4.20E+01$	18.6	ENSMUSG00000029096
Otud1	3.13	$1.10E+01$	75.13	ENSMUSG00000043415
Cygb	-1.13	$4.60E+01$	18.47	ENSMUSG00000020810
Gm11918	-2.07	$2.80E+02$	44.7	ENSMUSG00000080911
Gm8017	-1.12	$5.10E+02$	253.67	ENSMUSG00000063427
Lrrc30	1.38	$2.50E+01$	59.57	ENSMUSG00000073375
Ctgf	1.83	$4.10E+01$	122.88	ENSMUSG00000019997
Mgp	-0.86	$7.00E+02$	326.96	ENSMUSG00000030218
Krt17	6.36	$5.60E-02$	6.84	ENSMUSG00000035557
Txnip	-1.58	$4.30E+02$	106.39	ENSMUSG00000038393
Gm9493	-1.28	$3.90E+02$	199.33	ENSMUSG00000044424
Abca8a	-1.08	$5.40E+01$	19.64	ENSMUSG00000041828
Nfkbia	1.38	$1.90E+01$	42.96	ENSMUSG00000021025
Postn	1.68	$1.40E+01$	36.97	ENSMUSG00000027750
Irf2bp2	1.45	$8.30E+00$	18.39	ENSMUSG00000051495
Gm11808	-1.16	$1.00E+03$	443.31	ENSMUSG00000068240
Lce1a1	6.61	$0.00E+00$	17.05	ENSMUSG00000057609
Dusp18	1.93	$2.30E+00$	5.49	ENSMUSG00000047205
Ier5l	-2.76	$5.80E+00$	0.83	ENSMUSG00000089762
Dusp1	1.39	$2.70E+01$	56.55	ENSMUSG00000024190
Arrdc3	0.97	$5.90E+01$	82.6	ENSMUSG00000074794
Tpt1	-0.83	$1.60E+03$	973.43	ENSMUSG00000060126
Mmp2	-0.88	$6.50E+01$	30.17	ENSMUSG00000031740
D0H4S114	0.97	$8.60E+01$	132.64	ENSMUSG00000042834

Table A.5: 24.0hr genes sorted by p-value. rpkm1 = mock; rpkm2 = control. log 2(fold change) = control/mock. rpkm = reads per kilobase per million base pairs. $p < 0.001$.

gene symbol	**log2(fold change)**	**rpkm1**	**rpkm2**	**ENSEMBL ID**
Dcn	-0.8	$1.10E+03$	498.5	ENSMUSG00000019929
Gbp6	1.66	$7.50E+00$	16.03	ENSMUSG00000079362
Slc25a25	1.21	$4.50E+01$	85.85	ENSMUSG00000026819
Gbp10	1.88	$9.20E+00$	20.71	ENSMUSG00000054588
Cldn5	-1.7	$1.40E+01$	4.11	ENSMUSG00000041378
Krt10	3.76	$3.50E+00$	44.32	ENSMUSG00000019761
Nrip1	1.12	$8.40E+00$	12.81	ENSMUSG00000048490
Adh1	-1.16	$6.40E+01$	23.12	ENSMUSG00000074207
Lmo7	0.94	$3.60E+01$	57.61	ENSMUSG00000033060
Akap6	1.02	$1.10E+01$	18.6	ENSMUSG00000061603
Scara5	-1.1	$1.60E+01$	6.54	ENSMUSG00000022032
Uqcrq	-0.75	$1.60E+03$	882.35	ENSMUSG00000044894
Ifitm2	-1.03	$1.30E+02$	53.16	ENSMUSG00000060591
Arid5a	1.76	$3.40E+00$	9.36	ENSMUSG00000037447
Gm6181	-1.3	$2.40E+02$	78.44	ENSMUSG00000074092
Hivep2	0.98	$6.80E+00$	11.82	ENSMUSG00000015501
Fsd1l	1.07	$7.30E+00$	10.38	ENSMUSG00000054752
Gm8203	-0.89	$2.60E+02$	142.65	ENSMUSG00000060214
Ly6d	5.94	$1.60E-01$	15.19	ENSMUSG00000034634
Gpx3	-0.91	$2.50E+02$	111.54	ENSMUSG00000018339
Sec23a	0.92	$4.20E+01$	60.15	ENSMUSG00000020986
Retnla	2.91	$2.30E+01$	164.11	ENSMUSG00000061100
Ndufb11	-0.74	$5.70E+02$	265.63	ENSMUSG00000031059
Ttn	0.82	$8.80E+01$	141.84	ENSMUSG00000051747
Mettl7a1	-0.92	$4.80E+01$	22.41	ENSMUSG00000054619

Table A.5: 24.0hr genes sorted by p-value. rpkm1 = mock; rpkm2 = control. log 2(fold change) = control/mock. rpkm = reads per kilobase per million base pairs. $p < 0.001$.

gene symbol	**log2(fold change)**	**rpkm1**	**rpkm2**	**ENSEMBL ID**
Gm16276	-1.86	$8.80E+01$	17.02	ENSMUSG00000084755
Arrdc2	1.21	$2.40E+01$	50.74	ENSMUSG00000002910
Atrnl1	1.32	$5.70E+00$	11.32	ENSMUSG00000054843
Cox8b	-0.67	$2.60E+03$	1,367.38	ENSMUSG00000025488
Gm15430	-0.86	$2.70E+03$	975.71	ENSMUSG00000036305
Hist1h4h	-1.36	$2.00E+02$	62.89	ENSMUSG00000060981
Lnp	0.86	$3.40E+01$	49.27	ENSMUSG00000009207
Gm10196	-0.98	$4.10E+02$	124.58	ENSMUSG00000067058
Nfil3	2.53	$6.50E+00$	31.39	ENSMUSG00000056749
Foxo1	1.66	$6.00E+00$	16.83	ENSMUSG00000044167
Gm13826	-0.67	$1.90E+03$	986.44	ENSMUSG00000072692
Ltbp4	-0.77	$8.60E+01$	47.38	ENSMUSG00000040488
Zfp36	1.52	$1.00E+01$	22.94	ENSMUSG00000044786
Ppp2r3a	0.76	$6.30E+01$	80.07	ENSMUSG00000043154
Rps27a-ps2	-0.75	$1.10E+03$	490.39	ENSMUSG00000058838
8430408G22Rik	3.55	$1.30E+00$	11	ENSMUSG00000048489
Ly6a	-0.84	$1.70E+02$	73.66	ENSMUSG00000075602
Lars2	1.55	$1.90E+01$	49.9	ENSMUSG00000035202
mt-Nd2	0.66	$8.20E+03$	9,115.43	ENSMUSG00000064345
Tnfrsf12a	-1.69	$1.00E+02$	22.63	ENSMUSG00000023905
Trp53inp1	1.26	$5.50E+00$	9.62	ENSMUSG00000028211
Rpl18a	-1.19	$2.00E+02$	67.05	ENSMUSG00000045128
Cox7b	-0.66	$1.90E+03$	1,052.61	ENSMUSG00000031231
Gm6415	-0.89	$3.50E+02$	129.47	ENSMUSG00000083820
Ablim1	0.8	$2.50E+01$	33.28	ENSMUSG00000025085

Table A.5: 24.0hr genes sorted by p-value. rpkm1 = mock; rpkm2 = control. log 2(fold change) = control/mock. rpkm = reads per kilobase per million base pairs. $p < 0.001$.

gene symbol	**log2(fold change)**	**rpkm1**	**rpkm2**	**ENSEMBL ID**
Rps21	-1.61	$9.80E+02$	298.97	ENSMUSG00000039001

Table A.6: 168.0hr genes sorted by p-value. rpkm1 = mock; rpkm2 = control. log 2(fold change) = control/mock. rpkm = reads per kilobase per million base pairs. $p < 0.001$

gene symbol	**log2(fold change)**	**rpkm1**	**rpkm2**	**ENSEMBL ID**
Krt2	11.65	$0.00E+00$	$3.10E+01$	ENSMUSG00000064201
Krt1	9.94	$0.00E+00$	$2.10E+01$	ENSMUSG00000046834
Lor	8.51	$9.70E-02$	$2.70E+01$	ENSMUSG00000043165
Krt14	8.6	$0.00E+00$	$1.30E+01$	ENSMUSG00000045545
Krt5	8.3	$0.00E+00$	$8.60E+00$	ENSMUSG00000061527
Flg	8.13	$0.00E+00$	$1.20E+01$	ENSMUSG00000091340
Gsn	-1.13	$3.80E+03$	$7.20E+02$	ENSMUSG00000026879
Krt17	7.48	$0.00E+00$	$6.40E+00$	ENSMUSG00000035557
Calm4	5.33	$1.40E+00$	$2.50E+01$	ENSMUSG00000033765
Lce1a1	7.23	$0.00E+00$	$1.60E+01$	ENSMUSG00000057609
Dmkn	5	$1.50E+00$	$1.10E+01$	ENSMUSG00000060962
2310050C09Rik	7.16	$0.00E+00$	$7.30E+00$	ENSMUSG00000090314
Krt10	4.18	$4.50E+00$	$4.10E+01$	ENSMUSG00000019761
Asprv1	4.92	$3.20E-01$	$5.90E+00$	ENSMUSG00000033508
Lce1d	6.58	$0.00E+00$	$1.10E+01$	ENSMUSG00000078658
Lce1a2	6.52	$0.00E+00$	$1.10E+01$	ENSMUSG00000068890
Slc25a25	1.33	$6.10E+01$	$8.00E+01$	ENSMUSG00000026819
Myh4	-0.87	$5.50E+02$	$1.30E+02$	ENSMUSG00000057003
Lce1m	6.29	$0.00E+00$	$6.90E+00$	ENSMUSG00000027912
Lce1g	6.26	$0.00E+00$	$6.10E+00$	ENSMUSG00000027919
Lce1c	6.22	$0.00E+00$	$9.70E+00$	ENSMUSG00000042092
Mgp	-0.9	$1.30E+03$	$3.10E+02$	ENSMUSG00000030218
Lce1f	6.16	$0.00E+00$	$9.00E+00$	ENSMUSG00000042124
Gm94	6.1	$0.00E+00$	$6.00E+00$	ENSMUSG00000071858

Table A.6: 168.0hr genes sorted by p-value. rpkm1 = mock; rpkm2 = control. log 2(fold change) = control/mock. rpkm = reads per kilobase per million base pairs. $p < 0.001$

gene symbol	**log2(fold change)**	**rpkm1**	**rpkm2**	**ENSEMBL ID**
Itgb1bp3	-1.62	$2.80E+01$	$4.20E+00$	ENSMUSG00000004939
Lce1b	6.03	$0.00E+00$	$8.40E+00$	ENSMUSG00000027923
Scara5	-1.15	$2.90E+01$	$6.10E+00$	ENSMUSG00000022032
Clec3b	-1	$2.60E+02$	$5.40E+01$	ENSMUSG00000025784
Cox4i1	-0.77	$4.50E+03$	$9.40E+02$	ENSMUSG00000031818
Crct1	5.87	$0.00E+00$	$5.90E+00$	ENSMUSG00000027913
Mmp2	-0.88	$1.10E+02$	$2.80E+01$	ENSMUSG00000031740
Mt4	5.04	$2.60E-01$	$1.40E+01$	ENSMUSG00000031757
Zfp36	1.61	$1.20E+01$	$2.10E+01$	ENSMUSG00000044786
Rpl23a	-1.78	$3.70E+02$	$9.60E+01$	ENSMUSG00000058546
Uqcr10	-0.74	$3.20E+03$	$7.00E+02$	ENSMUSG00000059534
Cox7b	-0.76	$4.00E+03$	$9.80E+02$	ENSMUSG00000031231
Fbln2	-0.85	$1.00E+02$	$2.30E+01$	ENSMUSG00000064080
Arrdc3	0.89	$7.00E+01$	$7.70E+01$	ENSMUSG00000074794
Lce1h	5.56	$0.00E+00$	$5.20E+00$	ENSMUSG00000049593
Gm13826	-0.73	$4.30E+03$	$9.20E+02$	ENSMUSG00000072692
Htra3	-0.93	$7.80E+01$	$1.70E+01$	ENSMUSG00000029096
Uqcrq	-0.71	$3.90E+03$	$8.20E+02$	ENSMUSG00000044894
Lce1l	5.5	$0.00E+00$	$5.70E+00$	ENSMUSG00000046676
Perp	2.77	$2.50E+00$	$1.10E+01$	ENSMUSG00000019851
Defb6	5.47	$0.00E+00$	$1.30E+01$	ENSMUSG00000050756
Lce1i	5.45	$0.00E+00$	$5.10E+00$	ENSMUSG00000068888
Atp5o	-0.74	$9.10E+02$	$2.30E+02$	ENSMUSG00000022956
Serping1	-0.71	$2.60E+02$	$7.80E+01$	ENSMUSG00000023224
1100001G20Rik	3.86	$8.30E-01$	$1.60E+01$	ENSMUSG00000051748

Table A.6: 168.0hr genes sorted by p-value. rpkm1 = mock; rpkm2 = control. log 2(fold change) = control/mock. rpkm = reads per kilobase per million base pairs. $p < 0.001$

gene symbol	**log2(fold change)**	**rpkm1**	**rpkm2**	**ENSEMBL ID**
Adh1	-1.04	$1.20E+02$	$2.20E+01$	ENSMUSG00000074207
Irf2bp2	1.19	$1.30E+01$	$1.70E+01$	ENSMUSG00000051495
Ddit4	2.37	$4.00E+01$	$1.00E+02$	ENSMUSG00000020108
Rpl41	-0.65	$2.60E+03$	$6.10E+02$	ENSMUSG00000093674
Gpx3	-0.82	$4.50E+02$	$1.00E+02$	ENSMUSG00000018339
Dcn	-0.61	$1.30E+03$	$4.70E+02$	ENSMUSG00000019929
Pcolce	-0.75	$2.00E+02$	$4.90E+01$	ENSMUSG00000029718
Csrp3	-0.58	$5.90E+03$	$1.60E+03$	ENSMUSG00000030470
Inmt	-1.21	$1.00E+02$	$1.70E+01$	ENSMUSG00000003477
Dpep1	-1.14	$2.60E+01$	$4.90E+00$	ENSMUSG00000019278
mt-Co2	1.26	$0.00E+00$	$2.90E+04$	ENSMUSG00000064354
Slc15a2	-4.1	$1.50E+01$	$4.60E-01$	ENSMUSG00000022899
Rplp2-ps1	-0.63	$2.90E+03$	$6.90E+02$	ENSMUSG00000091018
Uqcrc1	-0.59	$7.20E+02$	$1.90E+02$	ENSMUSG00000025651
Cst3	-0.56	$5.80E+03$	$1.50E+03$	ENSMUSG00000027447
Aldh1a2	-1.39	$1.10E+01$	$2.10E+00$	ENSMUSG00000013584
Gm8017	-0.75	$9.40E+02$	$2.40E+02$	ENSMUSG00000063427
Ltbp4	-0.68	$2.10E+02$	$4.40E+01$	ENSMUSG00000040488
Gpx1	-0.65	$4.80E+02$	$1.10E+02$	ENSMUSG00000063856
Lmcd1	-0.56	$6.30E+02$	$2.00E+02$	ENSMUSG00000057604
Islr	-0.77	$5.90E+01$	$1.60E+01$	ENSMUSG00000037206
Mfap5	-0.73	$3.10E+02$	$7.60E+01$	ENSMUSG00000030116
Atp5d	-0.59	$8.80E+02$	$2.40E+02$	ENSMUSG00000003072
Apod	-0.68	$6.10E+02$	$1.80E+02$	ENSMUSG00000022548
Timm8b	-0.64	$7.60E+02$	$1.90E+02$	ENSMUSG00000039016

Table A.6: 168.0hr genes sorted by p-value. rpkm1 = mock; rpkm2 = control. log 2(fold change) = control/mock. rpkm = reads per kilobase per million base pairs. $p < 0.001$

gene symbol	**log2(fold change)**	**rpkm1**	**rpkm2**	**ENSEMBL ID**
Rpl8	-0.55	$2.10E+03$	$5.60E+02$	ENSMUSG00000003970
Fbln1	-0.88	$3.40E+01$	$7.70E+00$	ENSMUSG00000006369
Serpinf1	-0.99	$5.50E+02$	$1.10E+02$	ENSMUSG00000000753
Efemp1	-0.82	$6.40E+01$	$1.80E+01$	ENSMUSG00000020467
Romo1	-0.73	$5.80E+02$	$1.40E+02$	ENSMUSG00000067847
Ddit3	-0.83	$1.20E+02$	$2.90E+01$	ENSMUSG00000025408
Usmg5	-1.14	$1.40E+02$	$2.50E+01$	ENSMUSG00000071528
Hic1	-1.66	$5.60E+00$	$8.10E-01$	ENSMUSG00000043099
mt-Nd2	0.57	$7.60E+03$	$8.50E+03$	ENSMUSG00000064345
Mrps24	-0.7	$3.60E+02$	$7.20E+01$	ENSMUSG00000020477
Gm10222	1.98	$4.80E+03$	$6.70E+03$	ENSMUSG00000067736
Ndufs8	-0.64	$3.30E+02$	$8.00E+01$	ENSMUSG00000059734
Gm4604	-1.1	$1.40E+03$	$2.70E+02$	ENSMUSG00000091845
Errfi1	0.76	$4.50E+01$	$3.10E+01$	ENSMUSG00000028967
Psma7	-0.57	$7.30E+02$	$1.90E+02$	ENSMUSG00000027566
Mylpf	-0.5	$0.00E+00$	$2.00E+04$	ENSMUSG00000030672
Ndufb8	-0.53	$1.90E+03$	$4.70E+02$	ENSMUSG00000025204
Pi16	-0.89	$1.30E+02$	$2.70E+01$	ENSMUSG00000024011
Per1	0.63	$6.30E+01$	$6.00E+01$	ENSMUSG00000020893

Appendix B

Mock denervated vs. denervated muscle: top 100 differentially expressed genes

Table B.1: 6.0hr genes sorted by p-value. rpkm1 = mock; rpkm2 = denervated. log 2(fold change) = denervated/mock. rpkm = reads per kilobase per million base pairs. $p < 0.001$.

gene symbol	**log2(fold change)**	**rpkm1**	**rpkm2**	**ENSEMBL ID**
Clec2d	2.77	39.81	262.8	ENSMUSG00000030157
Tsc22d3	1.52	284.77	785.3	ENSMUSG00000031431
Pik3ip1	1.79	22.28	63.2	ENSMUSG00000034614
Angptl4	4.39	0.31	5.8	ENSMUSG00000002289
Myf6	1.92	89.62	337.3	ENSMUSG00000035923
Fkbp5	1.45	32.96	79.5	ENSMUSG00000024222
Gm129	−3.24	11.93	1.6	ENSMUSG00000038550
Gm12966	−1.81	167.5	48.6	ENSMUSG00000070729
Xirp1	−2.23	46.47	9.6	ENSMUSG00000079243
Otud1	−2.32	37.3	6.7	ENSMUSG00000043415
Atf3	−2.35	42.74	7.8	ENSMUSG00000026628
Nr1d1	−1.8	29.23	8.6	ENSMUSG00000020889

Table B.1: 6.0hr genes sorted by p-value. rpkm1 = mock; rpkm2 = denervated. log 2(fold change) = denervated/mock. rpkm = reads per kilobase per million base pairs. $p < 0.001$.

gene symbol	**log2(fold change)**	**rpkm1**	**rpkm2**	**ENSEMBL ID**
2310050B05Rik	−1.38	451.11	178.7	ENSMUSG00000085779
Klf4	−1.9	10.73	2.6	ENSMUSG00000003032
Fibin	1.93	75.67	268.7	ENSMUSG00000074971
Ctgf	−1.89	65.9	16.5	ENSMUSG00000019997
Adh1	1.36	27.5	73.1	ENSMUSG00000074207
Adrb2	1.38	12.48	31.7	ENSMUSG00000045730
Dyrk2	−2.32	12.89	2.8	ENSMUSG00000028630
Clk1	1.25	53.86	109.6	ENSMUSG00000026034
Arid5a	−2.15	8.39	1.6	ENSMUSG00000037447
Slc41a3	−1.54	29.7	10.5	ENSMUSG00000030089
Actr6	1.79	3.66	11.4	ENSMUSG00000019948
2210403K04Rik	−1.74	92.7	23.5	ENSMUSG00000085148
mt-Rnr1	1.63	372.13	1,066.00	ENSMUSG00000064337
Idh1	1.14	58.55	93.3	ENSMUSG00000025950
Ctla2a	1.43	12.32	33.6	ENSMUSG00000044258
Cited2	1.3	15.98	38.9	ENSMUSG00000039910
Slc6a6	−1.62	15.31	4.4	ENSMUSG00000030096
Sv2b	1.43	2.47	5.8	ENSMUSG00000053025
D4Wsu53e	1.4	182.13	506.9	ENSMUSG00000037266
Coq10b	−1.61	19.02	5.8	ENSMUSG00000025981
Cebpg	1.17	10.57	17.9	ENSMUSG00000056216
Chac2	1.61	5.83	16.2	ENSMUSG00000020309
Id1	−1.93	33.62	9.6	ENSMUSG00000042745
Nr4a1	−2.45	45.89	8.6	ENSMUSG00000023034
Atoh8	−1.9	6.85	2	ENSMUSG00000037621

Table B.1: 6.0hr genes sorted by p-value. rpkm1 = mock; rpkm2 = denervated. log 2(fold change) = denervated/mock. rpkm = reads per kilobase per million base pairs. $p < 0.001$.

gene symbol	**log2(fold change)**	**rpkm1**	**rpkm2**	**ENSEMBL ID**
Slc43a1	1.39	5.15	11.5	ENSMUSG00000027075
Amd1	1.39	10.33	21.5	ENSMUSG00000075232
Pde7a	1.05	18.05	28.3	ENSMUSG00000069094
3425401B19Rik	−1.45	35.44	13	ENSMUSG00000071540
P2ry2	−1.77	16.52	4.5	ENSMUSG00000032860
Cry2	−1.21	23.78	9.9	ENSMUSG00000068742
Med20	1.29	10.45	21.6	ENSMUSG00000092558
Nr3c2	−1.35	7.02	2.6	ENSMUSG00000031618
Pde4d	−1.52	36.68	11.4	ENSMUSG00000021699
Neat1	1.7	304.08	924.5	ENSMUSG00000092274
Myh4	−1.24	330.21	143.4	ENSMUSG00000057003
Slc7a2	1.02	6.21	10.4	ENSMUSG00000031596
Gadd45a	1.08	36.23	76.6	ENSMUSG00000036390
Dusp1	−1.29	34.24	14.7	ENSMUSG00000024190
Gpr157	−1.46	8.35	2.9	ENSMUSG00000047875
Sult1a1	1.26	11.09	24.5	ENSMUSG00000030711
Rhebl1	2.18	1.92	8	ENSMUSG00000023755
4832428D23Rik	1.33	7.48	14.5	ENSMUSG00000046828
2900092E17Rik	1.25	5.5	14.6	ENSMUSG00000030680
Fndc1	−1.23	13.66	4	ENSMUSG00000071984
Sgk1	0.88	118.83	188	ENSMUSG00000019970
Osgin1	1.39	5.86	11.5	ENSMUSG00000074063
Galntl2	0.96	7.94	13.7	ENSMUSG00000021903
Nuak1	−1.39	6.49	2.2	ENSMUSG00000020032
Gm8812	1.35	23.55	60.8	ENSMUSG00000083289

Table B.1: 6.0hr genes sorted by p-value. rpkm1 = mock; rpkm2 = denervated. log 2(fold change) = denervated/mock. rpkm = reads per kilobase per million base pairs. $p < 0.001$.

gene symbol	**log2(fold change)**	**rpkm1**	**rpkm2**	**ENSEMBL ID**
Ang	1.64	6.07	19.9	ENSMUSG00000072115
1600002K03Rik	1.39	11.64	30.5	ENSMUSG00000035595
Pfkfb1	1.01	22.21	40.3	ENSMUSG00000025271
Jun	0.89	35.59	63.7	ENSMUSG00000052684
Cxcr7	−1.51	15.4	4.9	ENSMUSG00000044337
Rps6ka5	1	9.78	16.2	ENSMUSG00000021180
Ddit4l	0.88	214.06	368.5	ENSMUSG00000046818
Sgk3	1.27	3.48	7.6	ENSMUSG00000025915
F2r	−1.33	7.75	2.6	ENSMUSG00000048376
Slc16a10	1.03	4.67	7.9	ENSMUSG00000019838
Rpia	1.36	4.38	10.3	ENSMUSG00000053604
Klf9	−1.11	47.05	19	ENSMUSG00000033863
D0H4S114	−1.02	117.24	54.4	ENSMUSG00000042834
Socs2	−1.56	14.05	4	ENSMUSG00000020027
Mafk	−1.42	15.05	5.4	ENSMUSG00000018143
Hoxa9	1.42	3.77	9.1	ENSMUSG00000038227
Rnf150	−1.19	5.06	2	ENSMUSG00000047747
Egflam	−1.4	14.88	4.7	ENSMUSG00000042961
Zfp866	1.39	3.53	5.4	ENSMUSG00000043090
Asb4	1.26	2.53	5.2	ENSMUSG00000042607
Trim16	−0.94	46.82	20.6	ENSMUSG00000047821
Slc35e4	−0.99	27.53	14.1	ENSMUSG00000048807
Hyal2	1.38	3.25	9	ENSMUSG00000010047
Crebl2	1.22	3.11	5.5	ENSMUSG00000032652
Ncbp2	1.03	19.11	28.4	ENSMUSG00000022774

Table B.1: 6.0hr genes sorted by p-value. rpkm1 = mock; rpkm2 = denervated. log 2(fold change) = denervated/mock. rpkm = reads per kilobase per million base pairs. $p < 0.001$.

gene symbol	**log2(fold change)**	**rpkm1**	**rpkm2**	**ENSEMBL ID**
Scara3	−1.29	6	2.3	ENSMUSG00000034463
Plin3	0.88	21.51	39.5	ENSMUSG00000024197
Gapdh	−1.62	177.94	191.7	ENSMUSG00000057666
1190005F20Rik	1.2	3	6.8	ENSMUSG00000053286
Ifi205	1.2	8.06	19.5	ENSMUSG00000054203
Nfil3	−1.71	35.08	11.7	ENSMUSG00000056749
Vegfa	−1.03	29.01	13.9	ENSMUSG00000023951
Zfp874b	1.1	3.3	6.1	ENSMUSG00000059839
9330159F19Rik	0.83	11.73	18.1	ENSMUSG00000004360
Fam110a	−2.05	5.05	1.2	ENSMUSG00000027459
Slc25a33	−1.08	40.24	19.5	ENSMUSG00000028982
Emp1	−1.37	54.19	17.2	ENSMUSG00000030208
Tead1	−1.76	5.61	2.3	ENSMUSG00000055320

Table B.2: 12.0hr genes sorted by p-value. rpkm1 = mock; rpkm2 = denervated. log 2(fold change) = denervated/mock. rpkm = reads per kilobase per million base pairs. $p < 0.001$.

gene symbol	**log2(fold change)**	**rpkm1**	**rpkm2**	**ENSEMBL ID**
Krt2	13.4	$0.00E+00$	$1,352.20$	ENSMUSG00000064201
Lor	9.4	$3.80E-02$	125	ENSMUSG00000043165
Krt14	10	$0.00E+00$	186.8	ENSMUSG00000045545
Krt10	5.5	$3.10E+00$	570.4	ENSMUSG00000019761
Krt24	9.8	$0.00E+00$	148.2	ENSMUSG00000020913
Hrnr	9.7	$0.00E+00$	50.5	ENSMUSG00000041991
Calm4	7	$5.50E-01$	222.7	ENSMUSG00000033765
Krt5	9.5	$0.00E+00$	107.5	ENSMUSG00000061527
Dsp	6.7	$4.30E-02$	16.1	ENSMUSG00000054889
Dmkn	5.8	$1.80E+00$	114.1	ENSMUSG00000060962
Dsg1a	9	$0.00E+00$	30.2	ENSMUSG00000069441
Nr4a1	-3.7	$6.90E+01$	10.2	ENSMUSG00000023034
Flg	8.6	$0.00E+00$	101.8	ENSMUSG00000091340
2310050C09Rik	8.2	$0.00E+00$	89.2	ENSMUSG00000090314
Perp	4.3	$1.40E+00$	77.1	ENSMUSG00000019851
Dsc1	8.2	$0.00E+00$	22.8	ENSMUSG00000044322
Otud1	-3.1	$4.10E+01$	8.1	ENSMUSG00000043415
Lce1a1	8	$0.00E+00$	120.2	ENSMUSG00000057609
Gm94	7.9	$0.00E+00$	110	ENSMUSG00000071858
Kprp	7.9	$0.00E+00$	26.1	ENSMUSG00000059832
Dsc3	7.8	$0.00E+00$	12.8	ENSMUSG00000059898
Tnfrsf12a	-2.7	$1.30E+02$	30.5	ENSMUSG00000023905
Slc25a25	-3.2	$6.40E+01$	12.4	ENSMUSG00000026819
Lypd3	7.7	$0.00E+00$	43	ENSMUSG00000057454

Table B.2: 12.0hr genes sorted by p-value. rpkm1 = mock; rpkm2 = denervated. log 2(fold change) = denervated/mock. rpkm = reads per kilobase per million base pairs. $p < 0.001$.

gene symbol	**log2(fold change)**	**rpkm1**	**rpkm2**	**ENSEMBL ID**
Spink5	7.7	$0.00E+00$	14.7	ENSMUSG00000055561
Lce1a2	7.6	$0.00E+00$	101.8	ENSMUSG00000068890
Lmcd1	-2.2	$6.30E+02$	207.4	ENSMUSG00000057604
Lce1b	7.6	$0.00E+00$	97.9	ENSMUSG00000027923
Serpinb5	7.5	$0.00E+00$	21	ENSMUSG00000067006
Pla2g2f	7.4	$0.00E+00$	20.7	ENSMUSG00000028749
Psapl1	7.4	$0.00E+00$	9.5	ENSMUSG00000043430
2210403K04Rik	-2.2	$1.40E+02$	50.1	ENSMUSG00000085148
Lce1d	7.3	$0.00E+00$	77.5	ENSMUSG00000078658
Lce1g	7.3	$0.00E+00$	52.8	ENSMUSG00000027919
Atf3	-2.5	$3.50E+01$	10.2	ENSMUSG00000026628
Cyp2b19	7.2	$0.00E+00$	26.4	ENSMUSG00000066704
Pof1b	6.2	$2.10E-02$	6.9	ENSMUSG00000034607
Cpa4	7.2	$0.00E+00$	16.4	ENSMUSG00000039070
Per1	-2.3	$5.20E+01$	19.5	ENSMUSG00000020893
Hal	7.2	$0.00E+00$	18.1	ENSMUSG00000020017
Lce1h	7	$0.00E+00$	59.2	ENSMUSG00000049593
Klk7	6.9	$0.00E+00$	21.2	ENSMUSG00000030713
Lce1l	6.9	$0.00E+00$	58.8	ENSMUSG00000046676
Ctgf	-2.1	$8.60E+01$	38.9	ENSMUSG00000019997
Tgm3	6.8	$0.00E+00$	14.6	ENSMUSG00000027401
Lce1m	6.8	$0.00E+00$	40.6	ENSMUSG00000027912
Crct1	6.8	$0.00E+00$	53.2	ENSMUSG00000027913
Aqp3	5.4	$1.10E-01$	14.9	ENSMUSG00000028435
Ggta1	-1.8	$4.40E+01$	23.8	ENSMUSG00000035778

Table B.2: 12.0hr genes sorted by p-value. rpkm1 = mock; rpkm2 = denervated. log 2(fold change) = denervated/mock. rpkm = reads per kilobase per million base pairs. $p < 0.001$.

gene symbol	**log2(fold change)**	**rpkm1**	**rpkm2**	**ENSEMBL ID**
Neat1	1.7	$3.50E+02$	$1,822.80$	ENSMUSG00000092274
Lce1i	6.7	$0.00E+00$	47.1	ENSMUSG00000068888
Lce1f	6.7	$0.00E+00$	65.1	ENSMUSG00000042124
Krt9	6.3	$2.30E-02$	6.5	ENSMUSG00000051617
Il1f5	6.6	$0.00E+00$	26.4	ENSMUSG00000026983
Trim29	5.9	$7.50E-02$	25.1	ENSMUSG00000032013
Ddit4	-2.2	$2.40E+01$	12.2	ENSMUSG00000020108
Ppp1r15a	-1.7	$3.80E+01$	14.5	ENSMUSG00000040435
Asprv1	7	$1.60E-01$	164.7	ENSMUSG00000033508
Dusp1	-1.8	$5.40E+01$	24.9	ENSMUSG00000024190
Col17a1	5.1	$5.10E-02$	5.9	ENSMUSG00000025064
Rab25	6.5	$0.00E+00$	33.9	ENSMUSG00000008601
Dsg1b	6.4	$0.00E+00$	10.6	ENSMUSG00000061928
Lce1e	6.4	$0.00E+00$	40.3	ENSMUSG00000068889
Serpina12	3.7	$2.00E-01$	7.7	ENSMUSG00000041567
Sfn	3.6	$6.20E-01$	22.1	ENSMUSG00000047281
Ly6d	7.3	$7.20E-02$	131.5	ENSMUSG00000034634
Acer1	6.3	$0.00E+00$	9.7	ENSMUSG00000045019
Dapl1	6.2	$0.00E+00$	47.5	ENSMUSG00000026989
Csrp3	-1.8	$4.60E+03$	$1,620.90$	ENSMUSG00000030470
Alox12e	6.2	$0.00E+00$	10.4	ENSMUSG00000018907
Gjb4	6.1	$0.00E+00$	14.6	ENSMUSG00000046623
Wfdc12	6.1	$0.00E+00$	32.8	ENSMUSG00000042845
Them5	6.5	$4.30E-02$	39.3	ENSMUSG00000028148
Id1	-2.1	$5.60E+01$	16.1	ENSMUSG00000042745

Table B.2: 12.0hr genes sorted by p-value. rpkm1 = mock; rpkm2 = denervated. log 2(fold change) = denervated/mock. rpkm = reads per kilobase per million base pairs. $p < 0.001$.

gene symbol	**log2(fold change)**	**rpkm1**	**rpkm2**	**ENSEMBL ID**
Abra	-1.6	$1.20E+02$	71.1	ENSMUSG00000042895
Sbsn	2	$6.40E+00$	71.2	ENSMUSG00000046056
Csrnp1	-2.4	$5.80E+00$	1.6	ENSMUSG00000032515
Cnfn	6	$0.00E+00$	33.1	ENSMUSG00000063651
Tacstd2	6.2	$2.60E-02$	21.1	ENSMUSG00000051397
Elovl4	3.9	$1.50E-01$	7.5	ENSMUSG00000032262
Pkp3	6.2	$1.20E-01$	30.3	ENSMUSG00000054065
Spsb1	-1.9	$1.10E+01$	6.4	ENSMUSG00000039911
Fsd1l	-1.5	$1.00E+01$	5.7	ENSMUSG00000054752
Sdr16c5	5.9	$0.00E+00$	18	ENSMUSG00000028236
Ifrd1	-1.4	$1.70E+02$	106.6	ENSMUSG00000001627
Serpinb12	5.9	$0.00E+00$	5.6	ENSMUSG00000059956
Slc25a33	-1.6	$2.40E+01$	12.4	ENSMUSG00000028982
Plin5	2.6	$8.10E-01$	8.9	ENSMUSG00000011305
Alox12b	6	$1.80E-02$	6.8	ENSMUSG00000032807
4833423E24Rik	5.9	$0.00E+00$	7.8	ENSMUSG00000075217
Rapgef4	-1.8	$1.70E+01$	9.2	ENSMUSG00000049044
Klk5	5.8	$0.00E+00$	14.5	ENSMUSG00000074155
Sdr9c7	5.8	$0.00E+00$	7.8	ENSMUSG00000040127
Fam25c	5.3	$1.10E+00$	113	ENSMUSG00000043681
Gm6166	3.4	$1.70E+00$	41.4	ENSMUSG00000074280
Mapk13	5.8	$0.00E+00$	6.9	ENSMUSG00000004864
Krt15	5.7	$0.00E+00$	10.3	ENSMUSG00000054146
Tigd4	1.3	$1.40E+01$	60.1	ENSMUSG00000047819
Srsf3	-1.4	$6.10E+01$	37	ENSMUSG00000071172

Table B.2: 12.0hr genes sorted by p-value. rpkm1 = mock; rpkm2 = denervated. log 2(fold change) = denervated/mock. rpkm = reads per kilobase per million base pairs. $p < 0.001$.

gene symbol	**log2(fold change)**	**rpkm1**	**rpkm2**	**ENSEMBL ID**
Nccrp1	5.7	$0.00E+00$	5.2	ENSMUSG00000047586

Table B.3: 24.0hr genes sorted by p-value. rpkm1 = mock; rpkm2 = denervated. log 2(fold change) = denervated/mock. rpkm = reads per kilobase per million base pairs. $p < 0.001$.

gene symbol	**log2(fold change)**	**rpkm1**	**rpkm2**	**ENSEMBL ID**
Coch	3.6	9.19	72.62	ENSMUSG00000020953
Myog	3	10.27	70.16	ENSMUSG00000026459
Agpat9	4.2	1.13	7.81	ENSMUSG00000029314
Ttyh1	4.7	0.23	10.59	ENSMUSG00000030428
Kcnj2	−2.7	19.61	1.74	ENSMUSG00000041695
Ppp1r3c	2.3	39.41	110.04	ENSMUSG00000067279
Cd82	2.6	20.55	78.7	ENSMUSG00000027215
Hdac4	2.4	14.59	54.71	ENSMUSG00000073617
Hdac9	−3.8	5.7	0.23	ENSMUSG00000004698
Alpl	4.4	1.62	29.45	ENSMUSG00000028766
2010003K11Rik	5.4	0.28	10.32	ENSMUSG00000042041
Crem	2.5	17.46	66.92	ENSMUSG00000063889
Fam83d	6.3	0.27	20.1	ENSMUSG00000027654
Dusp10	−2.6	22.05	2.38	ENSMUSG00000039384
Runx1	2.4	2.77	7.58	ENSMUSG00000022952
Gm9766	−4.7	7.37	0.2	ENSMUSG00000038594
G3bp2	2	35.68	74.45	ENSMUSG00000029405
2700016F22Rik	6.1	0.3	8.79	ENSMUSG00000091188
B3galt2	−4	7.86	0.24	ENSMUSG00000033849
Nfil3	3.2	6.34	48.79	ENSMUSG00000056749
Mt1	3	116.85	843.89	ENSMUSG00000031765
3425401B19Rik	−1.8	38.16	8.79	ENSMUSG00000071540
AI464131	1.8	18.36	45.79	ENSMUSG00000046312
Mt2	3.7	100.29	1,065.61	ENSMUSG00000031762

Table B.3: 24.0hr genes sorted by p-value. rpkm1 = mock; rpkm2 = denervated. log 2(fold change) = denervated/mock. rpkm = reads per kilobase per million base pairs. $p < 0.001$.

gene symbol	**log2(fold change)**	**rpkm1**	**rpkm2**	**ENSEMBL ID**
Nav3	−2.7	5.25	0.46	ENSMUSG00000020181
Scn5a	4.9	0.13	6.49	ENSMUSG00000032511
Nr4a3	4.6	0.88	12.01	ENSMUSG00000028341
Stat3	1.7	36.42	70.71	ENSMUSG00000004040
Zkscan6	2.7	2.14	10.19	ENSMUSG00000018347
S100a8	3.4	66.31	421.46	ENSMUSG00000056054
Enho	4.1	10.66	184.93	ENSMUSG00000028445
Txnip	−1.6	432.41	90.74	ENSMUSG00000038393
Maf	1.7	21.45	41.61	ENSMUSG00000055435
Jph1	−1.7	71.01	20.77	ENSMUSG00000042686
Lims1	−1.7	40.63	5.79	ENSMUSG00000019920
Cntfr	3.6	7.9	78.55	ENSMUSG00000028444
Serpina3n	2.2	7.26	26.9	ENSMUSG00000021091
Tgif1	2.1	7.25	26.83	ENSMUSG00000047407
Smad3	2	13.07	31.78	ENSMUSG00000032402
Pdpn	2.2	16.61	49.63	ENSMUSG00000028583
Bcl2l11	2	4.88	11.97	ENSMUSG00000027381
Itgb1bp3	2.9	22.4	109.68	ENSMUSG00000004939
Tmem182	−1.6	257.63	58.52	ENSMUSG00000079588
Rcsd1	−1.5	102.74	25.58	ENSMUSG00000040723
Rhou	1.7	12.09	25.5	ENSMUSG00000039960
Sgms1	1.6	36.88	46.48	ENSMUSG00000040451
Ggta1	1.6	18.17	31.09	ENSMUSG00000035778
Pvr	2.6	5.11	17.64	ENSMUSG00000040511
Srxn1	2.5	38.14	138.52	ENSMUSG00000032802

Table B.3: 24.0hr genes sorted by p-value. rpkm1 = mock; rpkm2 = denervated. log 2(fold change) = denervated/mock. rpkm = reads per kilobase per million base pairs. $p < 0.001$.

gene symbol	**log2(fold change)**	**rpkm1**	**rpkm2**	**ENSEMBL ID**
Evi2a	1.9	17.96	46.79	ENSMUSG00000078771
Sesn1	−1.6	28.65	5.66	ENSMUSG00000038332
Clu	1.7	47.29	129.31	ENSMUSG00000022037
Fam13a	−2.3	5.96	0.71	ENSMUSG00000037709
Rnf115	−2.1	107.28	18.83	ENSMUSG00000028098
Adamtsl2	4.4	0.88	10.83	ENSMUSG00000036040
Dag1	−1.5	33.4	8.49	ENSMUSG00000039952
Lgals3	1.5	57.68	149.83	ENSMUSG00000050335
Fzd4	−1.4	49.45	11.17	ENSMUSG00000049791
Csrp3	−1.5	2,678.25	698.6	ENSMUSG00000030470
Bcl9l	−1.8	6.84	1.57	ENSMUSG00000063382
Mybph	−1.7	112.43	30.92	ENSMUSG00000042451
Nbeal2	2	3.22	12.07	ENSMUSG00000056724
Lmcd1	−1.5	351.47	94.6	ENSMUSG00000057604
Myo10	1.5	7.36	12.61	ENSMUSG00000022272
Cited2	−1.6	24	6.14	ENSMUSG00000039910
Slc25a25	2.4	42.93	147.51	ENSMUSG00000026819
Ppp1r27	2.3	95.39	394.23	ENSMUSG00000025129
Lrig1	−1.5	18.34	4.61	ENSMUSG00000030029
Hsd17b7	1.6	5.7	10.14	ENSMUSG00000026675
Csdc2	2.1	4.69	13.26	ENSMUSG00000042109
Mtch1	1.9	114.38	308.2	ENSMUSG00000024012
Ptpn21	−1.6	11.42	2.5	ENSMUSG00000021009
Slc41a3	1.5	21.76	47.81	ENSMUSG00000030089
Pdp1	−1.8	112.03	17.09	ENSMUSG00000049225

Table B.3: 24.0hr genes sorted by p-value. rpkm1 = mock; rpkm2 = denervated. log 2(fold change) = denervated/mock. rpkm = reads per kilobase per million base pairs. $p < 0.001$.

gene symbol	**log2(fold change)**	**rpkm1**	**rpkm2**	**ENSEMBL ID**
Scx	2.2	21.87	119.64	ENSMUSG00000034161
Nudt18	2.6	6.18	23.14	ENSMUSG00000045211
Zbtb16	−1.6	14.77	3.39	ENSMUSG00000066687
2310010M20Rik	−1.6	41.17	9.52	ENSMUSG00000046345
Lmo7	−1.4	38.84	9.48	ENSMUSG00000033060
Relt	1.8	6	15.21	ENSMUSG00000008318
Slmap	−1.5	84.64	13.02	ENSMUSG00000021870
Nmt1	1.4	32.36	45.2	ENSMUSG00000020936
Mtus1	−1.6	63.89	11.38	ENSMUSG00000045636
2310075C17Rik	1.5	112.4	227	ENSMUSG00000089718
Creld1	1.4	22.92	49.2	ENSMUSG00000030284
Tigd4	−3.4	28.34	1.65	ENSMUSG00000047819
Clcn1	−1.4	82.68	22	ENSMUSG00000029862
Mgp	1.3	708	1,451.91	ENSMUSG00000030218
Eif4ebp2	−1.6	22.12	5.99	ENSMUSG00000020091
Lpin1	1.5	32.07	53.21	ENSMUSG00000020593
mt-Rnr1	1.2	750.21	1,068.53	ENSMUSG00000064337
Ppp2r3a	−1.3	65.02	14.86	ENSMUSG00000043154
Mat2a	1.4	80.25	121.08	ENSMUSG00000053907
Rnd1	2.5	3.16	12.69	ENSMUSG00000054855
Sbno2	1.6	4.07	10.08	ENSMUSG00000035673
Amot	−1.3	22.78	5.1	ENSMUSG00000041688
Pde4d	1.5	58.22	96.14	ENSMUSG00000074661
Tnfrsf19	−2.6	8.38	0.81	ENSMUSG00000060548
1110028C15Rik	−1.7	12.51	2.58	ENSMUSG00000026004

Table B.3: 24.0hr genes sorted by p-value. rpkm1 = mock; rpkm2 = denervated. log 2(fold change) = denervated/mock. rpkm = reads per kilobase per million base pairs. $p < 0.001$.

gene symbol	**log2(fold change)**	**rpkm1**	**rpkm2**	**ENSEMBL ID**
Hr	1.5	21.02	37.23	ENSMUSG00000022096

Table B.4: 168.0hr genes sorted by p-value. rpkm1 = mock; rpkm2 = denervated. log 2(fold change) = denervated/mock. rpkm = reads per kilobase per million base pairs. $p < 0.001$.

gene symbol	**log2(fold change)**	**rpkm1**	**rpkm2**	**ENSEMBL ID**
Dhrs7c	-5	$4.60E+02$	6.35	ENSMUSG00000033044
Odf3l2	-6.4	$1.30E+02$	0.49	ENSMUSG00000035963
Scn5a	7.8	$1.00E-01$	18.3	ENSMUSG00000032511
Ramp1	-5.5	$2.60E+02$	3.38	ENSMUSG00000034353
Ppp1r1a	-3.5	$1.40E+02$	4.85	ENSMUSG00000022490
4930513N10Rik	-3.5	$4.50E+01$	1.79	ENSMUSG00000074136
Mbp	-3.9	$3.40E+01$	0.97	ENSMUSG00000041607
Igfn1	7.2	$6.00E+00$	358.58	ENSMUSG00000051985
Grb14	-2.9	$1.80E+02$	17.34	ENSMUSG00000026888
Hhatl	-2.6	$2.70E+02$	20.57	ENSMUSG00000032523
Cmbl	-2.5	$1.20E+03$	87.05	ENSMUSG00000022235
Ckmt2	-2.4	$7.50E+02$	69.01	ENSMUSG00000021622
Rpl3l	-2.4	$1.10E+03$	97.43	ENSMUSG00000002500
Lynx1	-2.5	$1.20E+02$	10.45	ENSMUSG00000022594
Zmynd17	-2.3	$9.50E+02$	111.58	ENSMUSG00000021815
Chrng	6	$7.30E-01$	24.72	ENSMUSG00000026253
Myl2	-3.8	$1.20E+04$	342.26	ENSMUSG00000013936
Eepd1	-2.6	$7.50E+01$	5.17	ENSMUSG00000036611
Aif1l	4.2	$1.20E+01$	180.93	ENSMUSG00000001864
Gsn	-2.1	$4.00E+03$	384.24	ENSMUSG00000026879
Clca3	6.1	$1.50E-01$	7.12	ENSMUSG00000028255
Myh4	-2.4	$5.70E+02$	55.45	ENSMUSG00000057003
Myog	4	$1.30E+01$	106.53	ENSMUSG00000026459
Mylk2	-2.2	$1.30E+02$	13.13	ENSMUSG00000027470

Table B.4: 168.0hr genes sorted by p-value. rpkm1 = mock; rpkm2 = denervated. log 2(fold change) = denervated/mock. rpkm = reads per kilobase per million base pairs. $p < 0.001$.

gene symbol	**log2(fold change)**	**rpkm1**	**rpkm2**	**ENSEMBL ID**
Gdf5	7.7	$3.10E-02$	8.84	ENSMUSG00000038259
S100a8	5.6	$6.10E+01$	$1,557.43$	ENSMUSG00000056054
Apobec2	-2	$9.80E+02$	123.4	ENSMUSG00000040694
Myf6	3.2	$2.00E+02$	$1,073.08$	ENSMUSG00000035923
Tmem233	-2.1	$1.20E+02$	15.04	ENSMUSG00000079278
Ostn	-2.5	$2.10E+02$	19.97	ENSMUSG00000052276
Ampd3	3.3	$9.60E+00$	68.66	ENSMUSG00000005686
Wfdc1	-2.3	$1.70E+02$	15.3	ENSMUSG00000023336
Klhl33	-3.4	$4.20E+01$	1.91	ENSMUSG00000090799
Tcea3	-2	$4.00E+02$	40.21	ENSMUSG00000001604
Plekhh1	4.3	$9.00E-01$	10.46	ENSMUSG00000060716
Cox7a1	-2.1	$3.10E+03$	290.5	ENSMUSG00000074218
Ankrd1	5.2	$2.90E+01$	651.34	ENSMUSG00000024803
Smtnl1	-1.9	$6.70E+02$	76.86	ENSMUSG00000027077
Evc	-2.5	$4.30E+01$	2.91	ENSMUSG00000029122
Slc37a4	-2	$1.60E+02$	19.82	ENSMUSG00000032114
Gadd45a	4.1	$9.60E+01$	459.61	ENSMUSG00000036390
Pvr	3.5	$6.10E+00$	36.68	ENSMUSG00000040511
Slc41a3	-2.3	$5.30E+01$	6.03	ENSMUSG00000030089
Ckm	-1.8	$0.00E+00$	$2,361.30$	ENSMUSG00000030399
Ache	-2.2	$7.70E+01$	8.52	ENSMUSG00000023328
Lrig1	-2.2	$4.60E+01$	4.48	ENSMUSG00000030029
Ldhb	-2	$2.90E+02$	29.91	ENSMUSG00000030246
Myoz1	-1.8	$3.20E+03$	424.62	ENSMUSG00000068697
Riiad1	-3.3	$5.30E+01$	2.6	ENSMUSG00000028139

Table B.4: 168.0hr genes sorted by p-value. rpkm1 = mock; rpkm2 = denervated. log 2(fold change) = denervated/mock. rpkm = reads per kilobase per million base pairs. $p < 0.001$.

gene symbol	**log2(fold change)**	**rpkm1**	**rpkm2**	**ENSEMBL ID**
Sema6c	-2.9	$1.70E+02$	13.35	ENSMUSG00000038777
Timp1	3.7	$1.00E+01$	71.04	ENSMUSG00000001131
Scd1	2.7	$3.50E+01$	142.9	ENSMUSG00000037071
Camk2a	-1.8	$1.20E+02$	20.92	ENSMUSG00000024617
Krt18	6.3	$8.80E-01$	26.9	ENSMUSG00000023043
Prss55	-4.1	$2.40E+01$	0.58	ENSMUSG00000034623
Pvalb	-1.7	$0.00E+00$	3,250.83	ENSMUSG00000005716
Runx1	3.9	$1.70E+00$	23.16	ENSMUSG00000022952
Cst3	-2	$6.00E+03$	572.87	ENSMUSG00000027447
Pmp22	-1.9	$1.60E+02$	27.74	ENSMUSG00000018217
St3gal6	-1.9	$1.50E+02$	26.64	ENSMUSG00000022747
Gm16119	-2.4	$5.30E+01$	4.98	ENSMUSG00000010492
Klhl23	-2	$3.40E+01$	5.75	ENSMUSG00000042155
Ptp4a3	-1.7	$3.60E+02$	49.18	ENSMUSG00000059895
Ufsp1	-2.3	$8.20E+01$	8.44	ENSMUSG00000051502
Myl4	3.2	$6.70E+01$	241.15	ENSMUSG00000061086
Slpi	6.6	$1.90E-01$	11.25	ENSMUSG00000017002
Hist1h4h	-3.5	$3.00E+02$	11.02	ENSMUSG00000060981
H19	2.7	$3.60E+02$	843.05	ENSMUSG00000000031
Spp1	4.2	$1.20E+01$	116.88	ENSMUSG00000029304
Aes	-1.7	$8.60E+02$	107.26	ENSMUSG00000054452
2310065F04Rik	-2	$7.50E+01$	8.82	ENSMUSG00000087410
Krt80	3.3	$2.70E+00$	14.52	ENSMUSG00000037185
Fhl3	-1.7	$5.50E+02$	64.19	ENSMUSG00000032643
Clcn1	-1.7	$1.40E+02$	26.73	ENSMUSG00000029862

Table B.4: 168.0hr genes sorted by p-value. rpkm1 = mock; rpkm2 = denervated. log 2(fold change) = denervated/mock. rpkm = reads per kilobase per million base pairs. $p < 0.001$.

gene symbol	**log2(fold change)**	**rpkm1**	**rpkm2**	**ENSEMBL ID**
Ttyh1	4.3	$6.10E-01$	15.63	ENSMUSG00000030428
Myl10	−2.9	$5.60E+01$	2.86	ENSMUSG00000005474
Chrnd	2.7	$1.00E+01$	36.69	ENSMUSG00000026251
Uaca	−1.6	$5.20E+02$	69.71	ENSMUSG00000034485
Thra	−1.8	$1.30E+02$	16.11	ENSMUSG00000058756
Tuba8	−1.7	$2.00E+02$	24.76	ENSMUSG00000030137
Cd24a	−1.6	$2.70E+02$	50.38	ENSMUSG00000047139
Nov	−1.9	$4.80E+01$	8.47	ENSMUSG00000037362
Ampd1	−1.6	$1.20E+03$	205.81	ENSMUSG00000070385
Ankrd10	2.5	$2.70E+01$	79.37	ENSMUSG00000031508
Cntnap2	−3.1	$9.50E+01$	5.75	ENSMUSG00000039419
Col22a1	−1.7	$3.60E+01$	5.3	ENSMUSG00000079022
Tpi1	−1.6	$2.60E+03$	461.25	ENSMUSG00000023456
Cst6	2.6	$1.10E+01$	30.07	ENSMUSG00000024846
Col24a1	−2.2	$1.10E+01$	1.78	ENSMUSG00000028197
Abcb4	−1.6	$1.00E+02$	16.89	ENSMUSG00000042476
Slc25a4	−1.5	$5.50E+03$	959.9	ENSMUSG00000031633
Kcna7	−1.7	$6.20E+01$	9.03	ENSMUSG00000038201
Cd82	3.2	$2.90E+01$	155.49	ENSMUSG00000027215
Pygm	−1.5	$3.30E+03$	541.08	ENSMUSG00000032648
Tnnt2	2.7	$4.10E+01$	96.94	ENSMUSG00000026414
Ccbl1	−1.9	$5.40E+01$	6.4	ENSMUSG00000039648
Eno3	−1.4	$1.10E+04$	$2,043.79$	ENSMUSG00000060600
Slc27a1	−1.9	$4.80E+01$	5.13	ENSMUSG00000031808
Ncam1	2.2	$2.90E+01$	73.62	ENSMUSG00000039542

Table B.4: 168.0hr genes sorted by p-value. rpkm1 = mock; rpkm2 = denervated. log 2(fold change) = denervated/mock. rpkm = reads per kilobase per million base pairs. $p < 0.001$.

gene symbol	**log2(fold change)**	**rpkm1**	**rpkm2**	**ENSEMBL ID**
Atp13a3	2.6	$5.50E+00$	30.47	ENSMUSG00000022533